Analysis and Synthesis of ECG Signals for Diagnosis and Person Specific Information

A

Thesis submitted

for the award of the degree of

DOCTOR OF PHILOSOPHY

By

Ato Kapfo

DEPARTMENT OF ELECTRONICS AND ELECTRICAL ENGINEERING

INDIAN INSTITUTE OF TECHNOLOGY GUWAHATI

GUWAHATI - 781 039, INDIA

MARCH 2026

Certificate

This is to certify that the thesis entitled "**Analysis and Synthesis of ECG Signals for Diagnosis and Person Specific Information**", submitted by **Ato Kapfo** (146102031), a research scholar in the *Department of Electronics and Electrical Engineering, Indian Institute of Technology Guwahati*, for the award of the degree of **Doctor of Philosophy**, is a record of an original research work carried out by him under our supervision and guidance. The thesis has fulfilled all requirements as per the regulations of the institute and has reached the standard needed for submission. The results embodied in this thesis have not been submitted to any other University or Institute for the award of any degree or diploma.

Prof. Samarendra Dandapat,
Professor
Dept. of Electronics and Electrical Engg.
Indian Institute of Technology Guwahati
Guwahati - 781039, India.

Dated:
Guwahati.

Prof. Prabin Kumar Bora,
Professor
Dept. of Electronics and Electrical Engg.
Indian Institute of Technology Guwahati
Guwahati - 781039, India.

Dated:
Guwahati.

To

My beloved parents

Chikha Kapfo and Zülhinyi-ü Kapfo

for their prayers, love and encouragement

Acknowledgements

Blessed be the name of God forever and ever, for wisdom and might are His. **Daniel 2:20**

I am overwhelmed in all humbleness and gratefulness to acknowledge my depth to all those who have been instrumental in the successful completion of this dissertation. At the outset, I express my heartfelt gratitude to my PhD supervisors, Prof. Samarendra Dandapat and Prof. Prabin Kumar Bora, for providing me an opportunity to work under their guidance. Their invaluable guidance, insightful feedbacks, and genuine concern have helped me in every stage of my research work. This thesis would not have been possible without their sincere efforts, encouragement and inspiration.

I am thankful to my doctoral committee members, Dr. Tony Jacob, Prof. M. K. Bhuyan, and Dr. Salil Kashyap for their valuable suggestions on my work. I am deeply grateful to them for their insightful comments and constructive criticisms on the work to bring it to the current form. I am thankful to Prof. Senthilkumar Sivaprakasam of IIT Guwahati, for his guidance, care and support during the difficult stretch of my life. I would like to express my sincere thanks to the office staffs of the Department and Administration, canteen caterers, security personnels, and maintenance staff members for their help when required. I sincerely thank Visvesvaraya PhD Scheme, initiated by the Ministry of Electronics and Information Technology for providing financial support toward my PhD project.

Deep appreciation is expressed to all friends for their unwavering support, kindness, love and care even if each one isn't individually acknowledged. I am incredibly grateful to you and my appreciation knows no bounds. My sincere gratitude to all my friends and labmates of the EMST and Signal Informatics Laboratory for their selfless help and invaluable support during my research journey. I also extend my gratitude to Naga IITG Family, IITG EU, and NCF Guwahati for their prayers and constant moral support. I would like to thank the entire IITG fraternity for their help and kindness extended to me during my time at the institute.

My deepest gratitude goes to my parents, siblings, grandmother, cousins and extended family. Without their unconditional love, unceasing prayers, and sacrifice it would not have been possible for me to complete my PhD.

Ato Kapfo

Abstract

Electrocardiogram (ECG) is the graphical representation of the electrical signals of the human heart. In clinical practice, the ECG is used as a standard tool to assess cardiac activities and diagnose the myocardium condition. Any heart dysfunction is reflected in the ECG signal as a deviation from the normal characteristic of the healthy human heart. Variations in the morphological features often indicate specific cardiac pathologies. However, visually detecting subtle changes across 24-hour ECG recordings can be time-consuming, susceptible to human error, and a challenging task for medical professionals. This necessitates the development of automated computer-aided diagnostic (CAD) system using advanced signal processing techniques for accurate and efficient detection of cardiac abnormalities. The thesis introduces an approach that utilizes variational mode decomposition (VMD) to extract features for myocardial infarction classification using machine learning techniques. The anomalies of cardiac disorders are reflected in different leads of the 12-lead ECG. However, utilization of multiple electrodes restricts their usage in some applications, such as continuous monitoring, ambulatory monitoring, personalized healthcare, and remote monitoring. Thus, deriving the standard twelve-lead ECG from its subset without losing the diagnostic quality is essential to mitigate the mentioned challenges and reduce the complexity of the system. This thesis proposes to decompose the three predictor leads using discrete wavelet transform (DWT) and applies the long short-term memory (LSTM) algorithm on selected subbands to synthesize the 12-lead ECG signal. Furthermore, the synthesized ECG signals are expected to retain the person specific biometric information. In this direction, a hierarchical LSTM architecture

has been explored to investigate the effectiveness of synthesized ECG signals for person identification applications.

The first contributory work of the thesis introduces a multiscale approach for detection of myocardial infarction (MI) from multilead ECG. The variational mode decomposition (VMD) grossly decomposes the diagnostic components of ECG such as the P-wave, the QRS-complex and the T-wave into different modes. In MI pathology, the shape and the amplitude of the diagnostic components of multilead ECG (MECG) are different from the normal sinus rhythm (NSR). These pathological changes may affect the characteristics of the coefficients of MECG at different modes. The features evaluated from the coefficients of MECG will be helpful for detection of MI. The proposed multiscale approach is based on the evaluation of multiscale mode energy and eigenspace (MMEE) features of multilead ECG. The MMEE features of multilead ECG are fed as an input to various classifiers for MI detection. Experimental results shows that the proposed method is capable of accurately detecting MI and demonstrate the superior performance compared to the existing approaches.

In the second work, an enhanced ECG spatial resolution approach that exploits the spatio-temporal correlations within the hidden feature space is investigated. The proposed approach takes leverage of the enhanced inter-lead correlation of the ECG signal in the wavelet domain. This high correlation between different leads within the same wavelet scale can be effectively utilized to train an advanced recurrent neural network (RNN) model. The experimental results are evaluated using different diagnostic measures and similarity metrics to assess the preservation of diagnostic information and quantify any potential loss. The proposed framework is well founded, and accurate reconstruction is possible as it can capture clinically significant features and provides a robust solution against noise.

In the third work, an HLSTM architecture has been explored to investigate the

effectiveness of synthesized ECG signals for person specific information. The model examines the similarity of biometric information between the original and reconstructed signals from the same record at different layers of hierarchy. To evaluate the performance of the synthesis model, a novel metric called Person Identifiability (PI) has been introduced. Experimental results demonstrate that the synthesized ECG signals retain person specific characteristics comparable to those of the original signals.

Keywords: Electrocardiogram (ECG), Variational mode decomposition (VMD), Myocardial infarction (MI), ECG synthesis, Discrete wavelet transform (DWT), Long short-term memory (LSTM), Biometric identification, Person specific information, Hierarchical LSTM (HLSTM).

Contents

List of Figures

List of Tables

List of Abbreviations

AF	Atrial Fibrillation
AI	Artificial Intelligence
ANN	Artificial Neural Network
AWGN	Additive White Gaussian Noise
AV	Atrioventricular
BBB	Bundle Branch Block
BiGRU	Bidirectional Recurrent Unit
BPM	Beats Per Minute
CAD	Coronary Artery Disease
CD	Conduction Disturbances
CNN	Convolutional Neural Network
CVD	Cardiovascular Diseases
CT	Computed Tomography
CYD	Cardiomyopathy
DCT	Discrete Cosine Transform
DL	Deep Learning
DWT	Discrete Wavelet Transform
ECE	Energy Contribution Efficiency
ECG	Electrocardiogram
EEG	Electroencephalogram
EGG	Electroglottographic
EMD	Empirical Mode Decomposition

EWT	Empirical Wavelet Transform
FN	False Negative
FP	False Positive
HC	Healthy Control
HCM	Hypertrophic Cardiomyopathy
HLSTM	Hierarchical LSTM
ICA	Independent Component Analysis
IDWT	Inverse Discrete Wavelet Transform
IMFs	Intrinsic Mode Functions
IoT	Internet of Things
KNN	K-Nearest Neighbour
LA	Left Atrium
LAD	Left Anterior Descending
LCA	Left Main Coronary Artery
LCx	Left Circumflex
RMSE	Root Mean Square Error
LSTM	Long Short-Term Memory
LV	Left Ventricle
ML	Mason-Likar
MI	Myocardial Infarction
MPI	Myocardial Perfusion Imaging
MRI	Magnetic Resonance Imaging
NSR	Normal Sinus Rhythm
PCA	Principal Component Analysis
PI	Person Identifiability
PTB	Physikalisch Technische Bundesanstalt
RA	Right Atrium
RCA	Right Coronary Artery

RV	Right Ventricle
RMSE	Root Mean Square Error
RNN	Recurrent Neural Network
SA	Sinoatrial
SNR	Signal-to-Noise Ration
SVM	Support Vector Machine
TN	True Negative
TP	True Positive
VA	Ventricular Arrhythmia
VCG	Vectorcardiogram
VF	Ventricular Fibrillation
VMD	Variational Mode Decomposition
VT	Ventricular Tachycardia
WEDD	Wavelet Energy Diagnostic Distortion
WT	Wavelet Transform

1

Introduction

Contents

1. Introduction

Cardiovascular diseases (CVDs) are the chief contributor to mortality and disability worldwide, accounting for an estimated 17.9 million fatalities in 2019, or 32% of global deaths [1]. They are responsible for approximately 38% of all premature deaths globally [2]. Among the various types of CVDs, heart diseases such as cardiac arrhythmias and coronary artery disease (CAD) are particularly significant contributors. These cardiac disorders frequently deteriorate over time; therefore, if not treated, they can result in serious complications such as strokes and myocardial infarction. Early diagnosis and a deeper understanding of cardiac disorders are essential for initiating timely and appropriate treatment strategies [3]. The electrocardiogram (ECG), which records the heart's electrical activity, is a fundamental non-invasive clinical tool for detecting and diagnosing most cardiac disorders.

Contemporary diagnostic devices for assessing cardiovascular health include ECG, myocardial perfusion imaging (MPI), cardiac ultrasound, cardiac computed tomography (CT) angiography, CT calcium scoring, cardiac catheterization and cardiac magnetic resonance imaging (MRI). Among these, ECG stands out as a simple, non-invasive, easy application and cost-effective method widely employed by physicians and cardiologists to monitor and diagnose cardiac ailments [4]. The electrophysiological defects of the heart leave a distinct signatures on the ECG. The accurate identification of these signatures can aid in the diagnosis of cardiac abnormalities. Clinically, ECG recordings are typically acquired in two formats: (i) Holter ECGs or single-lead ambulatory which record the heart's electrical activity from a single perspective over long periods. These are particularly useful for the characterization and early diagnosis of rhythm disorders, such as atrial fibrillation (AF) (ii) the standard 12-channel ECG captures the heart's electrical activity from different perspectives in the frontal and transverse planes over multiple heartbeats. This format is commonly used to diagnose acute, spatially localized cardiac disorders such as cardiomyopathy (CYD), conduction disturbances (CD), and myocardial infarction (MI). As a result, meticulous analysis of both single- and 12-lead ECG signals is essential for diagnosing cardiac abnormalities, assessing risk, and evaluating the impact of medical interventions.

An experienced cardiologists diagnose cardiac ailments clinically by manually analyzing

key ECG characteristics, including the P-wave, the T-wave, the ST-segment, and the QRS complex [5]. However, due to the varied causes of cardiac conditions, pathological ECG waveforms exhibit dynamic variations in duration, amplitude, and morphological changes. Furthermore, as the disease progresses, subtle changes in pathological ECG features can appear in specific leads of a 12-lead ECG. Manually analyzing lengthy single-lead or 12-lead ECG recordings is not only labor-intensive and time-consuming but also prone to errors [6]. The visual assessment of diverse pathological manifestations also introduces subjectivity, leading to inter- and intra-rater variability [6, 7]. Therefore, there is a pressing need for automated ECG interpretation methods that can effectively capture disease variations and facilitate faster, more objective, and accurate clinical decision-making.

The advancement of emerging technology in developing miniature and wireless ECG devices with minimal complexity has recently gained significant popularity. The multichannel ECG signal is recorded with the aid of multiple electrodes attached to predefined locations on the surface of the human body. However, utilizing numerous electrodes compromises the patient's comfort and intensifies the overall intricacy of the system [8]. This challenge becomes even more pronounced in ambulatory conditions, where the use of a large number of electrodes complicates the recording process. The application of a derived 12-lead ECG system is effective in an area where monitoring and recording of a standard twelve-lead ECG is challenging [9]. In remote healthcare settings, where access to medical professionals with expertise in ECG diagnosis is limited, a derived ECG system plays a crucial role in facilitating data transmission, compression, and efficient healthcare delivery [10].

The growing adoption of wearable healthcare devices and remote healthcare has made personalized CVD diagnostic systems increasingly relevant. Advances in communication technology and the Internet of Things (IoT) have driven a shift toward artificial intelligence (AI)-based healthcare systems, raising concerns about the privacy and security of sensitive medical data recorded both in hospital settings and personal wearable devices. The ECG signal offers a viable biometric modality for securing healthcare information and identity recognition, as its unique morphological patterns vary from person to person. Additionally,

it is highly resistant to spoofing due to its inherent liveliness characteristics and minimal exposure to covert acquisition. As a result, ECG-based biometrics emerge as a practical solution not only for healthcare security but also for a wide range of applications, given its ease of acquisition and reliability [11].

This thesis aims to develop a reliable and efficient automated computer-aided-diagnostic (CAD) system capable of analyzing, interpreting, and visualizing the ECG signals to assist in the accurate diagnosis of cardiac abnormalities, minimizing the complexity and enhancing the security system for sensitive medical data. This chapter begins with an introduction to the physiological processes of the heart and the ECG signal. The following section discusses both the single-lead and multi-lead ECG signals, followed by the pathological manifestations of cardiac disorders. Furthermore, we present a brief introduction to the synthesis of the 12-lead ECG and person specific information from synthesized ECG. The scope of the present work is discussed at the end of the section.

1.1 The Physiology of the Heart and the Electrocardiogram

The human heart is an autonomous organ that serves as the central component of the cardiovascular system, responsible for pumping oxygenated blood throughout the body. A cross-sectional anatomy of the heart is shown in Figure 1.1. It is enclosed within a protective and fluid-filled sac called the pericardium and consists of four chambers: two upper atria and two lower ventricles—as well as four valves: the tricuspid valve, the pulmonary valve, the mitral valve, and the aortic valve [5]. The left and right atria are separated by a thin membranous wall known as the interatrial septum, while the left and right ventricles are divided by a thick muscular wall called the interventricular septum.

The heart facilitates blood circulation in a unidirectional manner. Deoxygenated blood from the body is first received by the right atrium through two large veins, the superior vena cava and the inferior vena cava [12]. It then flows from the right atrium (RA) to the right ventricle (RV) through the tricuspid valve, which prevents backflow into the atrium. The

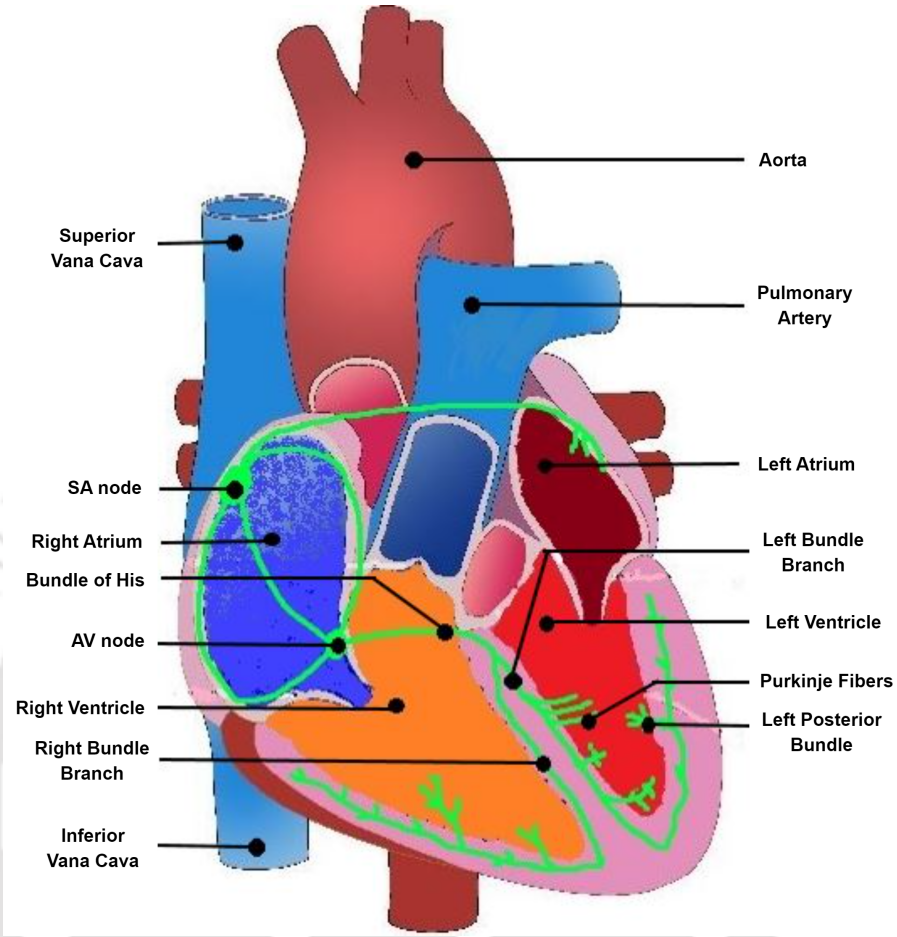

Figure 1.1: Cross-sectional anatomy of the heart.

right ventricle subsequently pumps the blood to the lungs through the pulmonary valve for oxygenation. Oxygen-rich blood returns to the left atrium (LA), from where it is transferred to the left ventricle (LV) via the mitral valve. The left ventricle then pumps the oxygenated blood into the aorta through the aortic valve, which distributes it throughout the body.

The heart's activity is regulated by an intrinsic electrical conduction system composed of specialized cardiac myocytes, or pacemaker cells. This conduction pathway consists of the sinoatrial (SA) node, atrioventricular (AV) node, His bundle, and Purkinje fibers [12]. Figure 1.2 illustrates the conduction system of the heart and the classical ECG waveforms. The electrical impulse originates in the SA node, spreading across the LA and RA to induce atrial contraction. This process, known as atrial depolarization, is represented by the P-wave on an ECG. The impulse then reaches the AV node, which acts as a relay station between the atria

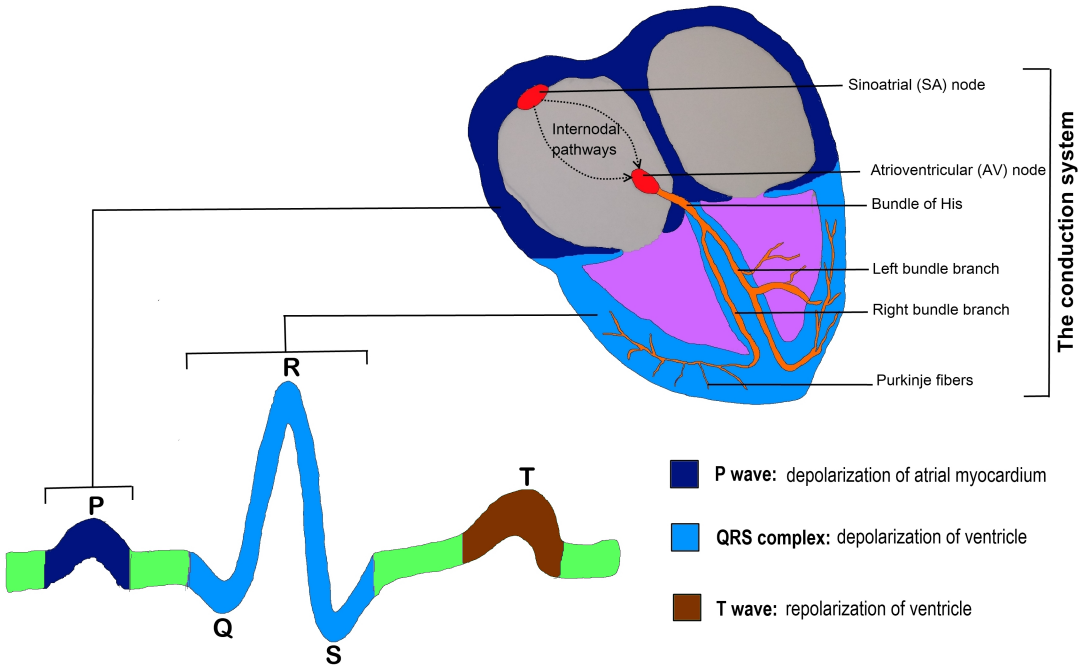

Figure 1.2: Conduction system of the heart and the classical ECG waveforms.

and ventricles. Subsequently, from the AV node, the electrical stimulus travels through the left and right bundle branches, stimulating the interventricular septum and triggering ventricular contraction. Ventricular depolarization is facilitated by the His bundle and Purkinje fibers. This event is characterized by the large QRS complex [5]. During ventricular depolarization, the RV pumps deoxygenated blood to the lungs, while the LV distributes oxygenated blood throughout the body. This is followed by ventricular repolarization, indicated by the T-wave on the ECG, and the heart enters the ventricular diastole phase.

The electrical activity of the heart, as recorded by the ECG, provides valuable insights into both its physiological function and pathological conditions. Each ECG cycle comprises different time-varying morphological features such as P-wave, QRS-complex and T-wave. As shown in Figure 1.3, each segment or wave of the ECG signifies the vital electrical events of the heart. The significance of each of the morphological features of the ECG signal are presented below.

- **P-wave:** The myocardial contracting cells of both the atria gets electrically stimulated

simultaneously by the conducting cells and this composite activation causes atrial depolarisation which generates P-wave in the ECG signal. Typically, the duration of the P-wave for a normal sinus rhythm (NSR) varies from 80 to 100 ms.

- **PR-interval:** The PR-interval represents the duration for the electrical impulse to travel from the SA node through the atria, AV node, and into the ventricles. In normal condition, the passage of PR-interval is of 120–200 ms.
- **QRS-complex:** The cardiac impulse then travels from the AV node to the His bundle, left and right bundle branches, and Purkinje fibers causing rapid depolarization of the ventricles, triggering ventricular contraction, resulting in a large QRS-complex in the ECG signal. The normal duration of QRS-complex is between 60-100 ms.
- **ST-segment:** Succeeding ventricular depolarisation, the muscle cells attain a plateau portion where no action potential occurs that proceeds about 120 ms, resulting to the isoelectric ST-segment in the ECG. The ST-segment represents the period between ventricular depolarization and repolarization.
- **T-wave:** Eventually, the ventricles enter the repolarization phase, which is reflected on the ECG as the T-wave. In NSR, the T-wave typically lasts between 100 and 250 ms.
- **QT-interval:** The QT-interval represents the total time for ventricular depolarization and repolarization. The QT interval typically ranges from 350 to 450 ms.
- **RR-interval:** The RR-interval on the ECG is the time between two consecutive R-waves, which correspond to the depolarization of the ventricles. It is a key measurement for evaluating both heart rate and rhythm. In a healthy adult with NSR, the RR-interval typically corresponds to a heart rate of 60–100 bpm.

The sequential process described above forms a single ECG heartbeat, inherently characterized by temporal dependencies within the waveform. In healthy control (HC) subjects, this cardiac cycle repeats regularly, producing a stable rhythm known as normal sinus rhythm

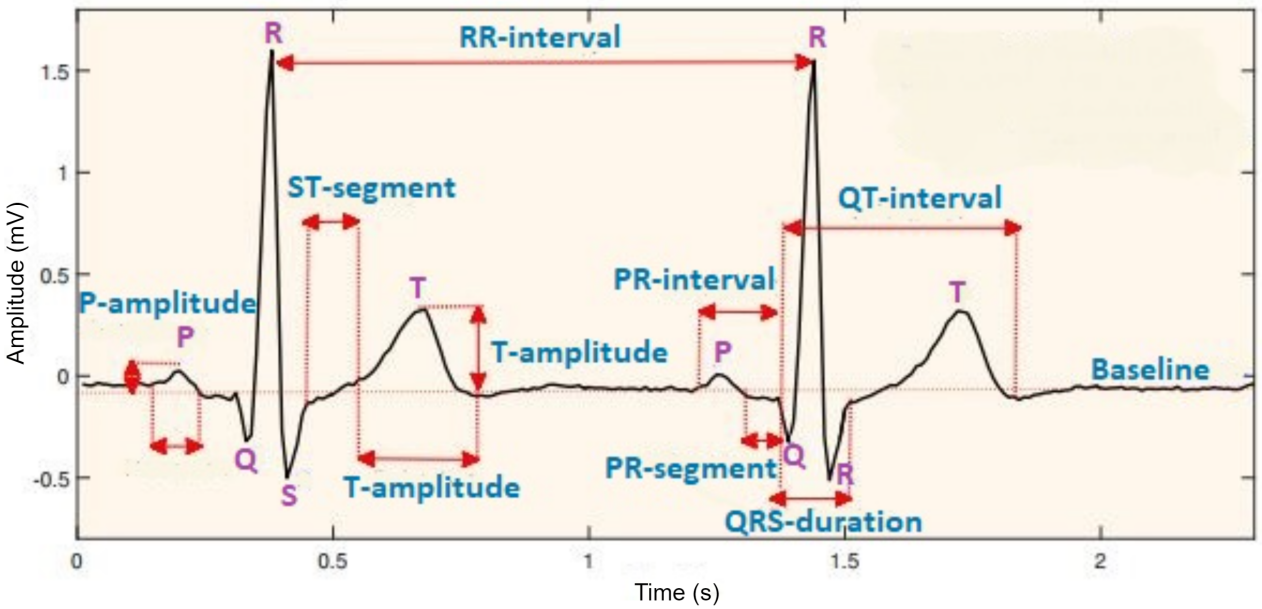

Figure 1.3: Morphological features of the ECG.

(NSR). As illustrated in Figure 1.3, the ECG captures essential information about the heart's electrical activity, meaning any dysfunction in the heart can manifest as observable morphological changes in the ECG signal. Analyzing these changes such as variations in amplitude, shape, duration offers critical understanding into cardiac pathophysiology [12]. In clinical practice, the most commonly used ECG systems for assessing cardiac health are the single-lead ECG and the standard 12-lead ECG [13]. The following sections provide a brief overview of these ECG recording systems.

1.2 ECG Leads

The heart's pumping action is initiated by rhythmic electrical impulses generated at the sinoatrial (SA) node and transmitted to different parts of the heart. An ECG is a graphical representation of this electrical activity over time, recorded using electrodes placed on the surface of the body. Since the human body conducts electricity, ECG signals can be recorded by positioning electrodes at specific locations, namely the wrists, ankles and chest. An ECG lead represents a vector projection of the heart's electrical activity, recorded using

two electrodes. The two types of ECG limb leads are unipolar and bipolar. Unipolar leads measure the difference in electrical potential between a limb electrode while the other serves as a reference. Bipolar leads measure a potential difference between two points on the body.

Since early 20th century, various methods have been developed for recording ECG signals, each employing distinct electrode placement configurations to capture the spatial progression of the heart's electrical impulses, thereby improving diagnostic accuracy [14]. Among these, the gold-standard 12-lead ECG and Holter ECG are widely used in clinical practice. The 12-lead ECG provides a comprehensive snapshot of cardiac activity, making it invaluable for diagnosing acute and chronic heart conditions. Meanwhile, Holter ECG monitoring enables continuous, long-term recording, allowing for the detection of intermittent arrhythmias and other cardiac abnormalities that might not be captured in a short-duration ECG.

Figure 1.4: Various single-lead ambulatory ECG recording setups and cardiac monitoring durations.

1.2.1 Single-Lead ECG

Single-lead ECG acquisition methods offer significant advantages for prolong cardiac examination due to their simplicity and practicality. These systems require only two electrodes, making them easy to acquire and use while also demanding minimal data storage. Although single-lead ECG signals may not provide a comprehensive cardiac assessment, they offer valuable insights into sustained heart health, arrhythmic abnormalities, and even biometric identification. For long-term cardiac monitoring, clinicians rely on portable ECG devices or Holter monitors, which allow for continuous recording over several hours or even days. Holter

ECG monitors are particularly valuable for detecting intermittent cardiac abnormalities that might be missed during a routine hospital visit [14]. Additionally, remote patient monitoring using Holter recorders plays a crucial role in the early detection and management of asymptomatic or silent cardiac abnormalities, enabling timely medical intervention. Recent advancements in wireless and sensor technologies have led to the development of portable wearable devices as shown in Figure 1.4. Most of these devices record single-lead ECG signals, typically from Lead I or Lead II. While smartwatches and handheld mobile are more suitable for intermittent monitoring, Holter ECG devices and cardiac monitoring Patch are well-suited for long-term ambulatory monitoring, allowing patients to record ECG readings whenever they experience abnormal sensations. These innovations enhance user convenience and compliance, making continuous ECG monitoring more accessible. Additionally, single-lead ECG signals are increasingly explored for biometric applications, benefiting from their ease of use and non-intrusive nature, which improve user acceptance.

1.2.2 Twelve-Lead ECG

Einthoven conceptualised a geometric arrangement of the three limb leads (I, II, III) as forming an hypothetical equilateral triangle known as Einthoven's triangle, with the heart positioned at its center. According to Einthoven's law, the sum of the potentials recorded in Leads I and III is equal to the electrical potential of Lead II. Later, Wilson introduced a central terminal which ultimately provide a foundation for recording additional electrocardiographic leads. This innovation enabled the establishment of unipolar lead systems (aVR, aVL, aVF), enhancing diagnostic accuracy. The six leads record projections of the three-dimensional heart electrical vector onto specific axes, providing multiple perspectives of cardiac function in the frontal plane. To further enhance ECG analysis, precordial leads (V1-V6) were introduced, allowing for the assessment of electrical activity in the horizontal plane. Figure1.5(a) shows Einthoven's triangle and the positions for placement of precordial leads.

The 12-lead ECG provides a comprehensive view of the heart's electrical activities from multiple angles, allowing healthcare professionals to assess heart function and detect cardiac

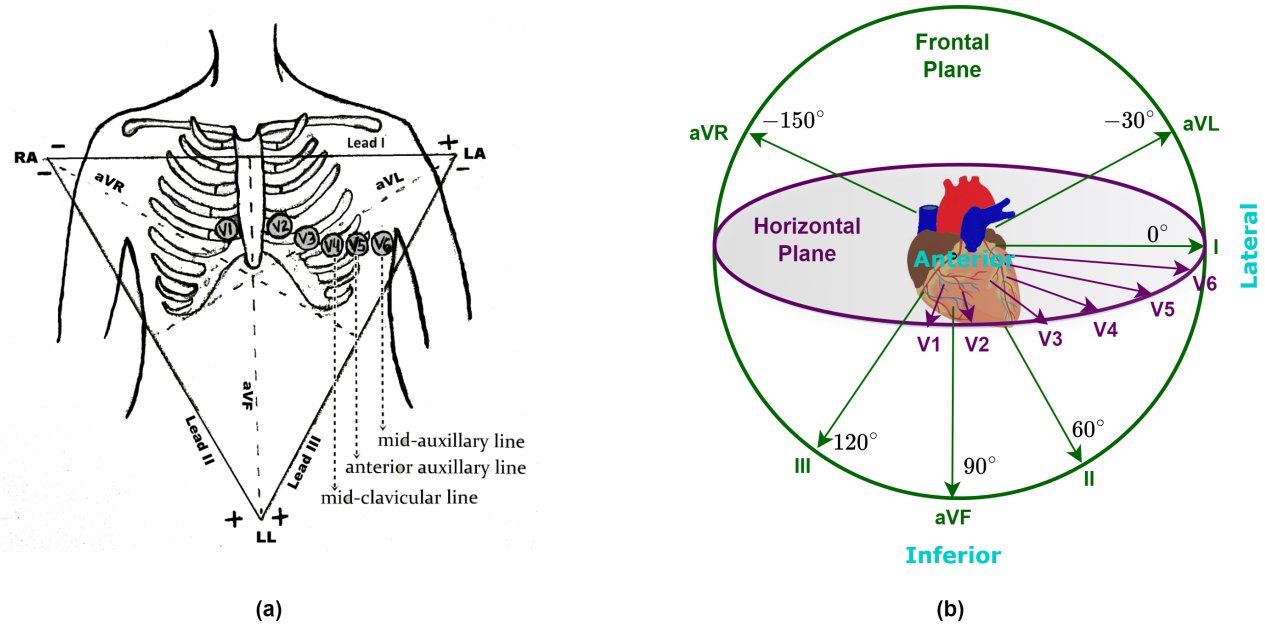

(a) (b)

Figure 1.5: Standard 12-lead ECG (a) Einthoven's triangle and the positions for placement of precordial leads. (b) The three-dimensional perspective of heart's electrical activity in both the horizontal and frontal planes

abnormalities. The "12-lead" or "12-channel" refers to the twelve different perspectives of the heart electrical activity, derived from a combination of electrodes placed on the specific location of the human body. The 12-lead ECG system is recorded using ten electrodes placed in a specific arrangement on the body's surface: four limb electrodes and six chest electrodes. Figure 1.6 illustrates the placement of these electrodes. They are labeled based on their respective positions on the patient limbs and chest (right arm (RA), left arm (LA), right leg (RL), left leg (LL), and chest electrodes (V1-V6)). The twelve leads derived from these electrodes are classified into three groups:

(i) Limb Leads (Bipolar Leads) – Derived from three limb electrodes:

- Lead I: Potential difference between LA and RA (LA-RA).
- Lead II: Potential difference between LL and RA (LL-RA).
- Lead III: Potential difference between LL and LA (LL-LA).

(ii) Augmented Limb Leads (Unipolar Leads) – aVR, aVL, and aVF measure the potential

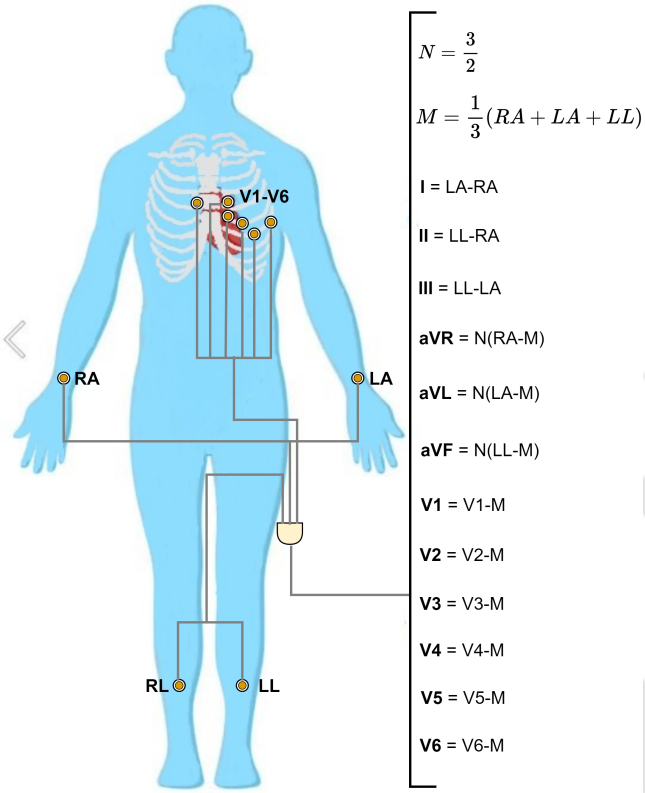

Figure 1.6: Placement of ten electrodes for recording standard 12-lead ECG.

difference between one limb electrode (RA, LA, or LL) and a reference electrode with a near-zero potential, rather than comparing the voltages between two extremities, as seen in bipolar limb leads. This near-zero potential is achieved within the electrocardiograph by connecting the three limb electrodes to a central terminal, known as Wilson's central terminal (M) [5].

(iii) Precordial (Chest) Leads – V1 to V6 measure the potential difference between the chest electrodes and the central terminal.

The heart is a three-dimensional organ, making it essential to assess its electrical activity from multiple perspectives for accurate diagnosis. The 12-lead ECG system visualize the heart's electrical signals from various unique angles in three-dimensional space as shown in Figure 1.5(b). In the frontal plane, lead I, lead II, and lead III views the heart at an orientation angles of $0°$, $60°$, and $120°$, respectively. Similarly, the augmented limb leads are positioned

as follows: Lead aVL at $-30°$, Lead aVR at $-150°$, and Lead aVF at $90°$. The precordial leads view the electrical signals from a horizontal plane. The anterior part of the heart is captured by lead V1 through V4. The inferior portion of the heart's electrical signals is seen using lead aVF, Lead II, and Lead III. Similarly, the right lateral is observed using lead aVR, while the left lateral portion of the heart is noticed through lead V5, lead V6, lead I, and lead aVL. Any deviations in these signals from their normal characteristics may indicate pathological signatures, which are crucial for detecting cardiac abnormalities. Thus, the 12-lead ECG captures the spatio-temporal variations of the heart's electrical activity, offering valuable insights into its function and aiding in a more comprehensive understanding of cardiac health.

Table 1.1: Normal characteristics of P-wave, QRS-complex and T-waves of the limb leads.

Waveform	Lead I	Lead II	Lead III	Lead aVR	Lead aVL	Lead aVF
P-wave	upright	upright	negative/upright	negative	negative	upright
QRS-complex	upright	upright	upright	negative	upright	upright
T-wave	upright	upright	negative/upright	negative	upright	upright

Table 1.2: Normal characteristics of P-wave, QRS-complex and T-waves of the precordial leads.

Waveform	Lead V1	Lead V2	Lead V3	Lead V4	Lead V5	Lead V6
P-wave	upright/biphasic	upright/biphasic	upright	upright	upright	upright
QRS-complex	rS-wave	rS-wave	equiphasic/upright	upright	upright	upright
T-wave	upright	upright	upright	upright	upright	upright

1.3 Normal Sinus ECG Signal

The normal sinus ECG is characterized by regular electrical stimuli of the healthy human heart that originates from the SA node, the natural pacemaker of the heart. Diagnosis of cardiac health depends on analyzing of essential features of the ECG signal, specifically the P-wave, QRS-complex, and T-wave. A detailed overview of the morphological characteristics of these waveforms in a sinus ECG signal is provided in Table 1.1 and Table 1.2. The sequential activation of the right and left atria is characterized by the P-wave. It begins with a propagation

of electrical activity of pacemaker cells in the SA node, typically propagates toward the left leg, forming an angle of approximately 60° with respect to the frontal plane. As a result, lead II displays a positive P wave, while lead aVR consistently records a negative P wave.

After atrial depolarization, ventricular depolarization occurs, giving rise to the QRS complex. Ventricular depolarization consists of two key phases: septum stimulation and simultaneous activation of both ventricles. The first phase, septal activation is characterized by q-waves; they are brief ($< 0.04s$ duration) and small amplitude. During this phase, they are observed in leads II, III, aVF when the QRS axis is to the right of $+60^\circ$, and in leads I and aVL when the QRS axis is to the left of $+60^\circ$. In the second phase, the left ventricle's electrical force dominates, shifting the net dipole toward the left ventricle. This results in a positive deflection (R-wave) in the left chest leads and a negative deflection (S-wave) in the right chest leads. As the QRS-complex progresses from lead V1 to V6, the R-wave height gradually increases, typically peaking around lead V4 or V5; a pattern known as normal R-wave progression. In contrast, the S-wave commence in V6 or V5 and progress in size to V2. S-wave in V1 is usually smaller than S-wave in V2. Eventually, the relaxation of the right and left ventricles of the heart is represented the T-wave represents. The normal T-wave typically follows the same direction as the QRS complex, except in the right precordial leads. In a normal ECG, the T wave is always inverted in lead aVR, while it is consistently upright in leads I, II, and V3–V6.

1.4 Cardiac Ailments: Pathological Manifestation in ECG Signals

This section presents a succinct overview of various cardiac ailments and their corresponding pathological changes in ECG signals. The discussion covers major cardiac ailments, including myocardial infarction (MI), hypertrophic cardiomyopathy, bundle branch block (BBB),and dysrhythmia.

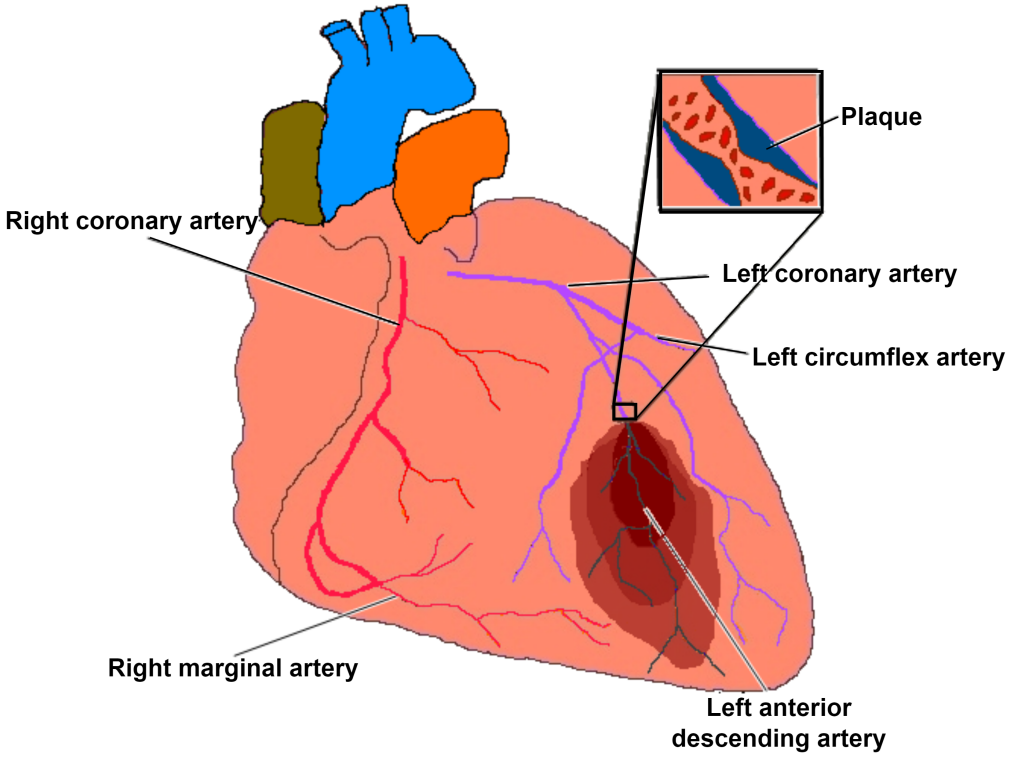

Figure 1.7: The coronary arteries and their anatomical relationships within the heart and the depiction of MI.

1.4.1 Myocardial Infarction

Myocardial infarction (MI) is a life-threatening heart condition caused due to the occlusion of a coronary artery, leading to reduced blood supply to the heart [13]. The coronary arteries are a network of blood vessels that encircle the heart, delivering oxygenated blood to the myocardium. The coronary arteries and their anatomical relationships within the heart and the depiction of MI are illustrated in Figure 1.7. The left main coronary artery (LCA) branches into left circumflex (LCx) artery and the left anterior descending (LAD) artery. The LCx artery supplies to the lateral wall of the left ventricle, while the LAD artery primarily responsible for perfusing the anterior wall of the left ventricle and the interventricular septum. The right coronary artery (RCA) supplies blood to the right atrium, right ventricle, and often the inferior portion of the left ventricle.

The pathogenesis of MI begins with the formation of plaques, composed primarily of

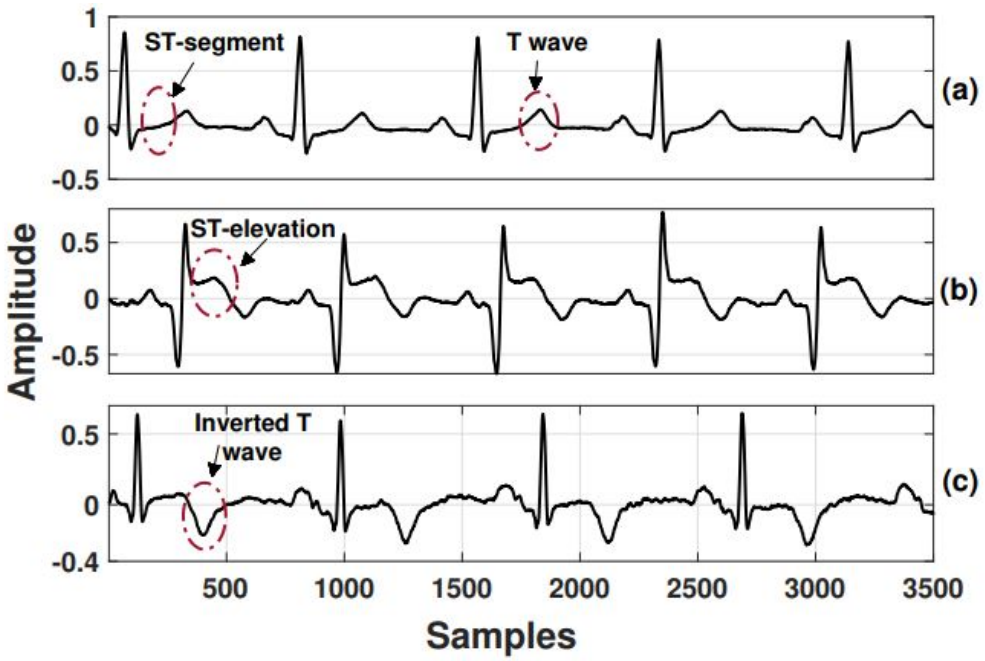

Figure 1.8: Healthy control ECG signal and pathological characteristics observed due to MI. (a) Normal ECG signal (b) MI with ST-elevation, and (c) MI with hyperacute T-wave peaking and inversion.

platelets, fibrin, and fat, which accumulate on the interior surface of the coronary arteries. This build-up leads to circulatory disruption and arterial occlusion, restricting blood flow to a portion of the heart and triggering the onset of MI. MI progresses through three distinct phases: ischemic, acute and necrosis. The first phase occurs when the blood flow in a coronary artery is restricted due to atherosclerotic plaque formation. In acute Phase, the condition worsens as ischemia intensifies, leading to increased damage to the cardiac tissue and in necrosis phase, the prolonged lack of oxygen results in myocardial tissue death (necrosis).

During MI, the morphology of the multi-lead ECG signal deviates from its normal characteristics. The ECG anomalies associated with MI such as the hyperacute T-Waves, T-wave inversion follows after the appearance of hyperacute T-waves, ST-segment elevation and the development of pathological Q-waves are observed in the 12-lead ECG. These characteristic ECG changes play a crucial role in the early detection and diagnosis of MI. The normal ECG and the two pathological characteristics of MI are shown in Figure 1.8.

1.4.2 Hypertrophic Cardiomyopathy

Hypertrophic cardiomyopathy (HCM) is a condition characterized by abnormal thickening (hypertrophy) of the heart muscle, which can impair the heart's ability to pump blood effectively. The thickened heart muscle can lead to serious complications, including chest pain, shortness of breath, and electrical abnormalities in the heart. These electrical disturbances may result in life-threatening arrhythmias or, in severe cases, sudden cardiac death. HCM primarily affects the septum, the wall separating the two lower chambers of the heart. In some cases, the thickened septum obstructs blood flow from the heart, a condition called obstructive hypertrophic cardiomyopathy. When there is no significant blockage of blood flow, the condition is referred to as nonobstructive hypertrophic cardiomyopathy. However, the heart's main pumping chamber, the left ventricle, may become stiff, making it difficult for the heart to relax properly. This stiffness reduces the ventricle's capacity to fill with blood, ultimately limiting the amount of blood pumped to the body with each heartbeat.

1.4.3 Bundle Branch Block

Bundle branch blocks (BBB) are ventricular conduction disorders caused by a blockage in either the left or right bundle branch, disrupting the normal electrical impulse transmission [15]. As a result, electrical signals travel asymmetrically, causing a delay in ventricular activation on one side of the heart. This disruption can affect the heart's pumping efficiency and overall cardiac function. The left BBB presents distinct morphological features, primarily characterized by a widened QRS-complex ($> 120ms$). In this condition, the entire ventricular depolarization is directed toward the left chest leads, resulting in broad and deep, and S-wave in lead V2 and a broad R-wave with notching at its peak in lead V6. T-wave inversion may be observed in the left precordial leads. Similarly, in right BBB, a delay in right ventricular activation displays a rSR complex, with a broad R-wave in lead V1, and lead V6 shows a broad S wave with a qRS-type complex. While BBB are not life-threatening, its presence can serve as an initial clue to underlying cardiac conditions, warranting further evaluation.

1.4.4 Dysrhythmia

Dysrhythmia and arrhythmia refer to irregularities in the heart's rate or rhythm, occurring when the heart beats too fast, too slow, or erratically. These disturbances may result from disruptions in the heart's electrical signaling system or structural changes in cardiac tissue, affecting the normal coordination of heartbeats. Other factors that contributes to dysrhythmia include, genetic factors, injury from a heart attack, heart disease, medical conditions, such as sleep apnea, thyroid disease, or high blood pressure, etc.

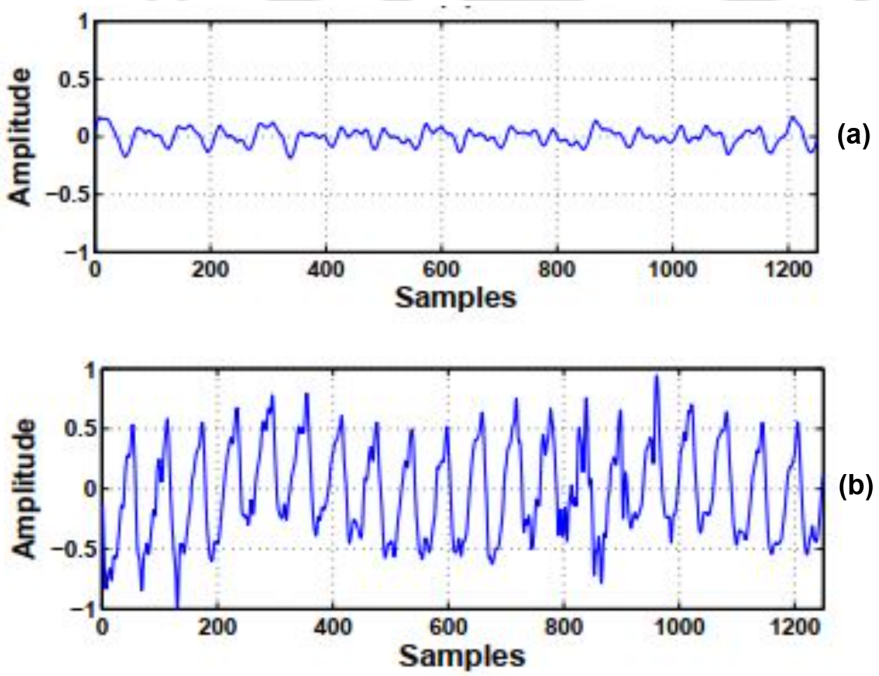

Figure 1.9: Subtypes of ventricular arrhythmias (a) Ventricular fibrillation occurrence in ECG. (b) Ventricular tachycardia occurrence in ECG.

Different types of dysrhythmia are bradyarrhythmias, supraventricular arrhythmias, and ventricular arrhythmias (VA). Bradyarrhythmias are associated with a heart rhythms with a rate under 60 beats per minute (BPM), commonly due to conduction disorder. Supraventricular arrhythmias are the types of arrhythmia that produce irregular heart's rate that occur in the upper chambers of the heart, while ventricular arrhythmias (VA) occur in the lower chambers of the heart. The subtypes of VA are ventricular fibrillation (VF) and ventricular tachycardia (VT). VF causes the ventricles to quiver instead of contracting and expanding and squeezing,

while VT is characterized by a fast, regular heartbeat exceeding 100 BPM, it can be brief or sustained for a longer duration, potentially leading to more severe complications. Figure 1.9 illustrates the occurrence of VF and VT in ECG. As can be seen from the Figure, VF and VT is characterized by irregular, squiggly lines with varying amplitudes without recognizable P waves, QRS complexes, or T waves, reflecting the heart's disorganized electrical activity.

1.5 Synthesis of the 12-lead ECG

In recent years, progressive advancement in technology have enabled the monitoring of cardiac condition through wearable devices, including mobile applications, patch monitors, and smartwatches, with enhancement in speed and quality. However, to keep track of ECG in these settings are typically inadequate to a single lead or a few leads, which may be insufficient for accurately diagnosing conditions affecting specific myocardial regions. Since the signatures of several cardiovascular diseases may appear in limb leads, precordial leads, or a combination of both. As a result, current clinical guidelines mandate the use of a standard 12-lead ECG for comprehensive and reliable diagnosis.

Spatially enhanced ECG systems are designed to improve the spatial resolution of ECG recordings by increasing the number of leads used for signal acquisition. According to volume conduction theory, developed by Burger and van Milaan, the human body is a 3-dimensional, uneven structure, and have volume conduction. This theory relied on the hypothesis that by projecting a heart dipole or heart vector on the lead vector in 3-D space, the voltage difference at any point on the surface of the torso can be determined [16]. The accuracy of electrical activity representation improves as the number of leads increases, as additional leads capture more details of the heart's electrical impulses. Higher spatial resolution is achieved when an ECG system records multiple leads simultaneously, offering a more detailed assessment of cardiac function. The spatial resolution of an ECG system is directly dependent on the number of electrodes used for signal acquisition. While increasing the number of electrodes enhances spatial resolution, it introduces practical limitations. A larger number of electrodes

may cause discomfort, reducing patient compliance. Simultaneously processing signals from numerous electrodes increases the complexity and expense of the recording system. In ambulatory settings, even acquiring a standard 12-lead ECG can be challenging. A reduced number of electrodes affects the spatial resolution of the recorded ECG, potentially impacting diagnostic accuracy.

A potential solution to the challenges associated with the mentioned issues is utilising fewer electrodes while employing a system that can enhance spatial resolution. This can be achieved by leveraging the intra-lead and inter-lead correlations among ECG signals. Systems designed to improve the spatial resolution of ECG recorded from a reduced lead set are commonly referred to as derived ECG systems [17, 18]. This systems utilize a pretrained linear or non-linear model that takes inputs from a specific set of leads (known as predictor leads) and generates the remaining leads [18]. The resulting ECG output, often termed spatially enhanced ECG, improves spatial resolution while maintaining diagnostic accuracy. Compared to conventional ECG recording systems, derived ECG systems offer several advantages including, lower cost, reduced complexity and enhanced patient comfort. Derived ECG systems are particularly useful in scenarios where recording, processing, or monitoring a standard 12-lead ECG is challenging, such as, personalized and continuous health monitoring, remote healthcare and ambulatory monitoring. The impediment of utilizing an array of ten skin-surface electrodes to record the twelve leads ECG in ambulatory monitoring can simplify by using minimal electrodes. In remote healthcare, a smaller number of electrodes facilitates data transmission and compression, improving telemedicine applications [10]. In applications like personalized and continuous health monitoring, minimizing the number of electrodes enhances patient comfort.

The standard 12-lead ECG system, recorded using ten electrodes, is the most widely used lead system among cardiologists. Due to its widespread clinical adoption, derived ECG systems have been developed to transform a smaller number of leads into a standard 12-lead ECG. One of the most commonly used derived ECG approaches involves reconstructing the full 12-lead ECG from a subset of leads, enabling a more efficient and practical alternative for

ECG acquisition while maintaining diagnostic accuracy.

1.6 Person Specific Information from Synthesized ECG

Biometric systems are essential for protecting privacy and securing data-driven intelligent technologies. With rapid advancements in artificial intelligence (AI), significant progress has been made across various biometric modalities, including speech, iris, face, gait, fingerprint, and ECG [19]. Among these, ECG signals stand out due to their resistance to spoofing attacks, stemming from their inherent liveliness, universal, while also providing valuable insights into an individual's psychological and clinical state [20]. Furthermore, ECG signals can be conveniently recorded using off-the-person setups, enhancing their practicality and accessibility.

ECG-based biometric systems hold promise across diverse applications, such as continuous authentication, mobile devices, and healthcare services [21, 22]. In particular, the growing demand for healthcare has underscored the importance of strong privacy and security measures to safeguard sensitive medical information. In this regard, ECG-based biometrics provide a compelling solution, especially in hospital environments, where they are less susceptible to deformation and environmental variability compared to other biometric modalities.

The ECG signal is a cyclostationary signal characterized by continual ECG beats. It is typically analyzed through five primary waveforms—the P-wave, QRS-complex, ST-segment, and T-wave along with associated intervals and segments [5]. Since ECG signals vary across individuals, these ECG waveforms, intervals, and segments also exhibit person specific differences. Beyond variations in the morphology of individual waveforms and segments, the relative differences between them may also contain biometric information in the synthesized ECG. Consequently, biometric features may be embedded across multiple temporal scales of the synthesized ECG signal.

1.7 Scope for the Present Work

The automated detection of MI using MECG remains a challenging task. VMD, introduced in signal processing literature, has shown promise for analyzing non-linear and non-stationary signals. It has been applied to ECG for tasks such as denoising and identifying various cardiac conditions. By decomposing the ECG signals into distinct modes or sub-signals, VMD may offer significant potential to extract diagnostic features that can aid in the detection of MI.

The anomalies of cardiac disorders provides valuable clinical information across multiple leads of the 12-lead ECG. However, utilizing 10 electrodes to record 12-lead ECG compromises the patient's comfort and intensifies the overall complexity of the system. Thus, synthesis of the 12-lead ECG from its subset without losing the diagnostic quality is essential to mitigate the challenges and reduce the complexity of the system. A model capable of simultaneously learning spatio-temporal correlations is better positioned to capture essential diagnostic features. This can be achieved through advanced recurrent neural network (RNN) based models, which are well-suited for extracting both spatial and temporal information from ECG signals.

The ECG signals is intrinsically time-varying, it may embed person specific information within the temporal variations of key ECG waveforms in the synthesized ECG. Deep learning (DL) models that explicitly focus on capturing these temporal variations may significantly enhance the extraction of robust biometric representations of the synthesized ECG signals.

The rest of the thesis are organised as follows:

Chapter 2 presents a literature review on automated cardiovascular disease (CVD) diagnosis methods, reconstruction of the 12-lead ECG and ECG-based biometric systems. Additionally, this chapter details the motivation behind this research.

Chapter 3 investigates the detection of myocardial infarction from a 12-lead ECG using the variational mode decomposition (VMD) technique. This chapter also presents the quantitative assessment of the proposed model and compares its effectiveness with the existing models.

Chapter 4 proposes a novel approach to synthesis of 12-lead ECG from a reduced lead

set that simultaneously leverages intra-lead and inter-lead correlations in ECG signals. This method employs long short-term memory (LSTM) to learn the spatio-temporal relationships between the lead signals. The performance is evaluated and compared against previously published methods.

Chapter 5 investigates the person specific information retained the synthesized ECG by leveraging the intra-beat and inter-beat variations of the ECG signal. Finally, conclusions of this thesis work and the future directions are presented in Chapter 6.

भारतीय प्रौद्योगिकी संस्थान गुवाहाटी
Indian Institute of Technology Guwahati

2

Analysis and Synthesis of Multilead ECG Signals: A Review

Contents

This chapter presents a review of the various approaches to feature extraction and classification of ECG, synthesis from subset of 12-lead, and biometric identification of ECG signals. Developing an intelligent automated diagnosis system for the analysis of ECG signals will be of immense advantage for the clinical diagnosis of cardiovascular diseases and to monitor the progress of undergoing treatment. ECG signal carries comprehensive information of the electrical and functional activities of the heart. The heart's rate, rhythm, and any potential abnormalities in its electrical conduction system are reflected in the ECG. These aberrations are quantifiable through the application of advanced signal processing and machine learning algorithms.

In clinical practice, the ECG is used as a standard tool to assess cardiac activities and diagnose myocardium conditions due to its non-invasive, cost-effective, and reliability. To acquire the standard 12-lead ECG, ten electrodes are positioned at a specific location on the human body's surface. The utilization of multiple electrodes for monitoring and recording is not suitable in some cases. These include remote healthcare, continuous monitoring, personalized healthcare, ambulatory monitoring, etc. The emerging technology and advancement in the development of miniature and wireless ECG with minimal complexity have gained popularity in recent times. Devising a system to synthesis a 12-lead ECG from its subset arises in situations where monitoring, recording, and/or processing ECG with the required number of electrodes poses challenges.

The ECG signal is not only useful for detecting CVDs but can be used as a potential source for biometric recognition traits due to its uniqueness. The properties of ECG such as liveliness detection, and combined information can enhance the security of biometric systems against fraudulent attacks. In the context of a biometric system utilizing ECG, the acquisition of signals can be made in different configurations. Although the 12-lead ECG format provides more information as they capture the cardiac activity from unique angles, they have impediment for real practical use for biometric recognition. Developing a system for ECG biometric by making use of the synthesized ECG will make an impact on the security of an individual.

The reviews pertaining to the prevailing and widely used algorithms for analyzing ECG signals are discussed in details in the succeeding sections.

2.1 Automated Detection of Myocardial Infarction from ECG

The primary objective of ECG-based automated detection systems is to quantify, characterize, extract, and identify the diagnostic information related to the cardiac ailments [4]. These systems can facilitate in expediting and enhancing the clinical workflow, reducing medical errors, and clinical decision-making [7]. Figure 2.1 illustrates the general operation of these systems, highlighting two key stages: training and testing.

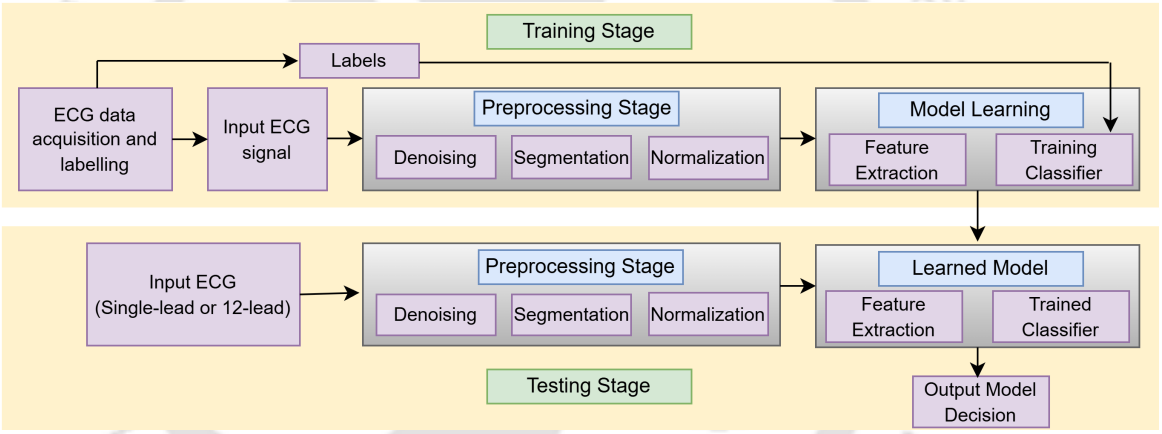

Figure 2.1: General block diagram of an ECG-based automated diagnosis system illustrating the training and testing phases.

During the training stage:

- ECG data, annotated with known diagnoses, is gathered.
- The data undergoes meticulous preprocessing and feature engineering to extract relevant patterns.
- The extracted features are used to train a powerful classification model.

In the testing stage:

- ECG signals from new patients are processed through the same preprocessing and feature engineering steps.

- The preprocessed data is fed to the trained model, which outputs a diagnosis decision.

This two-stage process, with its standardized data handling steps, paves the way for reliable and accurate diagnoses.

The training stage of the ECG-based diagnosis system is built upon clinical ECG data collected from a carefully chosen group of patients, ensuring it represents the specific clinical application. Depending on the focus, the data acquisition engage in either single-lead signals for targeted analysis or the 12-lead ECGs for comprehensive understanding. The dataset undergoes the complex labelling or annotation process where a committee of board-certified, experienced cardiologists, each with years of expertise, meticulously examine each ECG recording. Through their combined knowledge and careful consensus, they label each ECG as either normal or abnormal based on observed changes in the waveform [23].

In the initial stages of ECG processing, several crucial steps are undertaken to enhance data quality and facilitate accurate analysis. This preprocessing includes signal denoising, segmentation, and normalization, each of which plays a pivotal role in refining the ECG data [4].

Signal denoising: This is a critical step aimed at mitigating the impact of various noise artifacts that commonly affect ECG recordings. These artifacts encompass powerline interference, motion artifacts, muscle contraction noise, and respiratory noise. Their presence can obscure the delicate features of the ECG signal, potentially leading to misinterpretations and inaccurate diagnosis in clinical settings [4, 24]. Consequently, incorporating ECG denoising into the preprocessing stage is essential. The most common denoising methods employed to achieve optimal noise reduction and signal enhancement are adaptive filters [4], notch filters, band-pass filters, VMD [25], empirical mode decomposition [26], and empirical wavelet transform [27].

Segmentation: Following the denoising process, ECG signals undergo segmentation, which involves the delineation of an analysis window crucial for the diagnostic phase. Automated diagnosis systems commonly employ segmentation process, which can be broadly classified into two categories: (i) beat-based and (ii) frame-based. The former necessitates the detection

of the R-peak, followed by the application of a fixed window around the R-peak. This window captures the P-QRS-T characteristics, constituting a single heartbeat and encapsulating valuable intra-beat information. The beat-based segmentation approach has been extensively explored in diagnosing various conditions, including MI and ectopic beats [24, 28]. On the other hand, frame-based segmentation takes a different approach by selecting a blind excerpt from the ECG data for examination, eliminating the requirement for R-peak detection. The single-lead ECG segmentation focuses on intra-lead information, while the 12-lead ECG segmentation encompasses both inter-lead and intra-lead diagnostic information. This standardized technique has undergone extensive investigation in prior studies and serves as a reliable approach for diagnosing a spectrum of cardiac disorders [29, 30].

Normalization: The final phase of the preprocessing stage involves the normalization of the segmented ECG signals. In practical scenarios, the amplitudes of ECG data exhibit variations across acquisition devices and different subjects. To address this variability and facilitate standardized analysis, common normalization techniques, specifically the Z-score and min-max normalization methods, are widely employed for amplitude scaling. The former ensures a zero mean and unit variance, while the latter scales the ECG amplitudes into a range between 0 and 1 for the normalized signals. These normalization techniques play a crucial role in harmonizing the amplitudes of ECG data, thereby enhancing the consistency and reliability of subsequent analyses.

Subsequent to the preprocessing stage, the ECG signals, along with their corresponding instances associated with class labels, are inputted into the learning based techniques. In this phase, the model learns the essential parameters through supervised methods, enhancing the overall diagnostic performance. Over the past few decades, researchers have devised various model learning approaches tailored for automated ECG-based diagnosis.

2.1.1 Existing Methods for Detection of Myocardial Infarction

Over the past several decades, automated detection and classification of MI have been studied and developed based on the amalgamation of feature extraction using signal processing

tools and machine learning algorithms. Feature extraction, a pivotal step in this approach, is conducted under the guidance of medical experts. These experts curate a set of clinically informative features, comprehensively characterizing the specific cardiac abnormalities, which are then extracted from the preprocessed ECG data. This method reflects the evolution of model learning strategies employed in ECG-based diagnosis. The subsequent paragraphs delve into the historical context of these approaches and their evolution over time, highlighting the advancements made in optimizing the learning process for improved diagnostic accuracy.

The anomalies of MI in ECG can be characterised by the emergence of ST-segment elevation, hyperacute T-wave and inversion and pathological Q-wave. In early works to detect MI, researchers primarily relied on informative morphological features, specifically examining alterations that are indicative of MI. A notable milestone in this pursuit occurred in 1984 when Gallino et al. [31] studied the waveform of 2-lead ECG signal. This pioneering computer system extracted morphological features, encompassing the ST-segment deviation, the area and amplitudes of the R and S waves, as well as the RR interval. These features were quantified to delineate patterns associated with ischemia, contributing to the early exploration of automated methods for MI detection. Reddy et al. [32] used S-wave duration and amplitude, Q-wave duration and amplitude and R-wave amplitude as features to discriminate the ECGs of MI and normal. Bozzola et al. [33] used T-wave amplitude, the ratio of Q and R amplitudes, as well as Q and R-wave amplitudes and durations, as features. Heden et al. [34] utilized ST-segment parameters which includes T-wave amplitude, ST-slope and ST-J amplitude from standard twelve leads, and ultimately employed artificial neural network (ANN) to detect acute MI. In 2012, a comparable strategy was applied to 12-lead ECG by Arif et al. [35] and extract the characteristics of MI such as ST-segment deviation, T-wave amplitude and Q-wave amplitude. In their method the KNN classifier is used to estimate the feature set to discriminate between normal and MI. After two years, Safdarian et al. [36] extracted two time-domain features (integral of T-wave and the whole integral of an ECG cycle) to detect MI primarily in the left portion of the heart. The extracted features are given as input to four different classification models, namely, naive Bayes, KNN, multilayer perceptron, and probabilistic

neural network. In [37], Li Sun et al. employed polynomial fitting as a technique for feature extraction from ST segments. Subsequently, they applied a multiple instance learning (MIL) classifier to distinguish patients with MI from healthy control (HC) subjects. The efficacy of morphological features is highly dependent on correct delineation and segmentation of the ECG signal. Hence, the robustness of the extraction of these time-domain features is an issue that must be handled. Consequently, approaches relying on morphological features are prone to generating false MI alarms when confronted with various noise sources [38].

In subsequent investigations for MI detection, researchers shifted from explicitly evaluating morphological changes in the ECG and delved into the exploration of signal transformation techniques. Sadhukhan et al. [28] developed a diagnostic system for analyzing three leads (II, III, and V2) and utilized phase values of the Fourier harmonics as features through discrete Fourier transform (DFT) for MI detection. The pyramidal multiresolution of wavelet transform (WT) stands out as a widely employed method for feature extraction in MI identification by utilizing different mother wavelets. In this context, the Daubechies wavelet family emerges as the most prevalent choice for MI applications as it exhibits sufficient similarity with the ECG waveform. Various series of Daubechies wavelets have found application in MI detection, such as db4 [39], db6 [40, 41], and db9 [42]. Additionally, Daubechies Biorthogonal wavelets have been employed in specific analyses for multidimensional feature extraction, with examples including db7/8 [43] and db9/7 [44]. Padhy et al. [43] computed singular values and wavelet energy and considered them as features for identification of MI. Tripathy et al. [45] decomposed each of the standard twelve ECG leads to nine subband signals using empirical wavelet transform (EWT). The statistical features such as the entropy, the skewness, and the kurtosis are computed from the subband signals for the detection of MI pathology. In [39], ECG signal is subjected to discrete cosine transform (DCT) to obtain DCT coefficients. Data reduction method is used to reduce the coefficients and used as features for detection of CAD and MI. Although these signal decomposition methods operate implicitly and show promising performances but each technique suffers from critical drawbacks. While the Fourier transform provides information about the frequency content of a signal but fails

to capture the temporal evolution of signal components. The transform assumes that the signal characteristics remain constant over the entire duration, which may not be suitable for analyzing signals with nonsinusoidal components or time-varying characteristics, common in ECG signals. In discrete wavelet transform (DWT), the choice of predefined basis functions determines the compactness of the resulting wavelet representation. One demerit of the DWT in the analysis of ECG signal is the selection of a suitable mother wavelet that exhibits close similarity with the waveform of interest.

In recent publications, deep learning (DL) based approaches have garnered attention for their application in MI diagnosis. A noteworthy advantage of these methods lies in their ability to operate directly on raw ECG signals, bypassing the need for manually crafted features. This eliminates potential errors introduced in each processing step, particularly during preprocessing and segmentation. The earliest work for the detection of MI using convolutional neural network (CNN) was proposed by Acharya et al. [46]. In their work, they designed 11-layer deep CNN architecture and applied on two different datasets using single-lead ECG beats. A similar CNN model was investigated in another study [47], with a specific emphasis on MI identification utilizing lead V4 ECG beats. To capitalize on additional diagnostic information, Reasat et al. [48] extended their approach to incorporate a segment of three ECG leads (II, III, and aVF) for identifying patients with inferior MI. In a separate study, Liu et al. [49] formulated a multilead CNN architecture, leveraging four ECG leads (aVL, V2, V3, and V5) for the classification of HC and anterior MI ECG recordings.

The aforementioned methods focus on detecting localized MI, such as lateral or inferior MI, by utilizing a subset of 12-lead ECGs. This apriori selection of ECG leads tailored for specific MIs posses a limitation on the practical applicability of these methods in real-world diagnosis systems. In reality, patients may have MIs occurring at various spatial locations within the heart, including lateral, anterior, septal, and inferior regions. In an effort to enhance the reliability of MI diagnosis, Feng et al. [50] employs the 12-lead ECG records and investigates the use of integrated deep neural networks, specifically CNN and bidirectional gated recurrent unit (BiGRU) framework, for MI detection. The CNN module enables the

extraction of discriminative spatial features. Concurrently, the BiGRU module focuses on capturing crucial temporal features within each lead. The resulting features from these two modules are seamlessly fused to create comprehensive global features for subsequent classification. Strodthoff et al. [51] took a different approach by employing the standard 12-lead ECGs as input for their residual deep CNN model. Their method upon evaluation using 10-fold cross-validation achieved 89.7% specificity and 93.3% sensitivity.

2.2 Synthesis of 12-lead ECG

There are numerous systems available for recording ECG. These recording systems differ in the number of electrodes needed and the positioning of these electrodes on the surface of the body. The number of electrodes utilized in recording varies significantly, ranging from just a few to potentially hundreds. The spatial resolution of ECG diagnosis benefits from an increased number of electrodes, emphasizing the importance of electrode quantity in enhancing diagnostic capabilities. Numerous standards for electrode placement exist, each influencing the spatial distribution of information captured during ECG recordings. However, the utilization of multiple electrodes placed on the body surface for recording and monitoring is not suitable in some cases. These include remote healthcare, continuous monitoring, personalized health care, ambulatory monitoring, etc. The objective of this section is to discuss the literature of the derived ECG systems, elucidating their implementation through both linear and non-linear models.

2.2.1 Existing Methods for Synthesis of 12-lead ECG

The literature categorizes standard 12-lead derived or reconstruction systems into broad categories, as depicted in the accompanying Figure 2.2. One category encompasses derived systems based on subjects used for learning, including universal transform (applicable to any individual), population-specific transform (suitable for a group), and person-specific transform (applicable to an individual). The second category involves derivation from special lead systems (e.g., Frank, EASI, Mason-Likar) and derivation from limited lead systems, which

consist of a subset of the standard 12-lead ECG as source leads. The final category is based on the signal processing techniques employed for lead transformation, encompassing both linear and non-linear transformation methods.

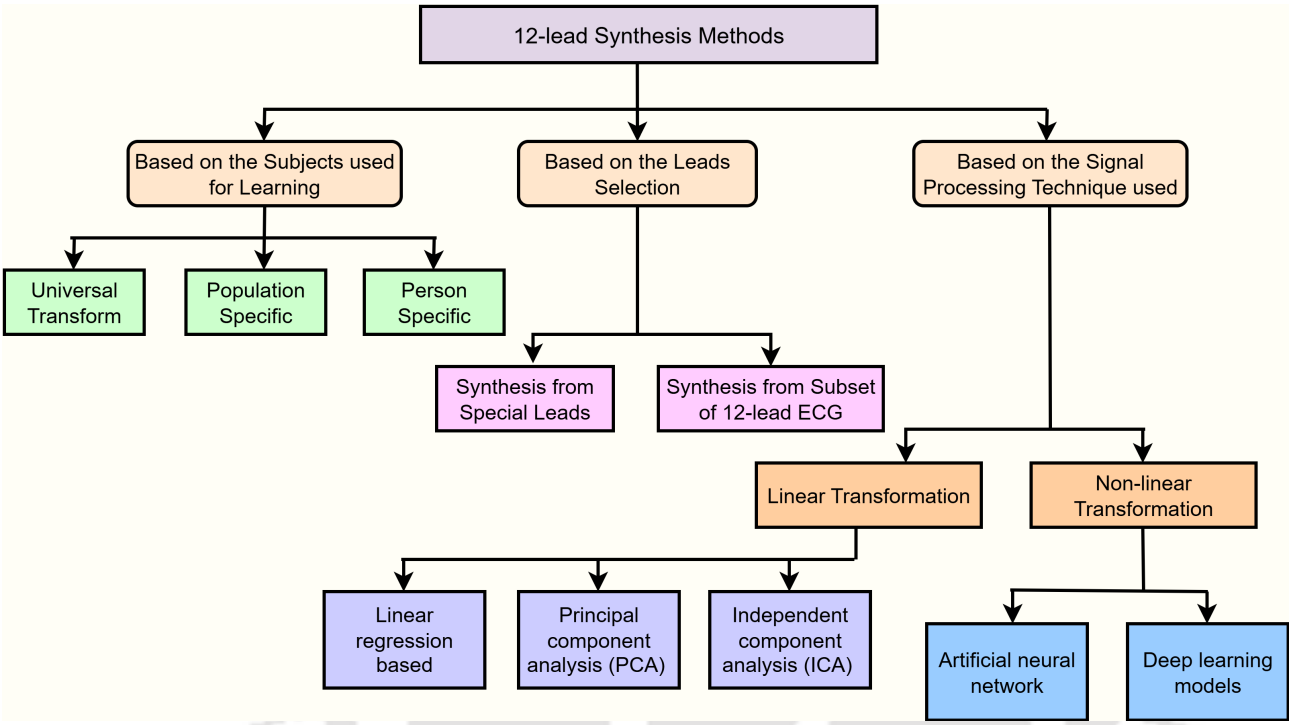

Figure 2.2: Categories of derived 12-lead ECG systems.

The foremost step in any 12-lead ECG derived systems is to simultaneously record standard twelve lead ECG and or special lead ECG followed by preprocessing [18]. In the subsequent event, selection of source leads and target leads is followed. The source leads are obtained from special lead systems or from the subset of 12-lead ECG system, serving as the basis for generating signals in the target lead. This transformation or conversion can be assessed using various metrics, ultimately leading to the synthesis of a 12-lead ECG. The signal quality of the reconstructed ECG are evaluated by comparing it with the original 12-lead ECGs. The 12-lead ECG derived systems can be broadly divided into two types and they are discussed in the following subsection. The first is from the special lead systems and the other is from limited or reduced lead system of the standard 12-lead ECG.

2.2.1.1 Synthesis from Special Lead Systems

Reconstruction of the standard 12-lead ECG from commonly used special lead systems, which include the vectorcardiogram (VCG), EASI, and Mason-Likar (ML) lead systems are as follows.

VCG to standard 12-lead ECG: VCG is based on the assumption that dipole is an adequate equivalent source for representing the hearts's electrical activity [52]. As the Frank system records 3-lead ECG (Vx, Vy, Vz) and is orthogonal, it can be useful to evaluate the dipole hypothesis as it posits that a minimum of three independent leads is sufficient to determine the potential difference at any point of the human torso [18]. Dower et al. [53] introduced the pioneering model-based derived system, known as Dower's universal transformation, establishing a relationship between the 3-lead VCG signal and the 12-lead ECG. They developed a simulator to derive the 12-lead from Frank leads. Despite its simplicity, a fixed transformation renders it less applicable in cardiac diagnosis applications due to variations among subjects and their pathological conditions [9]. Drew et al. [54] proposed a linear regression based population specific reconstruction of 12-leads ECG from VCG leads. The authors made three groups of the dataset including HC having 25 subjects, MI consisting 25 subjects and combination of HC and MI comprising 50 subjects. As their models are data driven and disease specific, reconstruction is better than Dower's universal transformation. With an aim to monitor remote healthcare, Maheshwari et al. [55] presented a linear regression based patient specific transformation for synthesis of twelve leads from VCG. Their model is data driven and designed for individual patients, the derived lead signals are more reliable than universal or population specific models.

EASI to standard 12-lead ECG: One of the widely used modified VCG lead system in ambulatory conditions and arrhythmia monitoring with great patient comfort is EASI lead system. Dower et al. [56] designed the first model based EASI to 12-lead ECG derived system using Frank lead vector derivations. Visual comparison of reconstruction results for 25 subjects excluding atrial and bundle branch blocks shows good resemblance. As their

model is based on universal transformation, it may not be suitable for diagnosis due to wide variations across time. Field et al. [9] proposed an improved EASI coefficients and compared to Dower's universal EASI coefficients using linear regression technique. They calculated 983 transformation matrices between EASI and 12-leads using 983 subjects simultaneous recordings. Using universal search method, the average of root mean square difference is measured. The best average score is selected and reported as an improved universal EASI coefficients. It has been shown that their model performs better than the model based universal Dower's coefficients.

Mason-Likar to standard 12-lead ECG: The Mason-Likar (ML) ECG acquisition system was developed in 1966 by Mason and Likar. Although the number of electrodes required by the Mason-Likar is same as standard twelve leads ECG, it is commonly used in exercise tests due to its reduced susceptibility to movement artifacts and muscle noise [57]. Man et al. [58] proposes a group specific conversion model using multiple linear regression to transform the ML system to standard 12-lead. An examination involving 180 subjects, encompassing conditions such as HC, arrhythmia, hypertension, and coronary heart disease, demonstrates satisfactory reconstruction, with root mean square difference as the evaluation metric. As highlighted in [18], it is crucial to acknowledge that the 12-lead ECGs obtained with the 10 electrodes positioned according to ML ECGs differ significantly from those acquired with standard electrode positioning. Hence, it requires simultaneous recording of the two systems (ML, 12-lead ECG).

2.2.1.2 Synthesis from a subset of 12-lead system:

The most popular and cost effective ECG derived system is the synthesis from a limited or reduced lead system, utilizing a subset of twelve leads as source leads. This derived system has numerous advantages as it does not require two simultaneous recording systems, which renders practically feasible, less complex and provides great comfort to the patients. Additionally, this derived system holds an extra advantage wherein eight out of the twelve leads are directly measured, with the standard electrode sites being familiar to clinicians. The

limited lead derived systems are based on linear or non-linear transformation techniques for synthesis and are discussed in the following paragraphs.

Over the past decade, several studies adopted linear transformation to achieve the goal of deriving 12-lead ECG from its subset. In 1989, Scherer et al. [59] introduced the first limited lead derived system, utilizing lead I, lead II and V2 as source leads. They designed two models based on ECG segment wise and beat wise reconstruction. Results indicate that segment-wise reconstruction outperforms beat-wise reconstruction. However, it's worth noting that since only MI subjects were used for estimating model parameters, its reliability for other cardiac abnormalities is limited. In [54], Drew et al. evaluated the performance of derived 12-lead ECG for diagnosing cardiac arrhythmia and MI. The source subset leads (I, II, V1, V5) were chosen for deriving the remaining independent target leads set (V2, V3, V4, V6). Evaluation over 649 subjects revealed a strong correlation between derived 12-lead ECGs and original 12-lead ECGs for diagnosing arrhythmia and MI. Nelwan et al. [8] investigated using linear regression model for generating the standard 12-lead from a different lead subsets. The analysis was performed on patient-specific and general reconstruction. It has been shown that, patient-specific performs better than general reconstruction as time progress. Maheshwari et al. [10] put forward a personalized lead reconstruction methodology that employs the principal component analysis (PCA) to generate the 12-lead ECG. They used PCA on 8 independent leads of 12-lead ECG and obtained 3 prominent PCs. Later, least square fit method was utilized to estimate transformation coefficients from 3 PCs to 8 leads ECG. The inter-lead correlation in the wavelet subband domain was investigated by Jiss et al. [60] and used this information in the derived 12-lead systems. They designed best source lead set for the reconstruction of standard twelve leads ECG using a novel diagnosability measure. Tsouri along with Ostertag [61] investigated usefulness of independent component analysis for synthesis using source leads (I, II, V2). The initial phase of their study involves fundamental preprocessing, encompassing the filtration of the ECG waveform and identification of QRS complexes. Following this, a training sequence derived from a single beat is utilized to generate a patient-specific transform that relates the independent components (ICs) from the

reduced lead set to the target 12 leads.

The non-linear transformation based methods emerge as a powerful techniques for deriving twelve leads ECG from a reduced lead set. It is reported that the production of electrical activity by the heart signals is not a purely linear process [62] [63]. For the applications to home care and ambulatory settings, Atoui et al. [64] presented a groundbreaking approach for obtaining complete 12-lead ECGs from a non-linear reconstruction method using ANN. They used three lead subset (I, II, V2) for deriving the five missing leads (V1, V3, V4, V5, V6) trained via a supervised backpropagation algorithm with three neurons in input layer, fifteen neurons in hidden layer and five neurons in output layer. Wang et al. [65] have developed synthesis system based on CNN to synthesize missing precordial leads of the 12-lead ECG signal. Their works include reconstructing the pathological ECG signal. Correlation coefficient is used as performance metric to assess their proposed methodology. designed a three-lead patch-type ECG device and used LSTM network to reconstruct the 12-lead ECG. The purpose of their study was to determine the viability of reconstruction obtained by the patch device.

2.3 Person Specific Information from Synthesized ECG

ECG-based biometric identification has garnered significant attention in recent years due to its potential applications in healthcare, access control, and secure authentication. The noninvasive nature of ECG collection, combined with its ability to be continuously monitored, makes it a promising candidate for both active and passive biometric systems. Additionally, the ECG signal is resilient to changes in external factors such as lighting, facial expressions, or skin conditions, which can affect the accuracy of traditional biometric methods.

However, the use of ECG signals for biometric identification presents unique challenges. These include the need for high-quality signal acquisition, robust feature extraction, and the development of algorithms capable of handling intra- and inter-subject variability. Furthermore, the ECG signal can be influenced by various factors such as physical activity, emotional state, and health conditions, which must be accounted for in the identification process.

This literature review aims to explore the current state of ECG biometric identification, examining the methodologies, challenges, and advancements in this field. The review will cover the fundamental principles of ECG signal processing, feature extraction techniques, classification methods, and the performance metrics used to evaluate ECG-based biometric systems. Additionally, it will discuss the practical implications of deploying ECG biometrics in real-world scenarios, highlighting the ongoing research efforts to overcome the existing limitations and enhance the robustness of ECG-based identification systems.

2.3.1 Existing Methods for Person Specific Information

Early advancements in biometric systems based on ECG utilized signal processing methods to extract distinctive features from ECG signal [19]. The initial efforts primarily focused on time-domain features extraction, such as temporal distance, slope, area, and amplitude, by identifying fiducial points [66–69]. One of the earliest studies in this domain was conducted by Biel et al., who extracted 30 features from each of the twelve leads [66]. They found out that best results are found using 10 features for biometric identification. Shen et al. introduced an ECG-based biometric recognition system utilizing seven fiducial features related to the QRS-complex [70]. Their approach was based on the premise that the QRS-complex is less influenced by heart rate variability, making it a reliable feature for biometric identification. Similarly, Palaniappan and Krishnan proposed five fiducial-based features from a single ECG beat, that is, QRS-interval, RR-interval, R-amplitude, RS-amplitude and QR-amplitude and tested using a neural network classifiers for individual identification [71]. A more comprehensive study on ECG-based biometric recognition was conducted by Israel et al. [67]. Fiducial points were identified and fed as input to the classification algorithm. Arteaga et al. proposed a mobile biometric authentication system with a cell phone heart surveil at different conditions and times [72]. Their system extracted two amplitudes and six time-based features and demonstrated high authentication performance with 4 sec of data for authentication. Taking a different approach, Lim et al. [68] introduced a Gaussian Mixture Model - Hidden Markov Model (GMM-HMM) framework, extracting eleven heartwave features,

followed by LDA and PCA for dimensionality reduction to discriminate individual. Huang et al. [73] presented a practical ECG-based authentication scheme capable of reliably verifying patients even in the presence of noisy ECG signals, while simultaneously ensuring differential privacy protection. Cordeiro et al. [74] developed a domain-specific architecture and employed 14 temporal and 10 fiducial points features for ECG based biometric identification.

The impediment in extracting robust and reliable time-domain features of ECG biometric have led researchers to explore more optimistic alternatives in transformed domains. Transform-domain methods utilize different signal processing techniques to convert ECG signals into a different domain, where biometric-relevant characteristics become more distinct and extractable. These approaches capture the unique characteristics of ECG without needing to identify specific fiducial points and offer improved feature representation. Plataniotis et al. [75] use autocorrelation and discrete cosine transform methods to extract features directly from the ECG signal. Their results yield high accuracy in identity recognition, demonstrating the effectiveness of the fiducial-free approach. Chiu et al., introduced the application of DWT on heuristically isolated pulses for ECG-based feature extraction [76]. Specifically, each heartbeat was identified by selecting 84 samples forward and 43 samples backward from the R peak in the ECG signal. DWT was then applied to extract relevant features, and Euclidean distance was used as the similarity measure for biometric identification. Irvine et al. [77] used PCA to extract the most significant features from the ECG signal. The advantages of their method include removal of the fiducial point extraction step and higher enrollment rates. Chan et al. [78] reported on ECG signals collected from 50 participants across three separate recording sessions. They introduced a new classification methodology using similarity measure based upon wavelet coefficients and achieved classification accuracy of 89%, which outperformed the correlation coefficient and percent residual distance measures. Lee and Kwak designed a robust PCA network based on time-frequency representation of ECG signals [79].

Of late, there has been a significant rise in the development of deep learning models for ECG-based biometric applications. These models seamlessly integrate feature extraction

and classification into a single end-to-end pipeline, eliminating the need for a separate feature extraction procedure. Among the various deep learning approaches, CNNs have been the most widely used, demonstrating effectiveness in learning robust biometric representations from ECG signals [80–84]. Srivastva et al. [85] developed a fine-tuned ensemble architecture by leveraging pre-trained deep neural networks for biometric recognition. In the study by Lynn et al. a bidirectional GRU network model was introduced for biometrics human identification [86]. However, a notable drawback of their proposed model is the variation in the segmented window length across different datasets necessitates further investigation to determine the optimal window size that effectively captures a single heartbeat for each specific dataset. Furthermore, in [87], a combination of CNN and LSTM based framework with a modified activation function was trained and tested in four databases is carried out for ECG biometric authentication.

2.4 Database

In this thesis, the data for analysis and experimentation are taken from the Physikalisch-Technische Bundesanstalt (PTB) database [88]. This non-commercial database was compiled by the National Metrology Institute of Germany for research, algorithmic benchmarking or educational use on PhysioNet. Professor Michael Oeff, M.D., gathered these ECGs from both healthy volunteers and patients with diverse heart conditions at the Department of Cardiology in the University Clinic Benjamin Franklin, Berlin.

The PTB database comprises of 549 records from 52 healthy subjects as well as 238 subjects diagnosed with cardiovascular diseases such as myocarditis, valvular heart diseases, myocardial hypertrophy, dysrhythmia, bundle branch block, cardiomyopathy, and myocardial infarction. The subjects age range from 17 to 87, with mean age 57.2; 81 women, with mean age 61.6, 209 men, and with mean age 55.5. Each record comprises 15 concurrently measured signals: the traditional 12 leads (I, II, III, aVR, aVL, aVF, V1, V2, V3, V4, V5, V6) and 3 orthogonal Frank leads (vx, vy, vz). The ECG signals in this database were sampled at

Table 2.1: The diagnostic classes of the PTB database

Diagnostic class	Number of subjects
Myocarditis	4
Miscellaneous	4
Valvular heart disease	6
Myocardial hypertrophy	7
Dysrhythmia	14
Bundle branch block	15
Cardiomyopathy	18
Myocardial infarction	148
Healthy controls	52

1kHz, with 16 Bit resolution ± 16.384 mV range. Most of these ECG records comprise of a comprehensive clinical summary encompassing details such as gender, age, diagnosis, and, when relevant, information regarding medical history, prescribed medications, hemodynamics, ventriculography echocardiography, and coronary artery pathology. Clinical summaries are not available for 22 subjects. The diagnostic categories for the remaining subjects are outlined in Table 2.1.

2.5 Motivation of this thesis work

Over the years, a lot of emphasis has been given to the ECG-based automated diagnosis system to detect MI. In the early efforts to detect MI, researchers primarily focused on analyzing informative time-domain features, particularly changes that signify the presence of MI. It is important to emphasize that the effectiveness of morphological features is heavily reliant on accurate delineation and segmentation of the ECG waveform. Therefore, ensuring the robustness of time-domain feature extraction is a critical challenge that must be addressed. As a result, methods that depend on morphological features are susceptible to generating

false MI alarms when exposed to various noise sources. In recent times, DL models emerge as a powerful methods for their application in MI diagnosis. Although DL techniques have shown promising results for ischemia and MI detection, the primary drawbacks associated with DL methods include their demanding computational requirements and the necessity for extensive datasets. Additionally, DL models are frequently characterized as "black boxes," given the inherent difficulty in comprehending the internal workings and decision-making processes of intricate neural networks. This lack of interpretability may pose challenges in clinical settings where transparency and interpretability are crucial for gaining trust and acceptance.

The anomalies of cardiac abnormalities is reflected in different leads of the 12-lead ECG. However, utilization of ten electrodes to record the standard 12-lead ECG restricts their usage in some applications, such as continuous monitoring, ambulatory monitoring, personalized healthcare, and remote monitoring. Thus, deriving the twelve-lead ECG from its subset without losing the diagnostic quality is essential to mitigate the mentioned challenges and reduce the complexity of the system. Moreover, the derived ECG methods discussed in the literature primarily leverage inter-lead or spatial correlations. However, none of these models are able to simultaneously exploit both spatial and temporal correlations. A model capable of learning spatio-temporal correlations concurrently could more effectively represent both intra-lead and inter-lead relationships. Such an approach would enhance reconstruction accuracy, ensuring better preservation of diagnostic information in the lead signals. This insight has inspired the adoption of neural network model for developing a more robust derived ECG model.

A biometric system designed for an application of practical personal recognition has certain challenges, including circumvention, applicability, and performance [89]. A user-friendly off-the-person ECG acquisition systems are crucial for wider adoption of biometric systems, but their low SNR makes detecting fiducial points, such as the R-peak, challenging. Since accurate fiducial point detection is vital for the success of existing methodologies, this limitation significantly impacts their reliability and performance. Additionally, as discussed

previously, direct acquisition of full 12-lead ECG signals may not always be feasible in certain environments. Synthesizing ECG signals from fewer leads enables biometric identification in resource-constrained scenarios while maintaining reliability. ECG biometrics derived from synthesized signals can provide a secure, non-invasive, and privacy-preserving alternative to traditional biometric systems, reducing concerns related to data misuse or replicate. Moreover, the synthesized ECG signals are expected to retain the person specific biometric information. It is worthwhile to investigate if the ECG signals synthesized from a reduced set retains person specific information. With these motivation, designing DL model that can learn the temporal variations within the synthesized ECG signal, biometric systems can achieve a balance between reliability, practicality, and scalability, driving advancements in secure identification technologies.

Driven by the aforementioned challenges, this thesis focuses on developing ML-DL-based automated ECG analysis methods to address these issues efficiently. The key contributions are as follows.

- A variational mode decomposition technique has been devised for robust and effective detection of MI from the multilead ECG. The VMD algorithm is applied to the 12 lead ECG. Variations in the mode coefficients obtained through VMD are linked to changes in feature values that encapsulate critical information about the ECG signal. One key feature is the multiscale mode energy, derived from the decomposed modes, which highlights significant differences in pathological signals. Additionally, the inter-lead correlations of the multiscale mode matrix (MSMM) influence its covariance structure, and these changes are captured in the eigenvalues of the MSMM. Consequently, these eigenvalues represent the pathological changes in the ECG signal and can serve as features for further analysis. The extracted feature subsets can be used to train classification models to distinguish between healthy controls and MI-affected individuals.

- An advanced recurrent neural network architecture has been devised to simultaneously examine the temporal and spatial correlation. Learning a model that can exploit this

spatio-temporal information in the ECG could generate lead signals while preserving important diagnostic information. The model employs LSTM model that exploits the enhanced inter-lead correlation of the ECG signal in the wavelet domain. The experimental results are evaluated using different diagnostic measures and similarity metrics. The proposed framework is well founded, and accurate reconstruction is possible as it can capture clinically significant features and provides a robust solution against noise.

- An hierarchical LSTM architecture has been explored to investigate the effectiveness of the synthesised ECG signals for person identification applications. Additionally, the model investigates the similarity of the biometric information present in the original signals and their reconstructed signals of the same record. A novel performance measure, i.e., person identifiability (PI), has been developed to evaluate the synthesis model. Experimental results show that the synthesised ECG signal contains similar biometric information compared to an original ECG signal.

भारतीय प्रौद्योगिकी संस्थान गुवाहाटी
Indian Institute of Technology Guwahati

3

Detection of Myocardial Infarction using Variational Mode Decomposition

Contents

Myocardial infarction (MI), generally known as “heart attack,” is a cardiovascular ailment and is one of the leading cause of mortality worldwide. The introduction chapter discussed that MI is caused by progressive atherosclerotic plaques occluding the coronary artery, resulting in an abrupt reduction in blood flow to the myocardium, ultimately leading to myocardial necrosis. MI exhibits a variety of morphological changes due to infarction locations and myocardium damage levels, and the pathological characteristics are depicted in different leads of the MECG. The 12-lead ECG is one of the most widely used diagnostic modalities for accurately assessing and localising MI pathology. According to the American Heart Association, if the type of MI is correctly identified and doctors take appropriate measures during the "golden hour" of MI patients, it may be possible to effectively reduce infarct size and mortality. Thus, an early diagnosis of MI is essential to initiate timely appropriate procedure that can prevent further infarction size and reduce mortality.

Over the past several decades, automated detection and classification of MI have been studied and developed based on the amalgamation of feature extraction using signal processing tools and machine learning algorithms. In feature extraction stage, several studies were adopted to capture the pathological characteristics which indicate the signature of MI such as Q-wave, ST-segment deviation, T-wave integral, T-wave amplitude and integral of single ECG cycle [35, 36, 90, 91]. The pyramidal multiresolution decomposition technique of DWT with different mother wavelets such as db4, db6 is a popular method for identification of MI [39, 41], and some works have implemented Daubechies biorthogonal wavelet [43, 44]. Empirical mode decomposition (EMD) was used for feature extraction to discriminate between normal and MI [39]. In [92], PCA is implemented for different orders of polynomial approximations and concluded that the 12 principal components (PCs) were found to be effective for the detection of MI. Alternatively, Liu et al. [93] use polynomial function and treated polynomial coefficients as features to classify MI patients and healthy controls. In the classification stage, the extracted feature vectors are fed as input to different classification algorithm for detecting MI. The most popular algorithms for classification are support vector machine (SVM) [44, 93], K-nearest neighbour (KNN) [39, 40], neural network [94, 95], decision trees [93, 96], and

random forests [37].

In this Chapter, a new method for automated detection of MI from 12-lead ECG is investigated. This approach is grounded on the analysis of multilead ECG to characterize the pathological changes of MI. Variational mode decomposition (VMD)-based feature extraction is proposed. The main advantage of the VMD technique over the other decomposition techniques, such as empirical mode decomposition (EMD) is that it is built on a sound foundation of mathematical theory. EMD is sensitive to noise and sampling. One caveat of DWT for analysis of MI is the hard band-limits of wavelet and inability to select appropriate mother wavelets. The VMD method has the edge over wavelet transform multiresolution technique because the DWT technique requires a predefined basis function like Daubechies, Symlet, Daubechies biorthogonal, etc. Implementation of different wavelet functions can result in different outcomes. Hence, the DWT efficiency depends on the choice of the mother wavelet and the decomposition level. In the existing literature, there is no proper justification for the use of a particular mother wavelet. So the selection of mother wavelet and analysis based on wavelet transform is a challenging task. In contrast, VMD is a data-driven and adaptive, decomposition model that assesses the relevant bands, and determines the associated modes simultaneously. This decomposition algorithm can reconstruct the decomposed ECG signal optimally (perfectly or in a least-squares sense). The main building blocks of VMD are the Wiener filter for denoising, the Hilbert transform to obtain single-side (non-negative) spectrum, and the harmonic mixing to translate the frequency spectrum to the baseband. Due to these inherent properties ingrained in this decomposition model, it outperforms its decomposition counterparts vis-à-vis EMD and DWT.

The VMD method is decomposition technique that decomposes the AM–FM signal into multiple subbands. It has gained wide popularity since its inception to analyse one-dimensional signals, such as epileptic seizure detection from the electroencephalogram (EEG) signals, and estimation of electroglottographic (EGG) signals [97, 98]. The VMD technique is found to be effective to eliminate noise, baseline wandering, and detection of cardiovascular diseases of the ECG signal. Prabhakararao and Manikandan [25] have used the VMD method to

extract baseline wander using frequency criterion and then subtract from the original signal. The performance results of their study ascertained that the VMD algorithm can effectively get rid of the baseline wanders without mangling the vital clinical information of the ECG signal. Lahmiri et al. [99] have used VMD and DWT for denoising of ECG signals. Tripathy et al. [100] decompose the ECG signal into five modes and extracted three different features from the first three modes for the detection of an arrhythmia. To the best of our knowledge, there is no article in the literature reporting MI diagnosis using VMD technique. Therefore, in this chapter, we propose a new algorithm for automated detection and classification of acute MI from HC subjects using 12-lead ECG signals.

The remaining portions of this chapter are structured as follows. The proposed VMD-based method to extract features that are related to MI, including preprocessing of an input ECG signal is described in Section 3.1. Furthermore, in Section 3.2, the ECG database used in this work is introduced briefly and presents the results and discussions in detail. In Section 3.3 conclusions are drawn.

3.1 Proposed Method for Detection of MI

In this Section, the proposed method for detection and localization of MI from multilead ECG is described. Figure 3.1 shows the block diagrams for detection and localization. The detection block comprises of preprocessing (noise filtering and beat based segmentation), evaluation of multiscale mode energy and eigenspace (MMEE) features and classification. In this block, the MI and the HC are classified using the MMEE features of multilead ECG frame. The following sub-sections briefly describe each part of the block diagram.

3.1.1 Preprocessing

MECG signal is corrupted with various types of noise. The preprocessing involves filtering unwanted noise and artifacts from a raw ECG signal. A moving average filter is utilized to remove the low-frequency baseline wandering [101]. The frame-based processing of MECG exploited the inter-lead, intra-beat, and intra-sample correlation information of the MECG

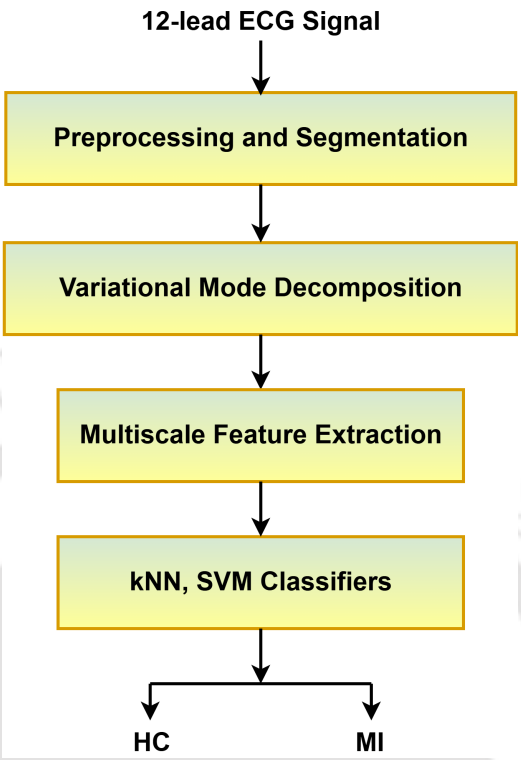

Figure 3.1: Block diagram for detection of MI

signal [102]. This information can facilitate to diagnose various CVD, including MI. The beat segmentation of the noise-free MECG signal is carried out by detecting R-peaks using Pan Tompkins algorithm, and segment 250 samples and 400 samples to the left of R-peaks and to the right of R peaks, respectively, resulting in 651 points in each sample at a sampling rate of 1 kHz [46, 103]. The first and last beats in all the datasets were excluded to maintain uniformity of the segmented beats. The R-peaks of lead I is used as a reference point to segment the remaining leads of MECG signals since all the 12 leads are recorded simultaneously. Each ECG beat has 651 samples, which covers all the characteristics of the ECG cycle.

3.1.2 Analysis of Multilead ECG using VMD

VMD method adaptively decompose MECG signal into a K ensemble number of band-limited sub-signals or principal modes v_k, where the modes are compactly supported around their center frequency [104]. The H^1 Gaussian smoothness determined the bandwidth of each mode of the shifted signal. The resulting constrained problem is formulated as

$$\min_{\{v_k\},\{\omega_k\}} \left\{ \sum_{k=1}^{K} \left\| \partial_t \left[\left(\delta(t) + \frac{j}{\pi t} \right) * v_k(t) \right] e^{-j\omega_k t} \right\|_2^2 \right\} \quad \text{s.t.} \quad \sum_{k=1}^{K} v_k(t) = v(t) \tag{3.1}$$

where $v(t)$ is the ECG signal, $\{v_k\} := \{v_1, v_2, ..., v_K\}$ represent the set of decomposed modes, $\{\omega_k\} := \{\omega_1, \omega_2, ..., \omega_K\}$ denotes the set of each center pulsation corresponding to k^{th} mode, t is the time, the number of modes is signified by K, ∂_t stands for the differential operation, and $*$ is the convolution.

The constrained problem of Equation 3.1 can be addressed by introducing Lagrangian multiplier and quadratic penalty term are employed to make the problem unconstrained. The augmented Lagrangian function is expressed as follows:

$$\mathcal{L}\left(\{v_k\},\{\omega_k\},\lambda\right) := \alpha \sum_k \left\| \partial_t \left[\left(\delta(t) + \frac{j}{\pi t} \right) * v_k(t) \right] e^{-j\omega_k t} \right\|_2^2 + \left\| f(t) - \sum_k v_k(t) \right\|_2^2 + \left\langle \lambda(t), f(t) - \sum_k v_k(t) \right\rangle \tag{3.2}$$

where λ(t) denotes the Lagrangian multiplier, α is the balancing parameter that control bandwidth, and $\delta(.)$ is the Dirac distribution. An optimization technique called alternate direction method of multipliers (ADMM) is rendered to solve Equation 3.2. All the modes gained is obtained in the Fourier domain and is given as

$$\hat{v}_k^{n+1}(\omega) = \frac{\hat{f}(\omega) - \sum_{i \neq k} \hat{v}_i(\omega) + \frac{\hat{\lambda}(\omega)}{2}}{1 + 2\alpha(\omega - \omega_k)^2} \tag{3.3}$$

The optimization of w_k also takes place in Fourier domain, the updated equation of w_k is shown as

$$\omega_k^{n+1} = \frac{\int_0^\infty \omega \left| \hat{v}_k(\omega) \right|^2 d\omega}{\int_0^\infty \left| \hat{v}_k(\omega) \right|^2 d\omega} \tag{3.4}$$

VMD is a parameterized method, and it has to initialize two tuning parameters in advance.

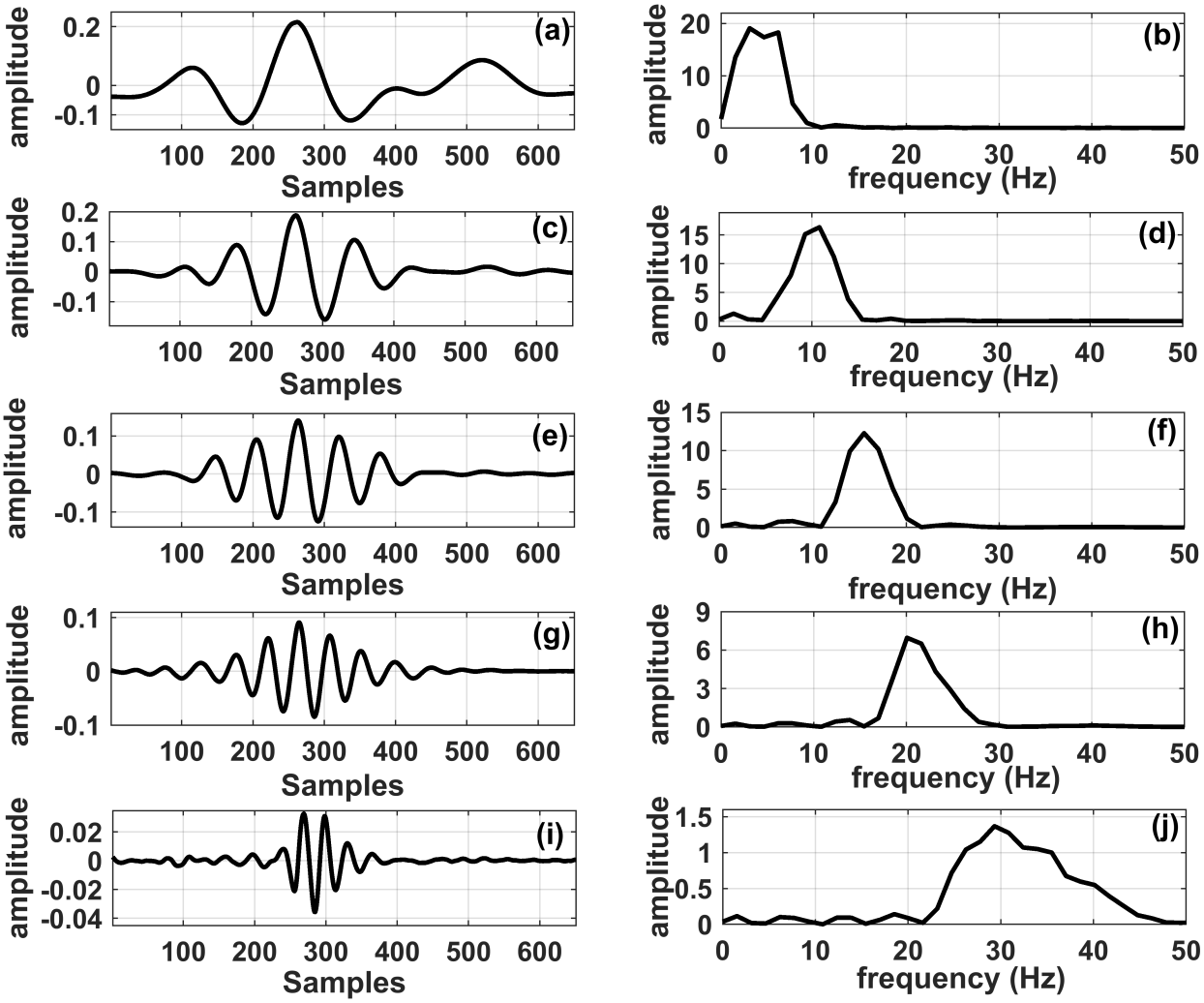

Figure 3.2: (a) Decomposed HC signal of mode 1 (b) Frequency response of mode 1 (c) Decomposed HC signal of mode 2 (d) Frequency response of mode 2 (e) Decomposed HC signal of mode 3 (f) Frequency response of mode 3 (g) Decomposed HC signal of mode 4 (h) Frequency response of mode 4 (i) Decomposed HC signal of mode 5 (j) Frequency response of mode 5.

These parameters are the bandwidth control parameter (α), and the number of modes (K) to be decomposed from the ECG signal. The correct choice of the values of α, and K capture the characteristics of the ECG signal in different decomposition modes. The experimental results reveal that a big value of α permits a low bandwidth in the decomposed modes. This results in mode mixing and also causes spurious mode in the higher level of mode decomposition. On the other hand, small values of α give rise to noise in the estimated mode. In this analysis, we have found that the corresponding parameters α of 1400 and K of 5 are considered the optimized parameters as it can capture the relevant components of the ECG signal. The different modes of the Healthy Control signal by VMD are illustrated in Figure 3.2, it shows the time domain signals of the first mode (a), second mode (c), third mode (e), fourth mode (g), and fifth mode (i) and (b), (d), (f), (h), and (j) depicts the corresponding frequency spectra of the decomposed mode, respectively. The dominant frequency of the spectrum of mode 1 is 3 Hz, which captures the P-wave and the T-wave. Mode 2 and mode 3 contain the characteristics of the QRS complex, and its dominant frequencies are around 12 Hz and 15 Hz, respectively. The spectrum of mode 4 and mode 5 depicts that the higher frequency of QRS complex is observed in these two modes. Their dominant frequencies are 20 Hz and 28.4 Hz, respectively.

3.1.3 Multiscale Mode Energy and Eigenspace Features

In this subsection, the proposed multiscale energy and eigenspace features of multilead ECG are assessed. Assuming that the significant information of ECG signal will reflect in the distribution of energy in different decomposition levels, the energy can be computed at different modes. The energy obtained from the coefficients along each decomposed mode is considered as multiscale mode energy [44], and it is given as

$$E_{cM^i_{j,k}} = \frac{\sum_{k=1}^{N_j}[cM^i_{j,k}]^2}{N_j} \tag{3.5}$$

where N_j is the number of coefficients. In this study, the multiscale mode energy features

from five decomposed modes of 12-standard leads are evaluated. Five multiscale mode energies of 12 features are extracted from one mode matrix. A total of 60 multiscale mode energies are chosen from the five mode matrices.

Myocardial infarction causes variation in electrical conduction properties of heart tissues due to obstruction in the inside wall of the coronary artery. These variations in values lead to a change in the morphological features of ECG signals, and they can be captured in different modes when subjected to the VMD algorithm, as shown in Figure 3.2. In order to quantify these changes, covariance structures of the multiscale mode matrices (MSMM) are analysed. When eigenanalysis is computed on mode matrices, the clinical diagnostic information related to MI presumably appears in eigenspaces. The covariance matrices are assessed from the MSMM, and it is evaluated as

$$C_{M_j} = \frac{1}{(N_j - 1)} \left([\mathbf{M_j}]^T [\mathbf{M_j}] \right) \tag{3.6}$$

where C_{M_j} is the covariance matrix at the jth mode. When Equation 3.6 is subjected to eigendecomposition the expression appears in the following equation

$$\mathbf{C_{M_j} V_{M_j}} = \mathbf{V_{M_j} \Lambda_{M_j}} \tag{3.7}$$

where Λ_{M_j} and V_{M_j} are the eigenvalues and eigenvectors of mode matrix, respectively. Eigenvector matrix V_{M_j} diagonalize the covariance matrix C_{M_j} as

$$\mathbf{V_{M_j} C_{M_j} V_{M_j}^{-1}} = \mathbf{\Lambda_{M_j}} \tag{3.8}$$

Λ_{M_j} is the diagonal matrix. The eigen values are the diagonal elements of the diagonal matrix. The eigenvectors constitute the vector directions of the new feature space of the covariance matrix, and the eigenvalues represent the magnitudes of those vectors. The eigenvector corresponding to the highest eigenvalue is the first principal component. The

eigenvalues are sorted from largest to smallest value and accordingly, the corresponding eigenvectors as it provides the significance of the components. The ordered eigenvalues in the mode matrix are

$$\lambda_{M_{j_1}}, \lambda_{M_{j_2}}, \lambda_{M_{j_3}}, ..., \lambda_{M_{j_N}} \tag{3.9}$$

In this work, six dominant eigenvalues from single covariance matrix is evaluated to create feature vectors. A total of 30 feature vectors are extracted from five covariance matrices.

3.1.4 Classification of MI and HC

In this work, for MI detection, 60 multiscale mode energy features and 30 multiscale eigenvalue features are evaluated from each multilead ECG beat. The features extracted from the multiscale mode energy and covariance matrices are concatenated and forms a 90-dimensional feature vector. The multiscale feature matrix is denoted as $Z \in R^{p \times q}$ where, p and q are the numbers. These feature subsets are provided as input to the KNN and the SVM algorithm to discriminate the two classes, i.e. healthy control and MI. In this study, the KNN and the SVM classifiers are used for MI detection. The class labels of both KNN and SVM classifiers for ith feature instance $(i = 1, 2, ..p)$ are given as $y \in (0, 1)$. where, 0 and 1 are the class labels for HC and MI classes. The training and the test instances of both KNN and SVM classifiers are selected using both hold-out cross-validation and 5-fold cross-validation approaches. In this work, for MI detection, the number of nearest neighbors and the distance metric for KNN classifier are selected as '5' and 'Euclidean', respectively. Similarly, for SVM classifier with linear kernel, the regularization parameter C = 30 is used. The regularization parameter C = 30 and the standard deviation $\sigma = 0.5$ are used for SVM classifier with RBF kernel function. The performance of both KNN and SVM classifiers on test data is evaluated using the metrics such as the sensitivity, the specificity and the accuracy.

Two supervised learning classifiers, K-nearest neighbour, and SVM are used to carry out the classification task of HC and MI. KNN is a non-parametric algorithm employed for

classification and regression problems. The algorithm predicts the target label by discovering the K nearest neighbor of the test data by using the distance measures. In this analysis, we have used euclidean distance and K = 5.

SVM is a two-category classification model defined by a separating hyperplane. The algorithm outputs the given labeled training data by defining optimal hyperplane in an N-dimensional space which categorizes the test feature set [105]. The training features set is $(\mathbf{x}_m, \mathbf{y}_m)$, *m* = 1, 2,...,n, $\mathbf{x} \in \mathbf{R}^j$, $y \in (+1, -1)$. The feature matrix of input multilead ECG can be represented, $\mathbf{Z} \in \mathbf{R^{j,k}}$ with each feature vector $\mathbf{z}_m \in \mathbf{R}^k$, $i \in 1, 2, ..., j$, where j is the number of feature set, and *k* is the length of the feature vector and (*k* = 90). The optimisation is based on the maximization of hyperplane, given by

$$min\frac{1}{2}\mathbf{w}^T\mathbf{w} + C\sum_{m=1}^{j}\varepsilon_m \tag{3.10}$$

subjected to $y_m(\mathbf{w}^T\phi(x_m) + b) \geq 1 - \varepsilon_m$, $\varepsilon_m \geq 1$ where w is the hyperplane, and C is the regularisation parameter. The kernel function $\phi(x_m)$ transform the training feature set (x_m) to the high-dimensional space. The constrained problem of Equation 11 is translated into the Lagrangian dual problem in order to make the problem unconstrained. The dual quadratic optimization problem produce new equation, given by

$$max_\mu L(\mu) = \sum_{m=1}^{q}\mu_m - \frac{1}{2}\sum_{m=1}^{q}\sum_{n=1}^{q}\mu_m\mu_n y_m y_n R(z_m, z_n) \tag{3.11}$$

subjected to $0 \leq \mu_m \leq C$, $m = 1, 2, ..., n$ and $\sum_{m=1}^{q}\mu_m y_m = 0$. μ_m is the Lagrange multiplier for every training point. The predicted output y_p for the test feature subset z_t from MECG is computed as

$$y_p = sgn\left[\sum_{m=1}^{\hat{q}}\mu_m y_m R(z_m, z_t)\right] \tag{3.12}$$

where $R(z_m, z_t)$ is the kernel function and $\hat{q}$ is the support vector. In this study, the linear

kernel and radial basis function (RBF) kernel are used. The RBF kernel used in this work is given as

$$R(z_m, z_t) = exp\left(\frac{\|z_t - z_m\|^2}{2\sigma^2}\right) \tag{3.13}$$

where the variance parameter σ^2 controls the width of Gaussian.

The classifiers performance are assessed using specificity, sensitivity, and accuracy. Specificity (Sp) of a test is the percentage of data that did not have MI and were correctly identified by the test. It is also called the true negative rate. The sensitivity (Se) is defined as the percentage of data that truly had MI and were correctly identified by the classifier. Accuracy (Acc) measurement system is the degree to which the result of a measurement conforms to the correct value. Specificity, sensitivity and accuracy are then formulated in the following equations:

$$Sp = \frac{TN}{FP + TN} \times 100 \tag{3.14}$$

$$Se = \frac{TP}{TP + FN} \times 100 \tag{3.15}$$

$$Acc = \frac{TP + TN}{TP + FP + FN + TN} \times 100 \tag{3.16}$$

where TP, FP, TN, and FN represent the MI patient correctly predicted as MI, healthy patient incorrectly diagnosed as MI, healthy patient predicted as healthy, and MI patient predicted as healthy, respectively.

3.2 Evaluation of the Proposed Method

The ECG data used in this study are taken from the PTB database. The 15 concurrently measured signals (standard 12-lead + 3 Frank leads) comprises 549 records from 290 subjects. 52 subjects are related to HC, and 148 subjects are related to MI out of 290

subjects. The dataset consists of 81 women, average age 61.6, and 209 men, average age 55.5. The 16-bit resolution over a $\pm$ 16.384 mV range of each ECG signal was sampled at 1000 Hz.

The features extracted from the multiscale mode energy and covariance matrices are concatenated and forms a 90-dimensional feature vector. These feature subsets are provided as input to the KNN and the SVM algorithm to discriminate the two classes, i.e. healthy control and MI. Each of these feature vectors corresponds to an instance. In this work, 8000, 12000, and 20000 instances are utilized for evaluation to investigate the performance of the models. Balanced datasets with a 1:1 class ratio of the instances are implemented for training and testing the classification models since the performance of the classifiers relies on the balance of the dataset to a great extent. In this study, 5 fold and 10 fold cross-validation statistical method are used to ensure the reliability of the predictive models of SVM and KNN classifiers, respectively. The performance of the classification models are shown in Table 3.1.

Table 3.1: Performance evaluation for KNN and SVM classifiers

No. of instances	KNN			SVM Linear			SVM RBF		
	Sp (%)	Se (%)	Acc (%)	Sp (%)	Se (%)	Acc (%)	Sp (%)	Se (%)	Acc (%)
8000	86.20	79.20	82.70	96.80	98	97.40	99.88	99.90	99.88
12000	82.60	77.20	79.20	96.93	97.52	97.22	99.77	99.70	99.73
20000	77.34	93.20	85.27	96.20	95.93	96.06	99.83	99.89	99.86

With 8000 instances the best performance is obtained for both KNN and SVM linear kernel with specificity of 86.20% and 96.80%, sensitivity of 79.20% and 98%, and accuracy values of 82.70% and 97.40%, respectively. Average specificity, average sensitivity, and average accuracy of SVM with RBF kernel function classifier are found to be 98.88%, 99.90%, and 99.88%, respectively, for 8000 instances. In this study, the best results for SVM with RBF kernel of $\sigma = 0.5$ is achieved for all the 3 different instances. The result shows that the less number of instances achieved better results compared to the higher number of instances. This may be because the sample values of the recorded data are different for different subjects.

As a result, the variability of the subjects may affect the performance of the classifiers.

From the acquired results of the classification algorithms, the end result of the RBF kernel function of SVM surpassed the SVM with linear kernel function and KNN classifiers. The linearly non-separable input features of the RBF kernel function of SVM is mapped to a high dimensional feature space [106]. Presumably, this is the reason the RBF kernel function of SVM achieved a better result than KNN and linear kernel SVM.

3.2.1 Performance Comparison with the Existing Methods

This subsection compares the classification results of the proposed method with the previously published works for automated detection and diagnosis of MI and is reported in Table 3.2. Safdarian et al. [36] extracted two time-domain features (integral of T wave and whole integral of an ECG cycle) to detect MI primarily in the left portion of the heart. The extracted features are given as input to four different classification models, namely, naive Bayes, KNN, multilayer perceptron, and probabilistic neural network. Naive Bayes give the best performance with an accuracy of 94.74%. A new technique to automatically detect MI called latent topic multiple instance learning without labeling heartbeats is developed in [37]. Their study shows specificity values of 88.1 $\pm$ 2.3 and sensitivity values of 92.3 $\pm$ 0.84. In [44], DWT decomposed segmented ECG beats up to 6th level of decomposition of standard 12 leads ECG. Multiscale energy features and eigenvalue features are extracted from wavelet subbands to form 72 dimensional feature vector. Their method for detection of MI obtained specificity, sensitivity, and accuracy of 99% 93% and 96%, respectively. The approach presented in [46] utilized convolutional neural network (CNN) algorithm to detect and discriminate the healthy control, and MI ECG beats from single-lead ECG. They analyzed the ECG beats with noise contaminated and noise eliminated and gained 93.53% and 95.22% accuracies, respectively.

Pathological characteristics of MI, such as T wave inversion, abnormal Q wave, and ST-segment elevation, are regarded by physicians as symptoms of MI [35]. These features are highly dependent on correct delineation and segmentation of the ECG signal. Hence, the robustness of the extraction of these time-domain features is an issue that must be handled.

Table 3.2: Summary of the classification performance of the proposed method in comparison with the other existing methods

Author	Number of leads	Database	Techniques and features	Classifier	Performance (%)
Sun et al. [37]	12 leads	Beat specific HC: 79 records MI: 369 records	ST segment detection Multiple instance learning	SVM	Sp = 88.1 Se = 92.3
Safdarian et al. [36]	1 lead (lead II)	Beat specific Subjects: 290 subjects	Integral of ecg cycle	Naive Bayes	Acc = 94.74
Sharma et al. [44]	12 leads	Frame specific 1074 frames for MI and HC	DWT Multiscale energy Multiscale eigen analysis	SVM	Sp = 99 Se = 93 Acc = 96
Acharya et al. [46]	1 lead (lead II)	Beat specific HC: 10,546 MI: 40,182	No feature extraction or feature selection	CNN	Sp = 94.19 Se = 95.49 Acc = 95.22
Liu et al. [49]	4 leads	Beat specific HC: 80 records MI: 167 records	No feature extraction or feature selection	Multilead CNN	Sp = 97.37 Se = 95.40 Acc = 96.22
Proposed work	12 leads	Beat specific HC: 8000 MI: 8000	VMD Multiscale mode energy Eigen values	SVM	Sp = 99.83 Se = 99.89 Acc =99.86

Several methods using single-lead ECG have been proposed and developed to detect the presence of MI [36, 46]. Liu et al. [49] used four leads (aVL, V2, V3, and V5) to detect anterior MI, including anteroseptal MI and anterolateral MI. The segmented ECG beats are used as input to multilead-CNN and obtained specificity of 97.37%, sensitivity of 95.40%, and accuracy of 96.00 %. Since MI occurs in different leads of MECG, analysis on all 12 leads will provide more useful information and yield a better result than single lead and fewer leads in detection. In this work, we have used standard 12 leads ECG signal for analysis. The framework for feature extraction in this study is similar to the method used in [44]. In their work, 1074 frames of within-class variations data of HC and MI multilead ECG are used for evaluation. Each frame consists of four ECG beats. They have used DWT to decompose the ECG signal up to the 6th level of decomposition, whereas in this work, the VMD technique is implemented. In our study, subject-wise validation approach is performed [107]. 10000 beats of MECG, both from HC and MI, are utilized for analysis in this work. Comparative analysis of the results shows that our proposed method exhibited better performance than DWT based

approach and other methods, as shown in Table 3.2.

3.3 Summary

In this chapter, a novel method is proposed to investigate the pathological characteristics of MI from MECG. Normal and pathology MI MECG signals are analyzed using VMD based approach. The preprocessed noise-free signal is subjected to the VMD algorithm. The changes that are observed in the mode coefficients from the VMD caused the variations in the values of different features that can capture useful information from a given ECG signal. The multiscale mode energy is one such feature acquired from the different decomposed mode that reflects the significant change of the pathological signal. Also, the interlead correlations of the MSMM affect the covariance structures, and the eigen values of the MSMM exhibit these changes. Therefore, the change in the ECG signal of a pathological signal can be represented by the computed eigen values and can be used as a feature. Hence, these extracted feature subsets can further be employed to train the classification models to discriminate between healthy control and MI. Analysis with number of multilead ECG data shows that the multiscale mode energy and eigenvalue features are capable of discriminating HC and MI. The proposed method achieved the highest classification performance from the SVM classifier with an RBF kernel and obtained 99.88% specificity, 99.90% sensitivity, and accuracy of 99.88%. The yielded results indicate that the proposed method is capable of successful detection of MI and achieved better results than existing methods.

4

Synthesis of Twelve-lead ECG from a Reduced Lead Set

Contents

The approaches discussed in chapter 2 primarily focused on leveraging the spatial or inter-lead correlation between the twelve-lead ECG signals within the transformed domain for model learning. However, the ECG signals inherently exhibit both inter-lead and intra-lead correlations [43]. Developing a model that effectively captures and utilizes this spatio-temporal information could enable the generation of lead signals without losing critical diagnostic details. In this chapter, we introduce an enhanced ECG spatial resolution approach that exploits the spatio-temporal correlations within the hidden feature space to improve ECG reconstruction accuracy.

The proposed approach take leverage of the enhanced inter-lead correlation of the ECG signal in the wavelet domain. The inter-lead correlation of a twelve-lead ECG in the wavelet subband is significantly higher compared to that of the original signals in the time domain [108]. This high correlation between different leads within the same wavelet scale can be effectively utilized to train non-linear models. By leveraging this enhanced correlation in the wavelet-transformed domain, it is possible to develop more accurate models that preserve the spatial relationships between leads while improving ECG signal reconstruction and diagnostic reliability.

Over the past decade, several studies have employed linear transformation techniques to derive the full 12-lead ECG from its subset [9, 18]. While these linear approaches can achieve high accuracy when electrode placement remains consistent [8, 54], they encounter significant challenges in real-world scenarios, particularly when serial ECGs are recorded over intervals of days or weeks without professional supervision. In such cases, variations such as electrode misplacement or external noise can degrade the quality of the recorded ECG, making accurate synthesis more difficult.

To address these challenges, non-linear methods, especially those based on ANNs have been explored for their potential to improve reconstruction accuracy and overcome the limitations of traditional linear techniques [64]. Indeed, existing literature provides ample evidence of the effectiveness of non-linear models as robust alternatives to conventional approaches [8, 109]. Furthermore, the electrogenesis of cardiac signals is not strictly a linear

process, further supporting the use of non-linear methods in ECG signal synthesis [62, 63].

4.1 Preprocessing

The standard 12-lead ECG signal is corrupted with different types of noise and baseline wander since it is recorded and captured by skin electrodes. The electrodes are sensitive to minor electrical variations in the skin, and noise from internal or external sources can easily be introduced, leading to incorrect interpretations. Hence, ECG preprocessing is essential in order to remove noise and produce a cleaner, more easily interpretable ECG. Baseline wander is a low-frequency (0–0.5 Hz) interference caused by changes in electrode impedance, body movement and respiration. The raw ECG signal is passed to the Butterworth high-pass filter to remove the baseline wander [43]. Furthermore, the processed ECG mean of each lead is removed, and the amplitude is normalized to 1.

4.2 ECG Signal Representation in Wavelet Domain

The DWT has an inherent ability that bears good time-frequency localization and effectively characterizes the ECG signal's behavior. In this work, the DWT is used to decompose the characteristics of the three predictor leads up to six levels of decomposition. Essential characteristics of ECG is captured by the approximation coefficients and detail coefficients at different scales. The nonstationary, transients, and time-varying characteristics inherent in physiological signals have revitalized attention to apply the DWT transformation to analyse and characterize the ECG signals. Such application using multiresolution properties includes noise removal [110], detecting cardiac abnormalities [43], delineation of ECG characteristics features [111], QRS detection [112], and ECG compression [108]. The DWT has the advantage that it grossly segments the important attributes of ECG into different subbands. The inter-lead correlation of 12-lead ECG in the wavelet subband is higher than that of the original time domain signals [108].

The multi-resolution analysis of the DWT enables detailed examination of the ECG signals

at the subband level. The pyramid algorithm operates through the filter bank implementation by passing the ECG signal through low-pass and high-pass filters, followed by decimation and is defined by the following equations:

$$y_{low}[n] = \sum_{m} x[m]u[2n - m] \tag{4.1}$$

$$y_{high}[n] = \sum_{m} x[m]v[2n - m] \tag{4.2}$$

where $y_{low}[n]$, $y_{high}[n]$ are the outputs of the low-pass (u) and high-pass (v) filters, respectively. In the next level of decomposition, the filter output of the low-pass filter is further processed by passing it again through a new low-pass filter and a high-pass filter and this continues for further levels.

In wavelet transform, there are numerous families of wavelets, such as Daubechies, Haar, Morlet, Daubechies biorthogonal, etc. The choice of predefined basis functions determines the compactness of the resulting wavelet representation. If the characteristics of the wavelet basis functions resemble the ECG signal, the more compact the representation [113]. Therefore, Daubechies 6 wavelet is used since its wavelet function matches the ECG signal pattern. In this work, the three preprocessed predictor leads defined by x_1, x_2, and x_{V2} are individually fed as an input to the DWT block as shown in Figure 4.1. The DWT decomposes these ECG leads to six levels of decomposition. The essential characteristics of the ECG signal are apportioned across different wavelet subbands based on their frequency content, with the lower frequency subbands containing the majority of the significant information [44].

4.3 Synthesis of Twelve lead using DWT based ANN model

The pyramidal multi-resolution DWT decomposes the ECG signal such that each level of decomposition correlates to a distinct frequency band, and the clinical information and important characteristics of the ECG signal are discovered in each subband. Hence, the

multi-resolution technique combined with an efficient algorithm with good applicability in modeling non-linear dynamical problems could give promising results in reconstructing the standard 12-lead ECG from the limited 3 leads.

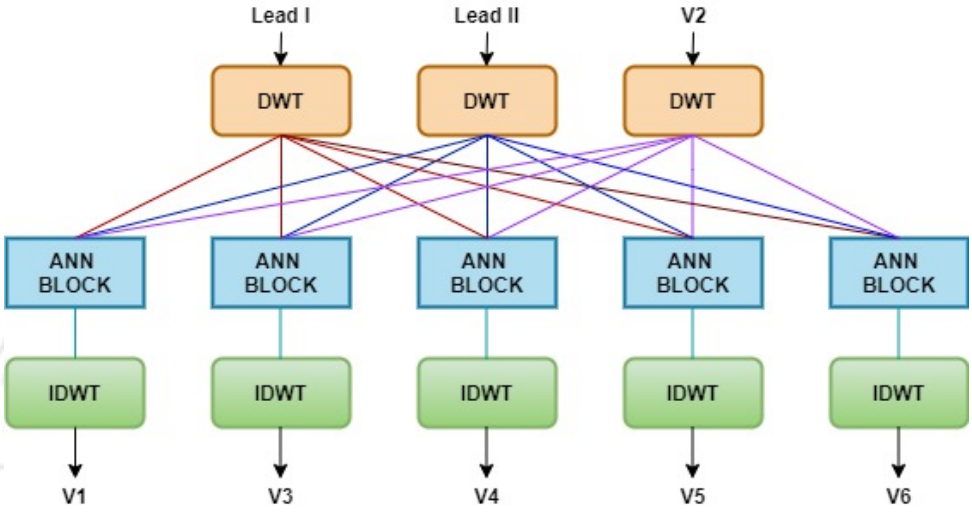

Figure 4.1: Block diagram of the proposed method

ANNs are widely-used to approximate non-linear biomedical signals with high generality. To synthesize the independent ECG signals i.e. V1, V3, V4, V5, and V6 from the predictor (I, II, V2) 12-lead ECG subset, we employed a set of multi-layer feed-forward ANNs which applied one input layer, one hidden layer and one output layer trained by means of the back-propagation algorithm. The relationship between the input and the output layers of the model are expressed by the biases and weights of the hidden layer. Each neuron's output is determined by the weights, along with the activation function. Back-propagation computes the derivatives of the activation functions in each successive neuron to obtain the optimal weights so as to generate the best outcome. The log sigmoid function is used as an activation function. In this work, 5 ANN block are employed to derive the 5 missing leads as shown in Figure 4.1. Each ANN block consist of seven individual ANN. The input to the first ANN is the approximation subband coefficient of the three predictor lead (I ,II, V2), and the input of the second ANN is the coefficient of the detail 6 subband and so on for the sixth and the seventh ANN respectively as shown in Figure 4.1. The outputs of the ANNs are the target coefficients. Each individual ANN consists of 3 input neurons (subband coefficients for each input), 10

hidden neurons, and an output layer.

The proposed method to reconstruct the standard 12-lead ECG involves several stages as shown in the block diagram in Figure 4.1. In this study, lead I, lead II, and precordial lead V2 are chosen as the predictor lead set as they achieved the good performance. In this work, the input three predictor leads I, II, and V2 is passed to DWT multi-resolution technique. The DWT decomposed the input ECG signal up to six levels of decomposition. The approximation coefficient and details coefficient obtained from the DWT are fed to the ANN. The multi-resolution technique has the ability to resolve the ECG signal into different frequency bands called the subbands. These subbands contain important attribute of the ECG signal. When each subband from the DWT decomposed ECG signal is given as an input to an ensemble of ANN algorithm, it is expected that the network may learn better than the whole frame of an input signal. ANN is proven to be an effective model to characterize an ECG signal due to its ability to map complex and nonlinear problems. The outcome from each ANN is fused and fed to the inverse discrete wavelet transform (IDWT). The output of the IDWT is the derived ECG signal, namely, V1, V3, V4, V5, and V6.

4.3.1 Performance Measures

The derived signals are compared with the original signals for assessing the performance of the proposed model. Standard closeness measures, namely, correlation coefficient (cc) and R^2 statistics, are used in this study. The cc is given as

$$cc = \frac{\sum_{i=1}^{N}(\mu_i - \bar{\mu})(\upsilon_i - \bar{\upsilon})}{\sqrt{\sum_{i=1}^{N}(\mu_i - \bar{\mu})^2}\sqrt{\sum_{i=1}^{N}(\upsilon_i - \bar{\upsilon})^2}} \tag{4.3}$$

where μ_i and υ_i are the values of the precordial original signal and synthesis signal, $\bar{\mu}$ and $\bar{\upsilon}$ are their mean values, respectively.

The root mean square error (RMSE) is the difference of the root-mean-square between the original and its reconstructed waveforms, and is defined as

$$RMSE = \sqrt{\frac{\sum_{i=1}^{N}(\mu_i - \upsilon_i)^2}{N}} \tag{4.4}$$

The variation of the diagnostic information between the actual and its reproduced version is measured by wavelet energy based diagnostic distortion (WEDD) [17]. It is given as

$$WEDD = \sum_{t=1}^{T+1} w_t WPRD_t, \quad t = 1, 2, ..., , T+1 \tag{4.5}$$

where WPRD is the wavelet percentage root mean square difference, w_t is the subband weight, and T is the decomposition level. The weight is evaluated as

$$w_t = \sqrt{\frac{\sum_{j=1}^{J_t} p_t^2(j)}{\sum_{n=1}^{T+1}\sum_{j=1}^{J_t} p_n^2(j)}} \tag{4.6}$$

where w_t is the weight of t^{th} subband, $p_t(j)$ denotes the wavelet coefficients of the original signal in t^{th} subband, and J_t is the length of wavelet coefficients in t^{th} subband.

WPRD is the inexactness obtain between the wavelet coefficients of the precordial original leads and its synthesis leads. WPRD can be expressed as

$$WPRD_t = \sqrt{\frac{\sum_{j=1}^{J_t}[p_t(j) - \bar{p}_t(j)]^2}{\sum_{j=1}^{J_t}[p_t(j)]^2}} \tag{4.7}$$

where $\bar{p}_t(j)$ is the wavelet coefficients of the synthesis signal in t^{th} subband.

4.4 Results of the DWT based ANN model

In this work, the PTB diagnostic ECG database is utilized to assess the proposed method. The database comprises 290 subjects with a total record of 549 from healthy volunteers as well as patients having various cardiovascular diseases are assembled. Each individual record contains standard 12 leads along with three vectorcardiogram orthogonal leads. The

Table 4.1: Performance evaluation of the DWT based ANN model for the reconstruction of 12-lead ECG

	r	R^2 (%)	WEDD (%)
V1	0.98	95.21	18.34
V3	0.98	95.65	14.04
V4	0.97	92.56	21.11
V5	0.97	93.00	20.63
V6	0.98	94.24	19.27
Average	0.98	94.13	18.68

15 leads are recorded simultaneously at a sampling rate of 1kHz, with a 16-bit resolution over a range of ± 16.384 mV. In this work, 16000 samples are used for training the model, and 10000 samples are used for reconstructing the derived lead sets.

Reconstruction accuracy for each lead subset of the reconstructed leads is compared with their originals. Overall waveform similarity is evaluated by standard closeness measures, namely, correlation coefficient (r), and coefficient of determination (R^2) between the reconstructions and their originals. The diagnostic closeness of the synthesized precordial leads with the original precordial leads is assessed by wavelet energy based diagnostic distortion (WEDD) measure [114]. The result of the proposed method is established from the average obtained value from the performance metrics of the five reconstructed precordial leads.

Table 4.1 shows the performance assessment of the proposed model. The lead V2 is used in the predictor lead set, hence the experimental result shown in Table 4.1 for five missing leads, namely, V1, V3, V4, V5, and V6. The WEDD value is low while the correlation coefficient and R^2 values are high. The higher average correlation value of 0.98 indicate that the reconstructed leads bear a good resemblance with their original. The average R^2 value of 94.13% shows that the proposed method achieved high-quality result for the set of data that has been evaluated. The WEDD obtained an average value of 18.68% indicate the synthesized leads preserve the significant diagnostic information. Taking account of the

individual precordial lead, lead V3 achieves the best result in terms of R^2, and WEDD with a value of 95.65%, and 14.04% respectively. From Table 4.1, it is observed that, based on the performance metrics the proposed model has the potential to synthesize the 12-lead ECG with minimal reconstruction error. The good performance obtained by the proposed system may be because the ANN learn better signal characteristics from a particular subset of the decomposed frequency bands from the decomposed DWT technique than the whole frame of the signal.

4.5 Synthesis of Twelve lead using DWT based LSTM Model

The recurrent neural network (RNN) architecture has recently become a popular choice, particularly to model chronological sequences. The RNN model operates in such a way that the neuron outputs are applied to their own inputs recursively. Thus to make a decision, the RNN cell considers both the past information and present data. However, the limitation of the conventional RNN in dealing with long-term dependencies is that the gradient of the backpropagated error either blows up (explode) or decays (vanish) exponentially. The LSTM network was introduced to overcome the vanishing and exploding gradient problem [115], and has emerged as one of the most popular RNN architectures to date. It is a novel recurrent network architecture designed to use feedback loops to retain past information and predict time-series data. The main advantage of the LSTM network is modeling sequential data and thus used to learn complex dynamics of the biomedical signals including ECG. Several works using LSTMs have been proposed in the classification of ECG signals and ECG biometrics [116–118]. The fundamental idea behind the LSTM cell are special structures consisting of memory cells and memory blocks, along with the multiple nonlinear gating units which regulate the flow of the information.

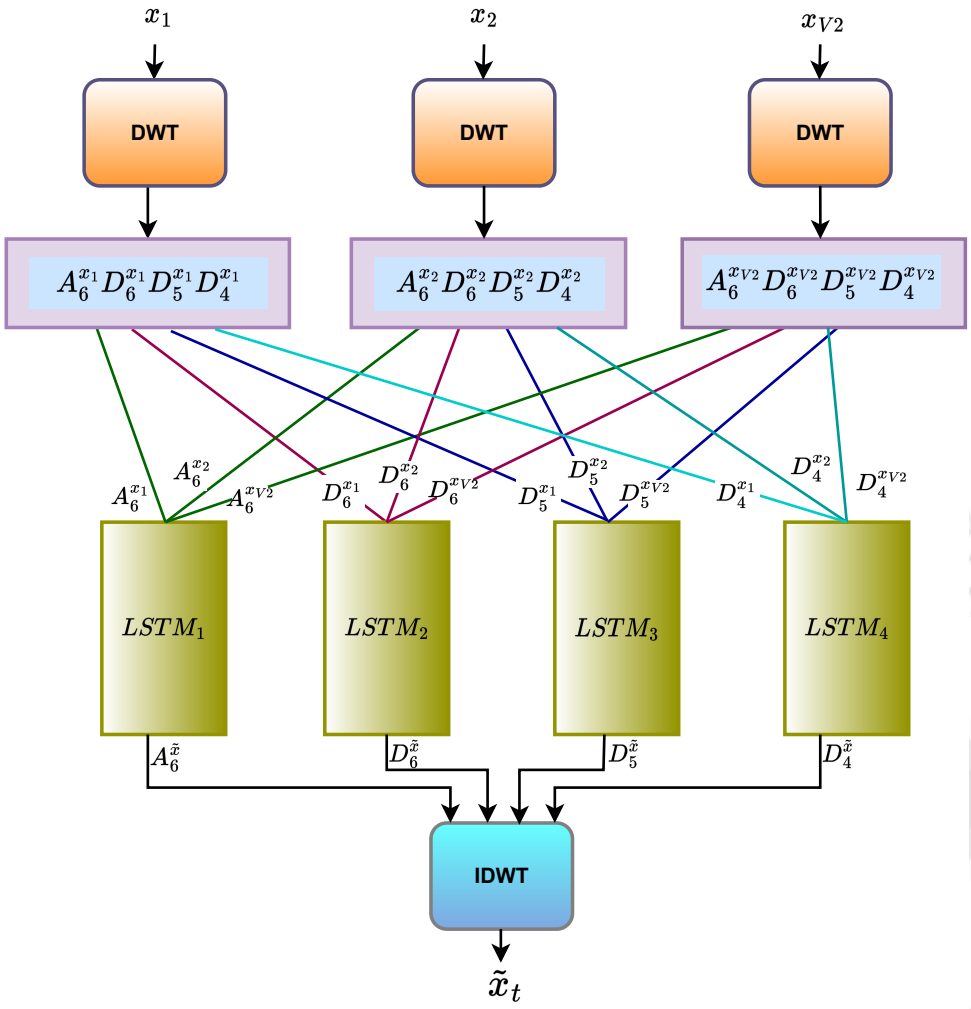

Figure 4.2: Block diagram of the DWT based LSTM proposed model

Figure 4.2 shows the block diagram of the DWT based LSTM proposed model. In this study, we used four LSTM networks to exploit the spatio-temporal information of the ECG signal. The output of the LSTM is fed to the inverse discrete wavelet transform in order to derive a missing precordial lead. For each derived lead, a separate network is trained with three predictor leads using training dataset. During estimation, the three predictor leads and corresponding network are used to get the targeted derived lead $\tilde{x}_t, (t \in \{V1, V3, V4, V5, V6\})$.

4.5.1 Energy based Subband Selection

The energy contributions of each subband in the wavelet domain are different. In this study, the relative wavelet subband energy is computed to analyze the energy contribution of the

Table 4.2: Energy contribution efficiency of the predictor leads

	I	II	V2
ECE A_6	37.3608	42.6670	34.7520
ECE D_6	24.7236	23.1034	21.0569
ECE D_5	27.1188	22.9986	26.2175
ECE D_4	10.0026	10.2596	16.0139
ECE D_3	0.5778	0.9712	1.3728
ECE D_2	0.1084	0.0955	0.2291
ECE D_1	0.1080	0.0846	0.3578

wavelet coefficients, and the subbands that have high energy (possess significant information) are used for further analysis. The energy contribution efficiency (ECE) is defined as the ratio of the energy of the wavelet coefficients of a particular subband and the total energy of the coefficients. The ECE of the approximation subband (A_6) and detail subbands $(D_1 - D_6)$ are calculated in this analysis. The ECE of the subband k, $k = 1, 2, ..., (K + 1)$ is defined as [119]

$$ECE = \frac{\sum_{n=1}^{N_k} y_k^2(n)}{\sum_{m=1}^{K+1}\sum_{n=1}^{N_m} y_m^2(n)}, \quad k = 1, 2, ..., (K + 1) \tag{4.8}$$

where $y_k(n)$ denotes the output of the k^{th} subband at point n, N_k is the number of elements in the k^{th} subband, and K is the number of decomposition levels. In order to observe the actual energy distribution of PQRST complex features, ECE values are calculated for zero mean ECG signals.

The ECE values of the subbands of the predictor leads are shown in Table 4.2. Most of the energy of the wavelet subbands follow descending characteristics. The approximation subband (A6) contributes the highest energy whereas the lowest detail subband (D1) contributes the least. The variation in ECE values reflects the variation in energy distribution across subbands. These experimental results clearly show that the ECE values of higher subbands (A6, D6, D5 and D4) are high while the lower detail subbands (D3, D2 and D1) are very low. In [114], it is reported that the significant information in the ECG signal is observed

in higher subbands, while the subbands D3 – D1 show primarily the noise components of the signal. Thus, in this work, the four higher subbands that possessed the dominant energy of the ECG signal are employed for further processing and fed as an input to LSTM networks. As shown in Figure 4.2, the approximation subbands $[A_6^{x_1}, A_6^{x_2}, A_6^{x_{V2}}]$ are given as input to the first LSTM network and the detail subbands $[D_6^{x_1}, D_6^{x_2}, D_6^{x_{V2}}]$ to the second LSTM network, and so on for other detailed subbands.

4.6 Results of the DWT based LSTM model

This study uses the publicly available PTB diagnostic ECG to assess the proposed model. The database has a well classified 549 ECG recordings related to healthy control and pathological signal. Each ECG signal is represented by 15 lead (standard 12-lead + 3 orthogonal leads) and digitised at a sampling rate of 1 kHz. In this work, the standard twelve leads are used, and the preprocessing is carried out to eliminate noise and artifacts using the method described in subsection 2.1. Subsequently, a total of 17,000 samples are utilized to carry out the experiment, of which 7000 samples are used for training the model, and 10,000 samples are used in the testing set.

In the experiment, we used LSTM with 150 hidden units, sequence input with 3 dimensions, and 1 fully connected layer, which was decided empirically by comparing the performance with varying numbers of hidden network units using training data. A batch size of 128 and an epoch number of 200 are used during the simulation. The time-step was 500, so the input data size is 3x500, and the output data size is 1x500. We employed Adam optimizer with an initial learning rate of 0.01. This experiment is conducted in a MATLAB environment.

In this work, ECE of the wavelet subbands are computed and the higher scales that contribute significant information of the ECG signal are employed for further analysis. In this study, we validate our proposed model by introducing noise in the ECG signal. The noises are modeled as additive white Gaussian noise. The analysis of the noise addition ECG signal is conducted in the testing phase and the results in detail are presented. Standard closeness

Table 4.3: Performance evaluation of the proposed method

	RMSE (mV)	r	R^2 (%)	WEDD (%)
V1	48.39	0.98	96.29	14.55
V3	69.16	**0.99**	**97.64**	**12.07**
V4	58.86	0.98	95.24	17.36
V5	57.59	0.97	94.97	17.91
V6	**42.29**	0.97	94.82	18.85
Average	55.28	0.98	95.79	16.15

metrics namely, correlation coefficient (r), RMSE, and R^2 statistics are used to assess the performance of the proposed model. The diagnostic variation between the original signal and the reconstructed signal is evaluated by WEDD. Table 4.3 presents RMSE, correlation, R^2, and WEDD values of the five missing precordial leads.

The table demonstrates the proximity effect mentioned in [9]. Leads close to the basis lead have better reconstruction results than those further away, as evidenced by the values of R^2 and WEDD of the V1 and V3 leads, which have higher values than other precordial leads due to their proximity to V2, one of the chosen predictor leads in this study. It is observed from the table that all the derived precordial leads bear high correlation values. The low average RMSE value of 55.28 mV and the higher average R^2 value of 95.79% indicate that the synthesized lead possesses a good similarity with the original signal. Using the proposed methodology, we have found that the value of R^2 for all the precordial leads is above 95%, which is practically retracing the original waveform. The low average value of 16.15% for WEDD suggests that the reconstructed leads retained the original signal without losing diagnostic information. Considering an individual lead, precordial lead V3 gives the best performance for correlation, R^2 and WEDD with the values of 0.99, 97.64%, and 12.07%, respectively, while lead V6 achieves the best RMSE value of 42.29 mV.

Table 4.4: Performance of the ablation study

	RMSE (mV)	r	R^2 (%)	WEDD (%)
with all the subbands	56.29	0.98	96.80	14.74
without D1, D2, and D3	51.41	0.99	97.79	13.78

4.6.1 Ablation study: performance with and without discarding lower subbands of the DWT

Table 4.4 shows the experimental results of the proposed method that is conducted (i) with all the subbands and (ii) discards the four lower subbands of the DWT. A total of 10 records is used in this study. As can be seen from the table, the analyzing performance without the lower subbands is superior to the one when all the subbands are considered. This means that the subbands D1, D2, and D3 can be removed without degrading the performance of the model. The results indicate that the higher subbands of the DWT contain diagnostically significant information of the ECG and the lower subbands are the noise components of the signal. The computational complexity is reduced when the four lower subbands are discarded.

In [120], a single LSTM network is used to synthesize the 12-lead ECG from a limited lead set. However, the correlation coefficient of their model achieves an average value of 0.95, while the proposed model obtains better performance with a correlation coefficient value of 0.98. This is due to the higher inter-lead correlation among the respective DWT subbands, and the four LSTM networks learns spatio-temporal information of the ECG characteristics adequately.

4.6.2 Performance of the Proposed Model in the Presence of Noise

The verification of the proposed system in the presence of noise was conducted by analysing the different levels of additive white Gaussian noise (AWGN). In Table 4.5, two SNR values of 10 dB and 20 dB are used for the analysis. A total of 10 records from the PTB database are used in this study. The performance of the proposed model in the presence of AWGN is

shown in Table 4.5. From the table, it is evident that the proposed method shows a promising performance even in the presence of noise.

Table 4.5: Performance of the proposed model in the presence of noise

	RMSE (mV)	r	R^2 (%)	WEDD (%)
10 dB	55.14	0.98	97.32	14.36
20 dB	52.68	0.99	97.64	13.95

4.6.3 Diagnosability of the Proposed Method

Diagnosability assesses the proposed method's ability to generate twelve leads for a given pathology that can discriminate from healthy control ECG [60]. It is defined as the ratio of the derived ECG classification accuracy (Acc_d) to that of the original ECG classification accuracy (Acc_o) and is computed as

$$Diagnosability = \frac{Acc_d}{Acc_o} \times 100 \tag{4.9}$$

Here accuracy is defined as, accuracy=(TP + TN)/(FP + FN + TP + TN) where FP denotes False Positive, TP denotes True Positive, FN denotes False Negative, and TN denotes True Negative. Acc_o is the accuracy obtained by the classifier when classifying between normal and pathological ECG. While Acc_d is computed in the same manner as the Acc_o but the pathological signal is generated by the proposed model. The inputs for the classification algorithm are the feature vectors extracted from the covariance matrices and the multiscale mode energy of the twelve leads. The feature extraction and classification techniques are implemented using the method described in [121]. In this work, diagnosability is implemented for three different types of pathological cases namely, myocardial infarction (MI), cardiomyopathy, and dysrhythmia. For MI, a total of 22 records, splitting 11 data each for MI and healthy control is used to train the model. The diagnosability result of 98.02% is achieved for the MI data. Similarly, 10 records each of healthy and pathological

data of cardiomyopathy is employed to test the diagnosability of the model. In this case, a diagnosability of 97.39% is obtained. For dysrhythmia, 18 records comprising healthy and pathological cases are used and achieved 98.27% diagnosability. The diagnosability results reveal that the classifier can distinguish between the healthy and pathological signal with very good accuracy using reconstructed leads. Thus, the reconstructed dataset of the different classes can discriminate healthy and pathological data with accuracy at par with the original dataset.

Table 4.6: Summary of selected studies conducted for the reconstruction of 12 lead ECG signals obtained from PTBDB.

			Performance			
Author	**Number of leads**	**Technique**	**RMSE (mV)**	**r**	**R^2(%)**	**WEDD (%)**
S.P. Nelwan *et al.* [8]	3	Linear Regression	88.69	0.96	88.61	26.03
G.Tsouri *et al.* [61]	3	Independent Component Analysis	95.56	0.93	86.72	26.99
S. Maheshwari *et al.* [10]	8	Principal Component Analysis	53.66	0.95	90.21	16.07
P. Kaewfoongrungsi *et al.* [122]	4	Support Vector Regression	94.74	0.97	-	26.64
H. Atoui *et al.* [64]	3	Artificial Neural Network	45.72	0.98	-	15.01
J. Lee *et al.* [123]	3	State Space Model	185.45	0.83	-	51.40
J.J. Nallikuzhy *et al.* [60]	3	Multi-scale Linear Regression	63.88	0.98	94.23	18.97
J.J. Nallikuzhy *et al.* [124]	3	Dictionary Learning	54.26	0.98	-	15.70
Lu-di Wang *et al.* [65]	3	CNN	-	0.94	-	-
Proposed method	3	DWT and LSTM	55.28	0.98	95.79	16.15

4.7 Performance Comparison with the Existing Methods

In this work, the proposed method is compared with the previously established works. Table 4.6 summarises the researchers' various techniques for the reconstruction of 12-lead ECG obtained from the same commonly accessible public PTB database. Most of the studies are conducted based on linear transformation techniques using independent three leads ECG signals as the basis leads. This includes linear regression (LR) model [8], independent component analysis (ICA) based model [61], ANN based model [64], state space (SS) model [123], multi-scale linear regression (mLR) model [60], and the dictionary learning (DL) model [124]. An investigation into the transformation of the standard 12-lead system from three predictor leads of our preliminary finding is presented in [125]. Our earlier work achieved a correlation value of 0.98, RMSE value of 78.00 mV, R^2 value of 94.93%, and WEDD value of 21.02%. The refinement in this work over the previous work includes subband selection based on energy contribution, noise added to the ECG signal, and fine-tuning of the LSTM parameters. This led to a significant improvement in the performance of the current work. Maheshwari et al. [10] conducted a study using eight leads ECG signals using PCA to synthesis 12-lead ECG. An investigation on a set of transfer function from SVR for deriving the 12-lead ECG from the lead I, lead II, V1, and V6 was studied by Kaewfoongrungsi et al. [122]. From Table 4.6, it can be seen that the proposed reconstruction methodology performs better than LR, ICA, SVR and mLR based models. The value of RMSE and WEDD using PCA model yields better result than our proposed model. Since PCA is applied on the eight independent leads, it certainly captures better information, ultimately improving the results. As can be seen from the table, the obtained results of the proposed model are comparable with that of the dictionary learning based model [124], but the limitation associated with the latter model is that once the types of datasets change, one needs to perform the dictionary learning process again. Besides, the reconstruction performance significantly depends on the accuracy of learned dictionaries. Atoui et al. [64] applied a nonlinear ANN using leads I, II, and V2 for the synthesis and obtained better results than the

proposed method. In their work, they segmented a 1 sec duration [P-onset - 18 ms, T-offset + 38 ms] representative cycle to determine the morphological features of PQRST onset and offset from every 10 sec ECG record. Eventually, the representative cycle of the original ECG signal was employed for further analysis. The limitation of their method is that the diagnostic information is lost during the extraction of a representative cycle, in which the reconstructed signal does not reflect the meaningful pathological changes for the pathological signal [65]. Another nonlinear method proposed by Wang et al. [65] using CNN to derive the standard 12-lead ECG achieves an average correlation coefficient of 0.94. Compared to the CNN model, our proposed methodology obtained a better result which is 0.98. The LSTM has an edge over the CNN method for the analysis of time-series data, as the former has the capability to capture long temporal dependencies due to the internal memory mechanism. The experimental results reveal that our proposed model can efficiently recover the original information with minimal loss while preserving the visual essence of the ECG signal.

LSTM has found many applications in the analysis of ECG signal for classification and person identification. However, in this work, our aim is to consolidate the significant diagnostic information present in twelve leads ECG onto three independent leads in order to minimize the number of channels and subdue the constraints from technical and medical science domains. One major advantage of the proposed model over other existing models is that our method provides a robust solution against noise. Experimental results reveal that the proposed method can learn spatial and temporal information of the ECG signal, presenting a good potential for reconstruction and the ability to discriminate between pathological and healthy control signal.

4.7.1 Performance Comparison with the Existing LSTM-based Approach

In [120], LSTM network is used to synthesize the 12-lead ECG from a limited lead set. A quantitative comparison with the proposed method in terms of correlation coefficient (r), RMSE, and R^2 statistics along with a diagnostic variation between the ground truth and the reconstructed signal i.e., WEDD are presented in Table 4.7. In this comparison, we have

evaluated the performances of both methods with and without the presence of noise. From the table, we can observe that in the case of noise-free conditions, the proposed method performs slightly better than the existing LSTM-based method [120]. To demonstrate the performance in the presence of noise, we varied the input noise level by changing the input signal's SNR from 20dB to 0dB. For better visualization, a comparison of reconstruction performance in the presence of noise is also shown in Figure 4.3. In the presence of a higher noise level, the performance of the existing LSTM-based method [120] significantly degrades. The proposed method can preserve better reconstruction quality even at higher noise levels. This is due to the lower subbands of the DWT being the noise components of the signal and are not involved in the reconstruction process of the proposed method. Besides, the proposed method exploits higher inter-lead correlation among the respective DWT subbands, and LSTM networks adequately learn spatiotemporal information of the ECG characteristics. As a result, the proposed method yields a noise-free and improved reconstruction of signals.

Table 4.7: Comparison of reconstruction performance with existing LSTM-based method in and without the presence of noise.

Input	Method	RMSE (mV)	r	R^2 (%)	WEDD (%)
Without noise	Sohn et al.	40.33	0.99	98.39	11.98
	Proposed	39.42	0.99	98.50	11.24
With SNR 20dB	Sohn et al.	47.42	0.99	97.95	13.12
	Proposed	43.51	0.99	98.06	11.36
With SNR 15dB	Sohn et al.	60.65	0.98	96.78	15.13
	Proposed	53.04	0.98	97.27	12.78
With SNR 10dB	Sohn et al.	95.39	0.96	92.90	19.46
	Proposed	69.02	0.98	96.00	14.33
With SNR 5dB	Sohn et al.	153.29	0.92	80.28	28.38
	Proposed	101.68	0.96	91.47	18.67
With SNR 0dB	Sohn et al.	256.20	0.84	60.86	45.85
	Proposed	173.67	0.89	74.87	28.06

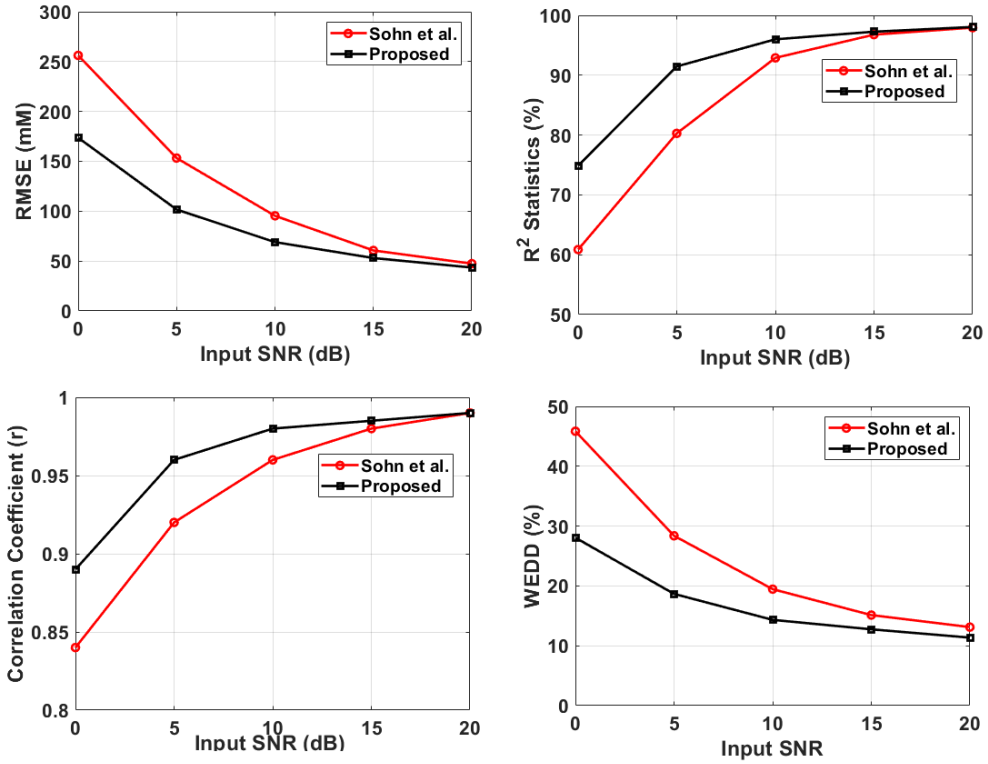

Figure 4.3: Comparison of reconstruction performance of the proposed method with existing LSTM-based method in terms of RMSE, correlation coefficient (r), R^2 and WEDD

4.7.2 Performance Comparison with Inter-patient Data

A set of experiments is also carried out to demonstrate the performance of unseen scenarios, i.e., inter-patient pathological data. For this, we have trained both the methods, i.e., the existing LSTM-based method [120] and the proposed method, with the healthy ECG data and tested on pathological data having a myocardial infarction. For visualization of the reconstruction performance, a representative reconstructed signal corresponding to lead V4 using both methods and ground truth is shown in Figure 4.4. In the figure, red represents ground truth, whereas blue and black represent the existing LSTM-based method [120] and the proposed method, respectively. It is clearly visible that with respect to ground truth, the proposed method shows less distortion compared to the existing LSTM-based method [120].

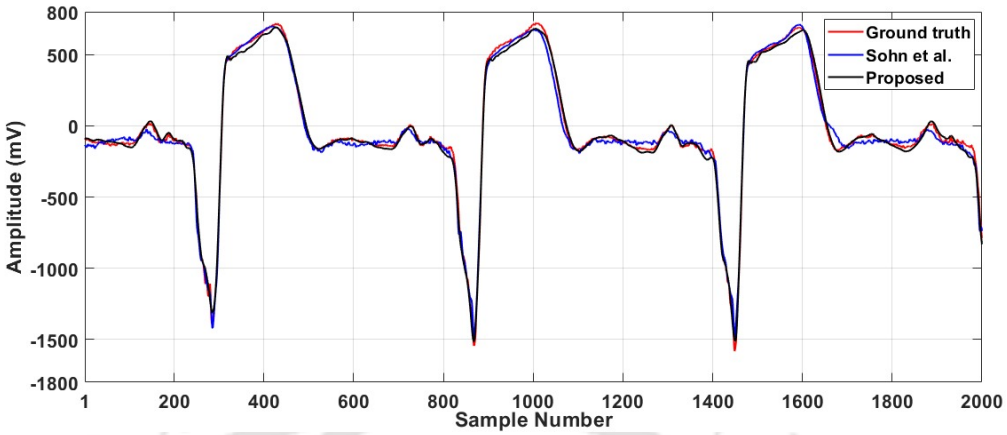

Figure 4.4: Comparison of reconstruction performance of the proposed method with existing LSTM-based method using inter-patient data.

4.8 Summary

This chapter sought to address the challenges faced by the cardiologists and the obstacles encountered during ambulatory monitoring, personalized health care, remote health care, telemonitoring, continuous monitoring, etc. We have proposed a novel reconstruction methodology based on long short-term memory approach on the wavelet subbands for reconstruction of the missing precordial leads of the standard 12-lead ECG and the results indicate that our method is well-founded and fine reconstruction quality can be established. The three-lead system used in this study needs no modifications to the standard electrode placement of a twelve-lead system, making it a viable clinical option. The proposed method attained high-performance results even with the addition of noise in the ECG signal. This implies that the proposed model can efficiently reconstruct the 12-lead ECG from three leads and has the potential to classify between cardiac diseases and healthy control ECG signals even when there is noise in the signal.

भारतीय प्रौद्योगिकी संस्थान गुवाहाटी
Indian Institute of Technology Guwahati

5

Person Specific Information from Synthesized ECG Signal

Contents

Biometric systems play a crucial role in safeguarding the privacy and security of data-driven intelligent technologies. With the substantial advancement of AI-based systems, there has been significant exploration across various biometric modalities, including, speech, iris, face, gait, fingerprint, and electrocardiogram (ECG) [89]. Among these, the ECG signal stands out for its resilience to spoofing attacks, owing to its intrinsic liveliness characteristics and provide valuable insights into a person's psychological and clinical status, offering multifaceted benefits beyond biometric identification. Moreover, ECG signals can be accessibly recorded using off-the-person setups, enhancing their usability. ECG-based biometric systems are applicable in a wide range of domains such as continuous authentication [21], healthcare services [22, 126], and mobile devices [72]. The growing demand for healthcare services has heightened the need for robust privacy and security measures to protect vital medical information. In this context, ECG-based biometric systems present a compelling solution, particularly in hospital settings, where they are less likely to be affected by deformation or environmental variations compared to other biometric modalities.

The ECG signal is a time-varying waveform with biometric information embedded in its temporal dynamics. In the existing literature, ECG-based biometric systems are generally categorized into two main approaches: fiducial point-based and non-fiducial point-based methods. The former relies on detecting specific landmarks in the ECG signal, most commonly the R-peak, or extracts numerous fiducial points prior to further analysis, while the latter does not require detecting any such points. The performance of fiducial point-based systems depends heavily on the precise identification of these fiducial points. Studies such as [21] and [80] addressed this challenge by identifying and discarding incorrectly detected R-peaks. They also employed an outlier removal algorithm designed to eliminate ECG beats that significantly deviate from the majority of beats associated with a given individual.

Over the past decade, various transform domain and time-domain methods have been investigated and proposed to extract biometric information from the single-lead or 12-lead ECG using signal processing techniques. The handcrafted features were then used to train machine learning classifiers for verification or identification tasks. However, the challenge

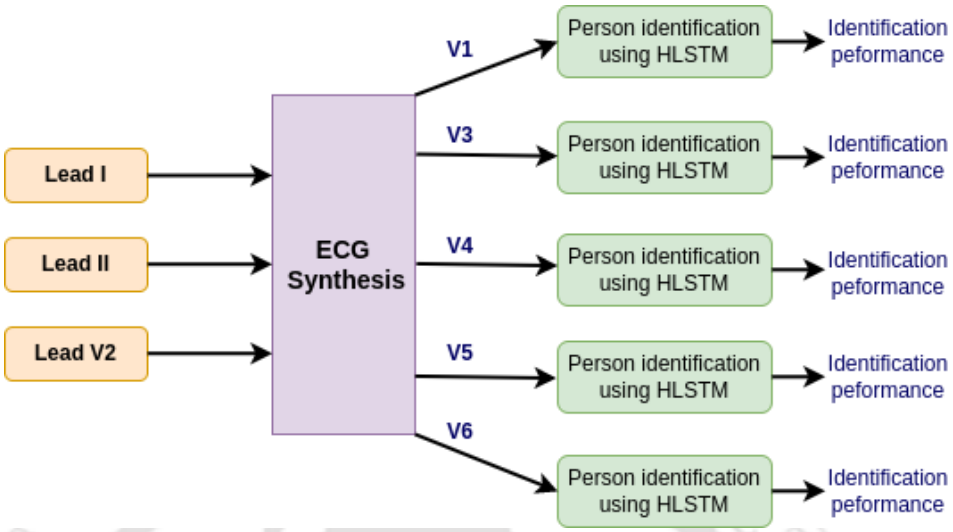

Figure 5.1: Block diagram of the proposed framework.

of extracting discriminative features consistently across individuals has limited the effectiveness of such approaches. Recent efforts have shifted towards leveraging deep learning models, which can automatically learn effective biometric representations directly from raw ECG signals in an end-to-end manner. According to the available literature, no study is conducted on biometric identification of the synthesized ECG. Therefore, in this chapter, we have investigated the effectiveness of the synthesised ECG signals for person identification applications.

We have used lead I, II, and V2 for the synthesis of the rest of the ECG leads. An LSTM based model using wavelet decomposed ECG signal is used for the synthesis of the ECG signals. Subsequently, each of the synthesised ECG signals is fed to a hierarchical long short-term memory (HLSTM) based biometric system to investigate the effectiveness of the reconstructed ECG signal for person identification application. This has led to the development of a new metric, i.e., person identifiability (PI), to evaluate the performance of a synthesis model.

The remaining portions of this chapter are structured as follows. In Section 5.1, the proposed framework is described. Section 5.2 describes the experimental setup. The results obtained in the experiment are discussed in Section 5.3. Finally, the summary of the chapter

is presented in Section 5.4.

5.1 Proposed Method for Person Identification

Figure 5.1 shows the block diagram of the proposed framework. In this work, we have used three leads, i.e., lead I, lead II, and lead V2 for the synthesis of lead V1, V3, V4, V5, and V6. Then, the HLSTM based biometric system is employed to obtain the identification performance using the synthesized leads.

5.1.1 ECG Synthesis Model

In this work, we have used the ECG synthesis model proposed in our previous work [125]. Figure 5.2 shows the block diagram for the ECG synthesis. The ECG synthesis module consists of a wavelet decomposition module followed by an LSTM based synthesis network. Three leads, i.e., lead I, lead II, and V2, are first preprocessed and then given as input to the synthesis module. During the preprocessing stage, the 12-lead ECG signal is downsampled to 500 Hz, followed by a filtering process as given in [125]. The amplitude and mean of the filtered ECG signal are normalized to one and zero, respectively. The preprocessed ECG signals are decomposed into six-level wavelet sub-bands, i.e., $[x^i_{A6}, x^i_{D6}, x^i_{D5}, x^i_{D4}, x^i_{D3}, x^i_{D2}, x^i_{D1}]$, where i = 1,2, and V2. Each sub-band signal from the three leads is concatenated and given as input to the LSTM module to synthesize the respective sub-band signal of another lead (i.e. $V_1, V_3, V_4, V_5,$ and V_6). Finally, the synthesized ECG signal is obtained by taking the inverse discrete wavelet transform of the synthesized sub-band signals.

5.1.2 Biometric System

In this work, we have employed the HLSTM based biometric system for the person identification [118]. The ECG signal is first preprocessed and segmented to give it as input to the HLSTM model. The preprocessing stage includes resampling the ECG signal to 200 Hz and then filtering it using a band pass filter with a lower cut-off frequency of 0.5 Hz and a higher cut-off frequency of 40 Hz. Following the preprocessing stage, the training ECG sequences

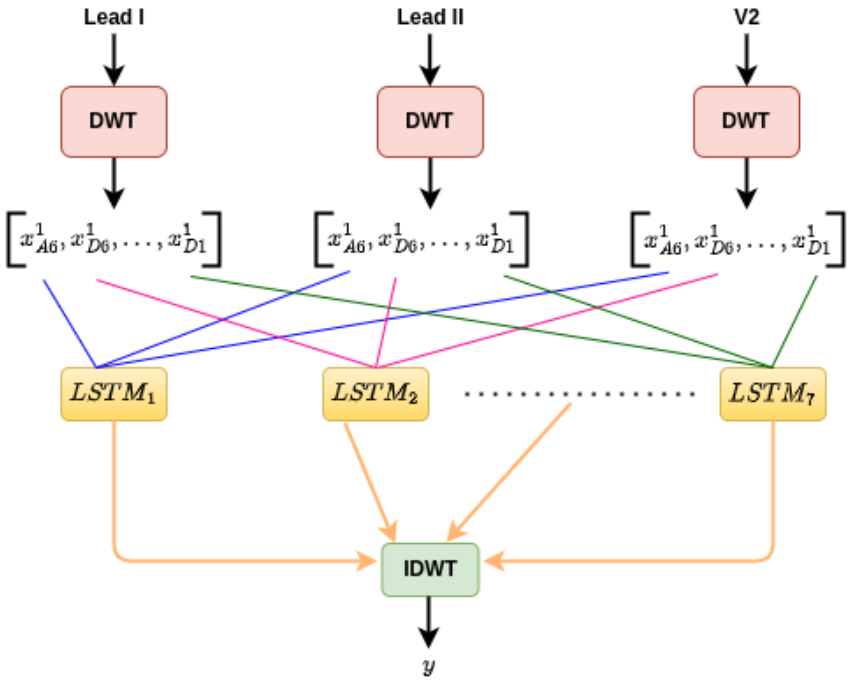

Figure 5.2: Block diagram of the ECG synthesis model

are extracted from the ECG signal using a 2 seconds rectangular window with an overlap of 0.75 fractions. The testing ECG sequences are extracted using the same rectangular window without any overlap. The process is similar to the method proposed in [118]. The ECG sequences are further segmented into smaller ECG segments using a 100 ms rectangular window with an overlap of 0.75 fractions. These smaller ECG segments are given as input to the HLSTM model at each time stamp.

Figure 5.3 shows the architecture of the HLSTM model. The HLSTM model consists of two layers of LSTM. The first layer of the LSTM takes the ECG segments are input. The output of the first layer of LSTM selected in an interval is given as input to the second layer of the LSTM. This allows the model to learn both the intra-beat and inter-beat variation of the ECG signal. The HLSTM model can encode long-term information of the ECG signal. Finally, the output of the second layer of the LSTM is given to an attention module to give more weight to the ECG segments with more biometric information. The attention weights are calculated using the Equation 5.1. Here, h_t is the output of the second layer LSTM at

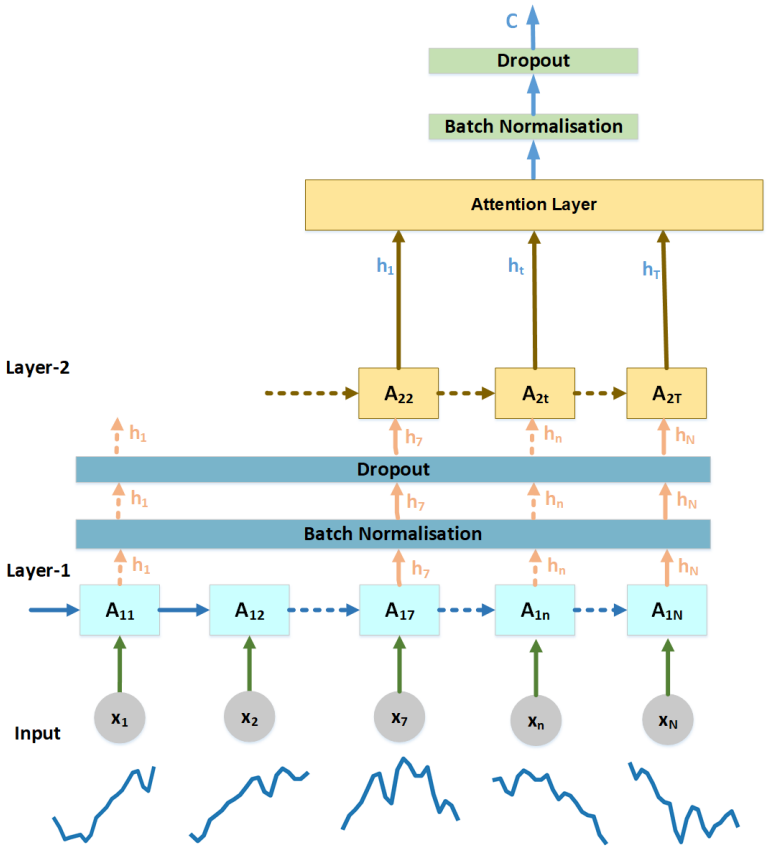

Figure 5.3: Network architecture of the HLSTM model.

time stamp t. Finally, the biometric representative vector c is obtained by taking the weighted summation of the hidden vectors at all the time stamps. This is shown in Equation 5.3.

$$\alpha_t = \text{softmax}(\text{score}(h_t)) = \frac{\exp(\text{score}(h_t))}{\sum_{t=1}^{T} \exp(\text{score}(h_t))} \tag{5.1}$$

$$\text{score}(h_t) = Wh_t + b \tag{5.2}$$

$$c = \sum_{t=1}^{t=T} c_t = \sum_{t=1}^{t=T} \alpha_t h_t \tag{5.3}$$

Finally, the context vector (C) is fed to a fully connected layer followed by a softmax function to obtain the posterior probability output ($\hat{P}(S_k/C)$) of the context vector belonging to a subject S_k. Finally, the candidate subject is identified by finding the maximum posterior probability corresponding to a subject.

$$\hat{P}(S_k/C) = softmax(WC + b) \tag{5.4}$$

5.1.3 Person Identifiability

Various performance measures have been developed to quantify the quality of the synthesized ECG signal, e.g. correlation coefficients (CC) [127], RMSE, WEDD, diagnosability etc. In this work, we have proposed a new performance measure, i.e., person identifiability (PI), to measure the performance of a synthesis model. The performance measure, PI, is defined using the accuracies obtained using the original ECG signal and the synthesized ECG signal.

$$PI = \begin{cases} 100, & \text{if } \frac{ACC_s}{ACC_o} \times 100 \geq 100 \\ \frac{ACC_s}{ACC_o} \times 100, & \text{otherwise} \end{cases} \tag{5.5}$$

5.2 Experimental Setup

In this work, we have used the publicly available PTB diagnostic ECG database. The database contains 549 recordings from 52 healthy subjects and 238 subjects with cardiac ailments. The ECG signals in this database are recorded using the standard 12-lead ECG recording setup and 3-orthogonal frank-lead system. In this work, we have considered the ECG signals recorded using the standard 12-lead ECG setup. Each ECG signal in this database is digitized at 1 kHz. In this work, an ECG signal of a duration of 14 seconds is used to train the neural network model designed for ECG synthesis. We have used an ECG signal of a duration of 20 seconds for testing the model.

The testing data of a duration of 20 seconds is again used in the training and testing process of the ECG biometric system. Out of the 20 seconds of duration, we have used 12 seconds of data for training the biometric system and 8 seconds of data for testing the biometric system. The train and test data are collected from different locations of the ECG

Table 5.1: Comparison of Person Identification Performance on Original ECG Signal (O) and Synthesized ECG Signal (S)

Leads	Type	Acc	EER	F1	Sen	Pre
V1	O	89.13	25.47	88.90	89.13	90.43
	S	86.96	31.27	87.00	86.96	89.40
V3	O	82.61	28.36	81.87	82.61	82.54
	S	83.70	28.01	82.52	83.70	83.70
V4	O	79.35	25.86	78.64	79.35	80.07
	S	79.35	29.27	76.25	79.35	75.93
V5	O	88.04	31.77	86.82	88.04	86.88
	S	80.43	37.97	78.19	80.43	78.19
V6	O	89.13	30.14	88.55	89.13	88.62
	S	85.87	37.06	83.73	85.87	86.18

signal. This is done by first extracting the training data and then the testing data is extracted. The training data for the ECG biometric system is extracted only from the original ECG signal (O). Whereas the testing data are extracted from both the original (O) and synthesized (S) ECG signals. This allows the comparison of the biometric information present in both the original and the synthesized ECG signal.

The performance of the synthesis model is evaluated using the correlation coefficients (CC), RMSE, WEDD, and person identifiability (PI). The person identification performance for both the original and the reconstructed ECG leads is obtained using accuracy (Acc), equal error rate (EER), F1 score (F1), sensitivity (Sen), and precision (Pre).

5.3 Results and Discussions

The performance of the person identification using the original ECG signal and the synthesized ECG signal is tabulated in Table 5.1. From Table 5.1, it can be observed that the person identification performance using the synthesized ECG signal is nearly the same as the original ECG signal. Maximum identification accuracy of 89.13% is obtained using the original ECG

signal of lead V1 and V6. Although the identification accuracy using the synthesized ECG signal follows the same trend, maximum identification accuracy of 86.96% is obtained using the synthesized ECG signal of lead V1. From Table 5.1, it can be observed that the model gives better performance using the synthesized ECG signal. This may be because of the fact that the synthesis model is able to learn person specific information and thus result in a better synthesized ECG signal which has fewer noises and deformations.

The performance of the synthesis model is tabulated in Table 5.2. From Table 5.2, it can be observed that the proposed PI performance measure gives performance consistent with other performance measures, i.e., CC, RMSE, and WEDD. The synthesized signal of lead V5 gives the worst performance, and the signal of lead V3 gives the best performance respective to the CC performance measure. It can be observed that the CC results are consistent with the PI performance measure. This shows that the PI performance measure can also be used for evaluating the performance of a synthesis model.

Table 5.2: Performance Evaluation of the Synthesized ECG Signal

Leads	CC	RMSE	WEDD	PI
V1	0.98	42.56	24.40	97.57
V3	0.99	71.72	17.94	100
V4	0.98	100.51	23.36	95.25
V5	0.97	87.13	20.42	91.36
V6	0.98	50.49	19.01	96.34
Average	0.98	70.48	21.02	97.1

5.4 Summary

In this work, we have analysed the effectiveness of the synthesised ECG signal for biometric applications. Experimental results show that the synthesised ECG signal contains similar biometric information compared to an original ECG signal. We have also developed a new performance measure, i.e., person identifiability (PI), for the ECG synthesis model. The

PI performance measure makes use of the identification accuracy of the original and the reconstructed ECG signal. We have shown that the proposed performance measure gives consistent results with the existing performance measures.

6

Conclusions

Contents

The growing prevalence and impact of CVDs on public health have underscored the urgent need for automated diagnostic and secure healthcare systems. Automated ECG interpretation methods are essential to facilitate rapid and reliable screening of cardiac abnormalities in both home-care and hospital-care settings. Such systems can significantly enhance cardiac disorders management and reduce healthcare costs. Consequently, the development of intelligent, automated techniques suitable for remote, portable ECG monitoring devices is vital for enabling early diagnosis and severity evaluation of cardiac conditions, thereby assisting physicians in commencing timely and effective treatment strategies, ultimately improving patient outcomes. In addition, advancements in wearable technologies, such as mobile applications, patch monitors, and smartwatches have made it possible to monitor cardiac health with greater speed and accuracy. However, these advancements also raise critical concerns regarding the privacy and security of sensitive medical data collected during diagnosis. In this context, the present thesis aims to develop an automated ECG interpretation and security system for the diagnosis of cardiac disorders using standard 12-lead ECG signal. The work in each chapter of this thesis is summarized as follows.

- Chapter 1 presents an insights into the electrophysiological activities of the heart and the graphical representation of cardiac conduction system in ECG system. This chapter discusses various ECG acquisition setups, including the single-lead ECG recording system, Holter monitoring, and the 12-lead ECG system. It further presents the morphological characteristics of normal ECG signals, as well as those linked to a range of cardiac abnormalities. Additionally, it presents a concise overview of the reconstruction of the 12-lead ECG.

- Chapter 2 presents a comprehensive literature review of existing automated methods for diagnosing myocardial infarction using 12-lead ECG signals, synthesis of the 12-lead ECG, and ECG-based biometric systems. While numerous approaches have been proposed for automated ECG interpretation and analysis, several research gaps remain inadequately addressed. The final section of this chapter highlights these gaps and

outlines the motivation behind the current research.

- Chapter 3 presents a new approach for detection of MI using multilead ECG. A VMD technique is used for quantifying diagnostic information of myocardial infarction from the ECG signal. Changes observed in the mode coefficients obtained through VMD are found to cause variations in the values of various features, which are used to extract clinically significant information from the ECG signals. Among these, multiscale mode energy is extracted from the decomposed modes and is shown to reflect substantial differences in pathological signals. Additionally, the inter-lead correlations present in the MSMM are found to affect its covariance structure, and these alterations are captured in the eigenvalues of the MSMM. Consequently, changes in pathological ECG signals are represented through these eigenvalues, which are then used as features. These extracted features are employed to train classification models aimed at distinguishing between healthy controls and individuals with MI. Among the classifiers tested, the SVM with a RBF kernel is found to deliver the highest performance, achieving 99.88% specificity, 99.90% sensitivity, and an overall accuracy of 99.88%. Based on the results obtained, it is concluded that the proposed method is capable of accurately detecting MI and demonstrates superior performance when compared to existing approaches.

- The standard 12-lead ECG system, recorded using ten electrodes, is the most widely used lead system among cardiologists. However, utilizing multiple electrodes may cause discomfort, reducing patient compliance. Simultaneously processing signals from numerous electrodes increases the complexity and expense of the recording system. In ambulatory settings, even acquiring a standard 12-lead ECG can be challenging. To address the above challenges, in Chapter 4, we presented an enhanced ECG spatial resolution approach that exploits the spatio-temporal correlations within the hidden feature space. The proposed approach take leverage of the enhanced inter-lead correlation of the ECG signal in the wavelet domain. This high correlation between different leads within the same wavelet scale can be effectively utilized to train RNN

model. The performance of the proposed model is assessed by standard closeness metrics namely, RMSE, correlation coefficient, and R^2 statistics. The diagnostic variation between the original signal and the reconstructed signal is evaluated by WEDD. The average RMSE, correlation, R^2, and WEDD values are 55.28, 0.98, 95.79%, and 16.15%, respectively. The results indicate that our method is well-founded and fine reconstruction quality can be established. The three-lead system used in this study needs no modifications to the standard electrode placement of a twelve-lead system, making it a viable clinical option. The proposed method attained high-performance results even with the addition of noise in the ECG signal. This implies that the proposed model can efficiently reconstruct the 12-lead ECG from three leads and has the potential to classify between cardiac diseases and healthy control ECG signals even when there is noise in the signal.

- Chapter 5 presents ECG based biometric system of the synthesized ECG by leveraging the temporal variation of the ECG signal. An LSTM based DWT is developed to generate the five leads from the three predictor leads. The HLSTM based biometric system is employed for the person identification. Each of the synthesised ECG signals is fed to a HLSTM based biometric system to investigate the effectiveness of the reconstructed ECG signal for person identification application. The person identification performance for both the original and the reconstructed ECG leads is obtained using accuracy (Acc), equal error rate (EER), F1 score (F1), sensitivity (Sen), and precision (pre). A new performance measure is developed, i.e., person identifiability (PI), for the ECG synthesis model. The PI performance measure makes use of the identification accuracy of the original and the reconstructed ECG signal. Experimental results shows that the person identification performance using the synthesized ECG signal is nearly the same as the original ECG signal. Maximum identification accuracy of 89.13% is obtained using the original ECG signal of lead V1 and V6. It is evident from the experimental results that the proposed performance measure gives consistent results with the existing performance measures.

6.1 Scope for the Future Work

The following would be the directions for future work.

- The proposed VMD based method can be extended for localization of MI. The VMD technique can be used for detection of other cardiac abnormalities such as bundle branch block, hypertrophy and cardiomyopathy.
- Most derived ECG models are patient-specific, as their personalized learning processes yield high reconstruction accuracy. However, existing global models often fail to preserve essential clinical information. Developing global models that maintain diagnostic integrity while enhancing reconstruction accuracy represents a promising direction for future research.
- The most convenient approach for ECG-based biometric systems is the off-the-person ECG recording setup. However, performance often declines in this setup due to the low signal-to-noise ratio (SNR), particularly in signals exhibiting significant baseline drift and abrupt fluctuations. Biometric identification and verification accuracy can be improved by enrolling and testing subjects using high SNR ECG signals. Therefore, developing a quality assessment algorithm based on estimating the periodicity of the ECG signal could be a valuable enhancement for ECG-based biometric systems.

References

[1] A. Update, "Heart disease and stroke statistics–2017 update," *Circulation*, vol. 135, pp. e146–e603, 2017.

[2] C. diseases (CVDs), "Cvd," https://www.who.int/news-room/fact-sheets/detail/cardiovascular-diseases-(cvds), Year Published/ Last Updated, accessed: January 2025.

[3] D. S. Celermajer, C. K. Chow, E. Marijon, N. M. Anstey, and K. S. Woo, "Cardiovascular disease in the developing world: prevalences, patterns, and the potential of early disease detection," *Journal of the American College of Cardiology*, vol. 60, no. 14, pp. 1207–1216, 2012.

[4] G. D. Clifford, F. Azuaje, P. McSharry, *et al.*, *Advanced methods and tools for ECG data analysis*. Artech house Boston, 2006, vol. 10.

[5] A. L. Goldberger, *Clinical Electrocardiography E-Book: A Simplified Approach*. Elsevier Health Sciences, 2012.

[6] C. Breen, R. Bond, and D. Finlay, "A clinical decision support tool to assist with the interpretation of the 12-lead electrocardiogram," *Health informatics journal*, vol. 25, no. 1, pp. 51–61, 2019.

[7] J. Schläpfer and H. J. Wellens, "Computer-interpreted electrocardiograms: benefits and limitations," *Journal of the American College of Cardiology*, vol. 70, no. 9, pp. 1183–1192, 2017.

[8] S. P. Nelwan, J. A. Kors, S. H. Meij, J. H. van Bemmel, and M. L. Simoons, "Reconstruction of the 12-lead electrocardiogram from reduced lead sets," *Journal of electrocardiology*, vol. 37, no. 1, pp. 11–18, 2004.

[9] D. Q. Feild, S. H. Zhou, E. D. Helfenbein, R. E. Gregg, and J. M. Lindauer, "Technical challenges and future directions in lead reconstruction for reduced-lead systems," *Journal of electrocardiology*, vol. 41, no. 6, pp. 466–473, 2008.

[10] S. Maheshwari, A. Acharyya, M. S. M. Schiariti, P. E. Puddu, *et al.*, "Personalized reduced 3-lead system formation methodology for remote health monitoring applications and reconstruction of standard 12-lead system," *International Archives of Medicine*, vol. 8, no. 1, 2015.

[11] H. P. Da Silva, A. Lourenço, A. Fred, N. Raposo, and M. Aires-de Sousa, "Check your biosignals here: A new dataset for off-the-person ecg biometrics," *Computer methods and programs in biomedicine*, vol. 113, no. 2, pp. 503–514, 2014.

[12] A. C. Guyton and J. E. Hall, *Text book of medical physiology*. Philadelphia, PA: Elsevier Saunders, 2006.

[13] M. A. Serhani, H. T. El Kassabi, H. Ismail, and A. Nujum Navaz, "Ecg monitoring systems: Review, architecture, processes, and key challenges," *Sensors*, vol. 20, no. 6, p. 1796, 2020.

[14] W. B. Fye, "A history of the origin, evolution, and impact of electrocardiography," *The American journal of cardiology*, vol. 73, no. 13, pp. 937–949, 1994.

[15] V. Kumar, A. K. Abbas, N. Fausto, and J. C. Aster, *Robbins and Cotran pathologic basis of disease, professional edition e-book*. Elsevier health sciences, 2014.

[16] H. Burger and J. Van Milaan, "Heart-vector and leads. part ii," *British heart journal*, vol. 9, no. 3, p. 154, 1947.

[17] D. D. Finlay, C. D. Nugent, J. G. Kellett, M. P. Donnelly, P. J. McCullagh, and N. D. Black, "Synthesising the 12-lead electrocardiogram: Trends and challenges," *European journal of internal medicine*, vol. 18, no. 8, pp. 566–570, 2007.

[18] I. Tomašić and R. Trobec, "Electrocardiographic systems with reduced numbers of leads—synthesis of the 12-lead ecg," *IEEE reviews in biomedical engineering*, vol. 7, pp. 126–142, 2013.

[19] J. R. Pinto, J. S. Cardoso, and A. Lourenço, "Evolution, current challenges, and future possibilities in ecg biometrics," *IEEE Access*, vol. 6, pp. 34 746–34 776, 2018.

[20] M. Li and S. Narayanan, "Robust ecg biometrics by fusing temporal and cepstral information," in *2010 20th International Conference on Pattern Recognition*. IEEE, 2010, pp. 1326–1329.

[21] W. Louis, M. Komeili, and D. Hatzinakos, "Continuous authentication using one-dimensional multiresolution local binary patterns (1dmrlbp) in ecg biometrics," *IEEE Transactions on Information Forensics and Security*, vol. 11, no. 12, pp. 2818–2832, 2016.

[22] S. Pirbhulal, H. Zhang, W. Wu, S. C. Mukhopadhyay, and Y.-T. Zhang, "Heartbeats based biometric random binary sequences generation to secure wireless body sensor networks," *IEEE Transactions on Biomedical Engineering*, vol. 65, no. 12, pp. 2751–2759, 2018.

[23] S. Romiti, M. Vinciguerra, W. Saade, I. Anso Cortajarena, and E. Greco, "Artificial intelligence (ai) and cardiovascular diseases: an unexpected alliance," *Cardiology Research and Practice*, vol. 2020, no. 1, p. 4972346, 2020.

[24] U. Satija, B. Ramkumar, and M. S. Manikandan, "A new automated signal quality-aware ecg beat classification method for unsupervised ecg diagnosis environments," *IEEE Sensors Journal*, vol. 19, no. 1, pp. 277–286, 2018.

[25] E. Prabhakararao and M. S. Manikandan, "On the use of variational mode decomposition for removal of baseline wander in ecg signals," in *2016 Twenty Second National Conference on Communication (NCC)*. IEEE, 2016, pp. 1–6.

[26] M. A. Kabir and C. Shahnaz, "Denoising of ecg signals based on noise reduction algorithms in emd and wavelet domains," *Biomedical Signal Processing and Control*, vol. 7, no. 5, pp. 481–489, 2012.

[27] J. Gilles, "Empirical wavelet transform," *IEEE transactions on signal processing*, vol. 61, no. 16, pp. 3999–4010, 2013.

[28] D. Sadhukhan, S. Pal, and M. Mitra, "Automated identification of myocardial infarction using harmonic phase distribution pattern of ecg data," *IEEE Transactions on Instrumentation and Measurement*, vol. 67, no. 10, pp. 2303–2313, 2018.

[29] V. K. Sudarshan, U. R. Acharya, S. L. Oh, M. Adam, J. H. Tan, C. K. Chua, K. P. Chua, and R. San Tan, "Automated diagnosis of congestive heart failure using dual tree complex wavelet transform and statistical features extracted from 2 s of ecg signals," *Computers in biology and medicine*, vol. 83, pp. 48–58, 2017.

[30] R. Tripathy, M. R. Paternina, J. G. Arrieta, A. Zamora-Méndez, and G. R. Naik, "Automated detection of congestive heart failure from electrocardiogram signal using stockwell transform and hybrid classification scheme," *Computer methods and programs in biomedicine*, vol. 173, pp. 53–65, 2019.

[31] A. Gallino, S. Chierchia, G. Smith, M. Croom, M. Morgan, C. Marchesi, and A. Maseri, "Computer system for analysis of st segment changes on 24 hour holter monitor tapes: Comparison with other available systems," *Journal of the American College of Cardiology*, vol. 4, no. 2, pp. 245–252, 1984.

[32] M. Reddy, L. Edenbrandt, J. Svensson, W. Haisty, and O. Pahlm, "Neural network versus electrocardiographer and conventional computer criteria in diagnosing anterior infarct from the ecg," in *Proceedings Computers in Cardiology*. IEEE, 1992, pp. 667–670.

[33] P. Bozzola, G. Bortolan, C. Combi, F. Pinciroli, and C. Brohet, "A hybrid neuro-fuzzy system for ecg classification of myocardial infarction," in *Computers in cardiology 1996*. IEEE, 1996, pp. 241–244.

[34] B. Hedén, H. Öhlin, R. Rittner, and L. Edenbrandt, "Acute myocardial infarction detected in the 12-lead ecg by artificial neural networks," *Circulation*, vol. 96, no. 6, pp. 1798–1802, 1997.

[35] M. Arif, I. A. Malagore, and F. A. Afsar, "Detection and localization of myocardial infarction using k-nearest neighbor classifier," *Journal of medical systems*, vol. 36, pp. 279–289, 2012.

[36] N. Safdarian, N. J. Dabanloo, and G. Attarodi, "A new pattern recognition method for detection and localization of myocardial infarction using t-wave integral and total integral as extracted features from one cycle of ecg signal," *Journal of Biomedical Science and Engineering*, vol. 2014, 2014.

[37] L. Sun, Y. Lu, K. Yang, and S. Li, "Ecg analysis using multiple instance learning for myocardial infarction detection," *IEEE transactions on biomedical engineering*, vol. 59, no. 12, pp. 3348–3356, 2012.

[38] M. Abdelazez, P. X. Quesnel, A. D. Chan, and H. Yang, "Signal quality analysis of ambulatory electrocardiograms to gate false myocardial ischemia alarms," *IEEE Transactions on Biomedical Engineering*, vol. 64, no. 6, pp. 1318–1325, 2016.

[39] U. R. Acharya, H. Fujita, M. Adam, O. S. Lih, V. K. Sudarshan, T. J. Hong, J. E. Koh, Y. Hagiwara, C. K. Chua, C. K. Poo, *et al.*, "Automated characterization and classification of coronary artery disease and myocardial infarction by decomposition of ecg signals: A comparative study," *Information Sciences*, vol. 377, pp. 17–29, 2017.

[40] U. R. Acharya, H. Fujita, V. K. Sudarshan, S. L. Oh, M. Adam, J. E. Koh, J. H. Tan, D. N. Ghista, R. J. Martis, C. K. Chua, *et al.*, "Automated detection and localization of myocardial infarction using electrocardiogram: a comparative study of different leads," *Knowledge-Based Systems*, vol. 99, pp. 146–156, 2016.

[41] E. Jayachandran, P. Joseph K, and R. Acharya U, "Analysis of myocardial infarction using discrete wavelet transform," *Journal of medical systems*, vol. 34, pp. 985–992, 2010.

[42] H. Pereira and N. Daimiwal, "Analysis of features for myocardial infarction and healthy patients based on wavelet," in *2016 Conference on Advances in Signal Processing (CASP)*. IEEE, 2016, pp. 164–169.

[43] S. Padhy and S. Dandapat, "Third-order tensor based analysis of multilead ecg for classification of myocardial infarction," *Biomedical Signal Processing and Control*, vol. 31, pp. 71–78, 2017.

[44] L. Sharma, R. Tripathy, and S. Dandapat, "Multiscale energy and eigenspace approach to detection and localization of myocardial infarction," *IEEE transactions on biomedical engineering*, vol. 62, no. 7, pp. 1827–1837, 2015.

[45] R. K. Tripathy, A. Bhattacharyya, and R. B. Pachori, "A novel approach for detection of myocardial infarction from ecg signals of multiple electrodes," *IEEE Sensors Journal*, vol. 19, no. 12, pp. 4509–4517, 2019.

[46] U. R. Acharya, H. Fujita, S. L. Oh, Y. Hagiwara, J. H. Tan, and M. Adam, "Application of deep convolutional neural network for automated detection of myocardial infarction using ecg signals," *Information Sciences*, vol. 415, pp. 190–198, 2017.

[47] U. B. Baloglu, M. Talo, O. Yildirim, R. San Tan, and U. R. Acharya, "Classification of myocardial infarction with multi-lead ecg signals and deep cnn," *Pattern recognition letters*, vol. 122, pp. 23–30, 2019.

[48] T. Reasat and C. Shahnaz, "Detection of inferior myocardial infarction using shallow convolutional neural networks," in *2017 IEEE region 10 humanitarian technology conference (R10-HTC)*. IEEE, 2017, pp. 718–721.

[49] W. Liu, M. Zhang, Y. Zhang, Y. Liao, Q. Huang, S. Chang, H. Wang, and J. He, "Real-time multilead convolutional neural network for myocardial infarction detection," *IEEE journal of biomedical and health informatics*, vol. 22, no. 5, pp. 1434–1444, 2017.

[50] L. Fu, B. Lu, B. Nie, Z. Peng, H. Liu, and X. Pi, "Hybrid network with attention mechanism for detection and location of myocardial infarction based on 12-lead electrocardiogram signals," *Sensors*, vol. 20, no. 4, p. 1020, 2020.

[51] N. Strodthoff and C. Strodthoff, "Detecting and interpreting myocardial infarction using fully convolutional neural networks," *Physiological measurement*, vol. 40, no. 1, p. 015001, 2019.

[52] E. Frank, "General theory of heart-vector projection," *Circulation Research*, vol. 2, no. 3, pp. 258–270, 1954.

[53] G. E. Dower, H. B. Machado, and J. Osborne, "On deriving the electrocardiogram from vector-cardiographic leads," *Clinical cardiology*, vol. 3, no. 2, pp. 87–95, 1980.

[54] B. J. Drew, M. M. Pelter, D. E. Brodnick, A. V. Yadav, D. Dempel, and M. G. Adams, "Comparison of a new reduced lead set ecg with the standard ecg for diagnosing cardiac arrhythmias and myocardial ischemia," *Journal of electrocardiology*, vol. 35, no. 4, pp. 13–21, 2002.

[55] S. Maheshwari, A. Acharyya, P. E. Puddu, and M. Schiariti, "Reduced lead system selection methodology for reliable standard 12-lead reconstruction targeting personalised remote health monitoring applications," *Computer Methods in Biomechanics and Biomedical Engineering: Imaging & Visualization*, vol. 2, no. 2, pp. 107–120, 2014.

[56] G. E. Dower, A. Yakush, S. B. Nazzal, R. V. Jutzy, and C. E. Ruiz, "Deriving the 12-lead electrocardiogram from four (easi) electrodes," *Journal of electrocardiology*, vol. 21, pp. S182–S187, 1988.

[57] R. E. Mason and I. Likar, "A new system of multiple-lead exercise electrocardiography," *American heart journal*, vol. 71, no. 2, pp. 196–205, 1966.

[58] S.-C. Man, A. C. Maan, E. Kim, H. H. Draisma, M. J. Schalij, E. E. van der Wall, and C. A. Swenne, "Reconstruction of standard 12-lead electrocardiograms from 12-lead electrocardiograms recorded with the mason-likar electrode configuration," *Journal of Electrocardiology*, vol. 41, no. 3, pp. 211–219, 2008.

[59] J. A. Scherer, J. M. Jenkins, and J. M. Nicklas, "Synthesis of the 12-lead electrocardiogram from a 3-lead subset using patient-specific transformation vectors: an algorithmic approach to computerized signal synthesis," *Journal of electrocardiology*, vol. 22, 1989.

[60] J. J. Nallikuzhy and S. Dandapat, "Spatial enhancement of ecg using diagnostic similarity score based lead selective multi-scale linear model," *Computers in biology and medicine*, vol. 85, pp. 53–62, 2017.

[61] G. R. Tsouri and M. H. Ostertag, "Patient-specific 12-lead ecg reconstruction from sparse electrodes using independent component analysis," *IEEE journal of biomedical and health informatics*, vol. 18, no. 2, pp. 476–482, 2013.

[62] R. Modre, M. Seger, G. Fischer, C. Hintermuller, D. Hayn, B. Pfeifer, F. Hanser, G. Schreier, and B. Tilg, "Cardiac anisotropy: Is it negligible regarding noninvasive activation time imaging?" *IEEE Transactions on Biomedical Engineering*, vol. 53, no. 4, pp. 569–580, 2006.

[63] R. M. Gulrajani, "The forward and inverse problems of electrocardiography," *IEEE Engineering in Medicine and Biology Magazine*, vol. 17, no. 5, pp. 84–101, 1998.

[64] H. Atoui, J. Fayn, and P. Rubel, "A novel neural-network model for deriving standard 12-lead ecgs from serial three-lead ecgs: application to self-care," *IEEE transactions on information technology in biomedicine*, vol. 14, no. 3, pp. 883–890, 2010.

[65] L.-d. Wang, W. Zhou, Y. Xing, N. Liu, M. Movahedipour, and X.-g. Zhou, "A novel method based on convolutional neural networks for deriving standard 12-lead ecg from serial 3-lead ecg," *Frontiers of Information Technology & Electronic Engineering*, vol. 20, no. 3, pp. 405–413, 2019.

[66] L. Biel, O. Pettersson, L. Philipson, and P. Wide, "Ecg analysis: a new approach in human identification," *IEEE transactions on instrumentation and measurement*, vol. 50, no. 3, pp. 808–812, 2001.

[67] S. A. Israel, J. M. Irvine, A. Cheng, M. D. Wiederhold, and B. K. Wiederhold, "Ecg to identify individuals," *Pattern recognition*, vol. 38, no. 1, pp. 133–142, 2005.

[68] C. L. P. Lim, W. L. Woo, S. S. Dlay, and B. Gao, "Heartrate-dependent heartwave biometric identification with thresholding-based gmm–hmm methodology," *IEEE Transactions on Industrial Informatics*, vol. 15, no. 1, pp. 45–53, 2018.

[69] Y. Huang, G. Yang, K. Wang, H. Liu, and Y. Yin, "Learning joint and specific patterns: A unified sparse representation for off-the-person ecg biometric recognition," *IEEE Transactions on Information Forensics and Security*, vol. 16, pp. 147–160, 2020.

[70] T.-W. Shen, W. J. Tompkins, and Y. H. Hu, "One-lead ecg for identity verification," in *Proceedings of the second joint 24th annual conference and the annual fall meeting of the biomedical engineering society][engineering in medicine and biology*, vol. 1. IEEE, 2002, pp. 62–63.

[71] R. Palaniappan and S. M. Krishnan, "Identifying individuals using ecg beats," in *2004 International Conference on Signal Processing and Communications, 2004. SPCOM'04.* IEEE, 2004, pp. 569–572.

[72] J. S. Arteaga-Falconi, H. Al Osman, and A. El Saddik, "Ecg authentication for mobile devices," *IEEE Transactions on Instrumentation and Measurement*, vol. 65, no. 3, pp. 591–600, 2015.

[73] P. Huang, L. Guo, M. Li, and Y. Fang, "Practical privacy-preserving ecg-based authentication for iot-based healthcare," *IEEE Internet of Things Journal*, vol. 6, no. 5, pp. 9200–9210, 2019.

[74] R. Cordeiro, D. Gajaria, A. Limaye, T. Adegbija, N. Karimian, and F. Tehranipoor, "Ecg-based authentication using timing-aware domain-specific architecture," *IEEE transactions on computer-aided design of integrated circuits and systems*, vol. 39, no. 11, pp. 3373–3384, 2020.

[75] K. N. Plataniotis, D. Hatzinakos, and J. K. Lee, "Ecg biometric recognition without fiducial detection," in *2006 Biometrics symposium: Special session on research at the biometric consortium conference*. IEEE, 2006, pp. 1–6.

[76] C.-C. Chiu, C.-M. Chuang, and C.-Y. Hsu, "A novel personal identity verification approach using a discrete wavelet transform of the ecg signal," in *2008 International Conference on Multimedia and Ubiquitous Engineering (mue 2008)*. IEEE, 2008, pp. 201–206.

[77] J. M. Irvine, S. A. Israel, W. T. Scruggs, and W. J. Worek, "eigenpulse: Robust human identification from cardiovascular function," *Pattern Recognition*, vol. 41, no. 11, pp. 3427–3435, 2008.

[78] A. D. Chan, M. M. Hamdy, A. Badre, and V. Badee, "Wavelet distance measure for person identification using electrocardiograms," *IEEE transactions on instrumentation and measurement*, vol. 57, no. 2, pp. 248–253, 2008.

[79] J.-N. Lee and K.-C. Kwak, "Personal identification using a robust eigen ecg network based on time-frequency representations of ecg signals," *IEEE access*, vol. 7, pp. 48 392–48 404, 2019.

[80] E. J. da Silva Luz, G. J. Moreira, L. S. Oliveira, W. R. Schwartz, and D. Menotti, "Learning deep off-the-person heart biometrics representations," *IEEE Transactions on Information Forensics and Security*, vol. 13, no. 5, pp. 1258–1270, 2017.

[81] R. D. Labati, E. Muñoz, V. Piuri, R. Sassi, and F. Scotti, "Deep-ecg: Convolutional neural networks for ecg biometric recognition," *Pattern Recognition Letters*, vol. 126, pp. 78–85, 2019.

[82] Y. Zhang, Z. Xiao, Z. Guo, and Z. Wang, "Ecg-based personal recognition using a convolutional neural network," *Pattern Recognition Letters*, vol. 125, pp. 668–676, 2019.

[83] Y. Li, Y. Pang, K. Wang, and X. Li, "Toward improving ecg biometric identification using cascaded convolutional neural networks," *Neurocomputing*, vol. 391, pp. 83–95, 2020.

[84] J. R. Pinto, M. V. Correia, and J. S. Cardoso, "Secure triplet loss: Achieving cancelability and non-linkability in end-to-end deep biometrics," *IEEE Transactions on Biometrics, Behavior, and Identity Science*, vol. 3, no. 2, pp. 180–189, 2020.

[85] R. Srivastva, A. Singh, and Y. N. Singh, "Plexnet: A fast and robust ecg biometric system for human recognition," *Information Sciences*, vol. 558, pp. 208–228, 2021.

[86] H. M. Lynn, S. B. Pan, and P. Kim, "A deep bidirectional gru network model for biometric electrocardiogram classification based on recurrent neural networks," *Ieee Access*, vol. 7, pp. 145 395–145 405, 2019.

[87] A. J. Prakash, K. K. Patro, M. Hammad, R. Tadeusiewicz, and P. Pławiak, "Baed: A secured biometric authentication system using ecg signal based on deep learning techniques," *Biocybernetics and Biomedical Engineering*, vol. 42, no. 4, pp. 1081–1093, 2022.

[88] M. Oeff, H. Koch, R. Bousseljot, and D. Kreiseler, "The ptb diagnostic ecg database," *National Metrology Institute of Germany*, 2012.

[89] A. K. Jain, A. Ross, and S. Prabhakar, "An introduction to biometric recognition," *IEEE Transactions on circuits and systems for video technology*, vol. 14, no. 1, pp. 4–20, 2004.

[90] A. Jaleel, R. Tafreshi, and L. Tafreshi, "An expert system for differential diagnosis of myocardial infarction," *Journal of Dynamic Systems, Measurement, and Control*, vol. 138, no. 11, p. 111012, 2016.

[91] R. Remya, K. Indiradevi, and K. A. Babu, "Classification of myocardial infarction using multi resolution wavelet analysis of ecg," *Procedia Technology*, vol. 24, pp. 949–956, 2016.

[92] J. T.-Y. Weng, J.-J. Lin, Y.-C. Chen, and P.-C. Chang, "Myocardial infarction classification by morphological feature extraction from big 12-lead ecg data," in *Trends and Applications in Knowledge Discovery and Data Mining: PAKDD 2014 International Workshops: DANTH, BDM, MobiSocial, BigEC, CloudSD, MSMV-MBI, SDA, DMDA-Health, ALSIP, SocNet, DMBIH, BigPMA, Tainan, Taiwan, May 13-16, 2014. Revised Selected Papers 18*. Springer, 2014, pp. 689–699.

[93] B. Liu, J. Liu, G. Wang, K. Huang, F. Li, Y. Zheng, Y. Luo, and F. Zhou, "A novel electrocardiogram parameterization algorithm and its application in myocardial infarction detection," *Computers in biology and medicine*, vol. 61, pp. 178–184, 2015.

[94] T. Lahiri, U. Kumar, H. Mishra, S. Sarkar, and A. D. Roy, "Analysis of ecg signal by chaos principle to help automatic diagnosis of myocardial infarction," 2009.

[95] N. Maglaveras, T. Stamkopoulos, C. Pappas, and M. G. Strintzis, "An adaptive backpropagation neural network for real-time ischemia episodes detection: development and performance analysis using the european st-t database," *IEEE Transactions on Biomedical Engineering*, vol. 45, no. 7, pp. 805–813, 1998.

[96] T. P. Exarchos, M. G. Tsipouras, C. P. Exarchos, C. Papaloukas, D. I. Fotiadis, and L. K. Michalis, "A methodology for the automated creation of fuzzy expert systems for ischaemic and arrhythmic beat classification based on a set of rules obtained by a decision tree," *Artificial Intelligence in medicine*, vol. 40, no. 3, pp. 187–200, 2007.

[97] P. Das, M. S. Manikandan, and B. Ramkumar, "Detection of epileptic seizure event in eeg signals using variational mode decomposition and mode spectral entropy," in *2018 IEEE 13th International Conference on Industrial and Information Systems (ICIIS)*. IEEE, 2018, pp. 42–47.

[98] G. J. Lal, E. Gopalakrishnan, and D. Govind, "Accurate estimation of glottal closure instants and glottal opening instants from electroglottographic signal using variational mode decomposition," *Circuits, Systems, and Signal Processing*, vol. 37, pp. 810–830, 2018.

[99] S. Lahmiri, "Comparative study of ecg signal denoising by wavelet thresholding in empirical and variational mode decomposition domains," *Healthcare technology letters*, vol. 1, no. 3, pp. 104–109, 2014.

[100] R. Tripathy, L. Sharma, and S. Dandapat, "Detection of shockable ventricular arrhythmia using variational mode decomposition," *Journal of medical systems*, vol. 40, pp. 1–13, 2016.

[101] R. M. Rangayyan and N. P. Reddy, "Biomedical signal analysis: a case-study approach," *Annals of Biomedical Engineering*, vol. 30, no. 7, pp. 983–983, 2002.

[102] M. S. Manikandan and S. Dandapat, "Wavelet-based electrocardiogram signal compression methods and their performances: A prospective review," *Biomedical Signal Processing and Control*, vol. 14, pp. 73–107, 2014.

[103] J. Pan and W. J. Tompkins, "A real-time qrs detection algorithm," *IEEE transactions on biomedical engineering*, no. 3, pp. 230–236, 1985.

[104] K. Dragomiretskiy and D. Zosso, "Variational mode decomposition," *IEEE transactions on signal processing*, vol. 62, no. 3, pp. 531–544, 2013.

[105] C. Cortes and V. Vapnik, "Support-vector networks," *Machine learning*, vol. 20, pp. 273–297, 1995.

[106] N. Cristianini and J. Shawe-Taylor, *Support Vector Machines and other kernel-based learning methods*. Cambridge, 2004.

[107] S. Ansari, N. Farzaneh, M. Duda, K. Horan, H. B. Andersson, Z. D. Goldberger, B. K. Nallamothu, and K. Najarian, "A review of automated methods for detection of myocardial ischemia and infarction using electrocardiogram and electronic health records," *IEEE reviews in biomedical engineering*, vol. 10, pp. 264–298, 2017.

[108] L. Sharma, S. Dandapat, and A. Mahanta, "Multichannel ecg data compression based on multiscale principal component analysis," *IEEE Transactions on Information technology in Biomedicine*, vol. 16, no. 4, pp. 730–736, 2012.

[109] S. Mitra, S. K. Pal, and P. Mitra, "Data mining in soft computing framework: a survey," *IEEE transactions on neural networks*, vol. 13, no. 1, pp. 3–14, 2002.

[110] H.-Y. Lin, S.-Y. Liang, Y.-L. Ho, Y.-H. Lin, and H.-P. Ma, "Discrete-wavelet-transform-based noise removal and feature extraction for ecg signals," *Irbm*, vol. 35, no. 6, pp. 351–361, 2014.

[111] S. Banerjee, R. Gupta, and M. Mitra, "Delineation of ecg characteristic features using multiresolution wavelet analysis method," *Measurement*, vol. 45, no. 3, pp. 474–487, 2012.

[112] A. Sharma, S. Patidar, A. Upadhyay, and U. R. Acharya, "Accurate tunable-q wavelet transform based method for qrs complex detection," *Computers & Electrical Engineering*, vol. 75, pp. 101–111, 2019.

[113] H. Yang, S. Bukkapatnam, and R. Komanduri, "Nonlinear adaptive wavelet analysis of electrocardiogram signals," *Physical Review E—Statistical, Nonlinear, and Soft Matter Physics*, vol. 76, no. 2, p. 026214, 2007.

[114] M. S. Manikandan and S. Dandapat, "Wavelet energy based diagnostic distortion measure for ecg," *Biomedical Signal Processing and Control*, vol. 2, no. 2, pp. 80–96, 2007.

[115] S. Hochreiter and J. Schmidhuber, "Long short-term memory," *Neural computation*, vol. 9, no. 8, pp. 1735–1780, 1997.

[116] J. H. Tan, Y. Hagiwara, W. Pang, I. Lim, S. L. Oh, M. Adam, R. San Tan, M. Chen, and U. R. Acharya, "Application of stacked convolutional and long short-term memory network for accurate identification of cad ecg signals," *Computers in biology and medicine*, vol. 94, pp. 19–26, 2018.

[117] O. Yildirim, U. B. Baloglu, R.-S. Tan, E. J. Ciaccio, and U. R. Acharya, "A new approach for arrhythmia classification using deep coded features and lstm networks," *Computer methods and programs in biomedicine*, vol. 176, pp. 121–133, 2019.

[118] D. Jyotishi and S. Dandapat, "An ecg biometric system using hierarchical lstm with attention mechanism," *IEEE Sensors Journal*, vol. 22, no. 6, pp. 6052–6061, 2021.

[119] M. S. Manikandan and S. Dandapat, "Wavelet threshold based tdl and tdr algorithms for real-time ecg signal compression," *Biomedical Signal Processing and Control*, vol. 3, no. 1, pp. 44–66, 2008.

[120] J. Sohn, S. Yang, J. Lee, Y. Ku, and H. C. Kim, "Reconstruction of 12-lead electrocardiogram from a three-lead patch-type device using a lstm network," *Sensors*, vol. 20, no. 11, p. 3278, 2020.

[121] A. Kapfo, S. Dandapat, and P. Kumar Bora, "Automated detection of myocardial infarction from ecg signal using variational mode decomposition based analysis," *Healthcare Technology Letters*, vol. 7, no. 6, pp. 155–160, 2020.

[122] P. Kaewfoongrungsi and D. Hormdee, "Support vector regression-based synthesis of 12-lead ecg system from the standard 5 electrode system using lead v1," *Engineering and Applied Science Research*, vol. 43, pp. 494–498, 2016.

[123] J. Lee, M. Kim, and J. Kim, "Reconstruction of precordial lead electrocardiogram from limb leads using the state-space model," *IEEE Journal of Biomedical and Health Informatics*, vol. 20, no. 3, pp. 818–828, 2015.

[124] J. J. Nallikuzhy and S. Dandapat, "Spatial enhancement of ecg using multiple joint dictionary learning," *Biomedical Signal Processing and Control*, vol. 54, p. 101598, 2019.

[125] A. Kapfo, S. Datta, S. Dandapat, and P. K. Bora, "Lstm based synthesis of 12-lead ecg signal from a reduced lead set," in *2022 IEEE International Conference on Signal Processing, Informatics, Communication and Energy Systems (SPICES)*, vol. 1. IEEE, 2022, pp. 296–301.

[126] S. Mian Qaisar and A. Subasi, "Cloud-based ecg monitoring using event-driven ecg acquisition and machine learning techniques," *Physical and Engineering Sciences in Medicine*, vol. 43, no. 2, pp. 623–634, 2020.

[127] R. M. Rangayyan, *Biomedical signal analysis*. John Wiley & Sons, 2015, vol. 33.

भारतीय प्रौद्योगिकी संस्थान गुवाहाटी
Indian Institute of Technology Guwahati

LIST OF PUBLICATIONS

Journal Publications:

1. Ato Kapfo, S. Dandapat, and P. Kumar Bora. "Automated detection of myocardial infarction from ECG signal using variational mode decomposition based analysis." *Healthcare Technology Letters*, 7(6)(2020), pp.155-160.

2. Ato Kapfo, S. Datta, S. Dandapat, and P. Kumar Bora. "A wavelet subband based LSTM model for 12-lead ECG synthesis from reduced lead set." *Biomedical Engineering Letters*, (2024) pp.1-11.

Book Chapter:

1. Ato Kapfo, S. Datta, S. Dandapat, and P. Kumar Bora. "Artificial Neural Network Based Synthesis of 12-Lead ECG Signal from Three Predictor Leads." *In Pattern Recognition and Data Analysis with Applications*, pp. 625-634. Singapore: Springer Nature Singapore, 2022.

Conference Publications:

1. Ato Kapfo, S. Datta, S. Dandapat, and P. Kumar Bora. "LSTM based Synthesis of 12-lead ECG Signal from a Reduced Lead Set." *In 2022 IEEE International Conference on Signal Processing, Informatics, Communication and Energy Systems (SPICES)*, vol. 1, pp. 296-301. IEEE, 2022.

2. Ato Kapfo, D. Jyotishi, S. Dandapat, and P. Kumar Bora. "Person Identification from Synthesized ECG Signal." *In 2022 IEEE Silchar Subsection Conference (SILCON)*, pp. 1-5. IEEE, 2022.